

AD A100455



FILE COPY

LEVEL 4

2

FRANK J. SEILER RESEARCH LABORATORY

FJSRL TECHNICAL REPORT 81-0005

MAY 1981

12 221

**A LIQUID CHROMATOGRAPHY
DETECTOR FOR TRANSITION
AND RARE-EARTH METAL
IONS BASED ON A CUPRIC
ION-SELECTIVE ELECTRODE**

FJSRL-TR-81-1115

R. CAMERON/DOREY

OTIC
ELECTE
JUN 22 1981

A

APPROVED FOR PUBLIC RELEASE;
DISTRIBUTION UNLIMITED.

PROJECT 2303

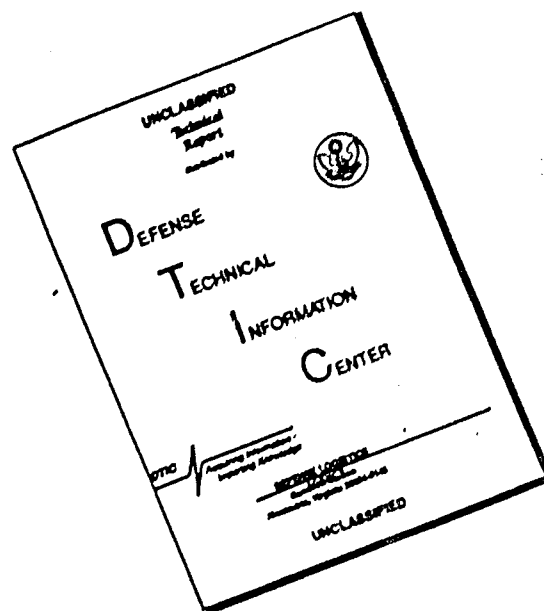
17 F3

AIR FORCE SYSTEMS COMMAND
UNITED STATES AIR FORCE

319 920

81 6 17 012

DISCLAIMER NOTICE



THIS DOCUMENT IS BEST QUALITY AVAILABLE. THE COPY FURNISHED TO DTIC CONTAINED A SIGNIFICANT NUMBER OF PAGES WHICH DO NOT REPRODUCE LEGIBLY.

FJSRL-TR-81-0005

This document was prepared by the Energetic Materials Division, Directorate of Chemical Sciences, Frank J. Seiler Research Laboratory, United States Air Force Academy, CO. The research was conducted under Project Work Unit Number 2303-F3-05, Chemical Structure/Bonding Decomposition Relationships, Capt R. Cameron Dorey was the Project Scientist.

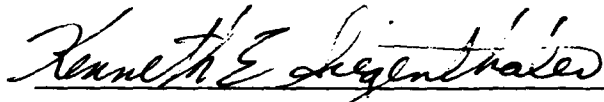
When U. S. Government drawings, specifications or other data are used for any purpose other than a definitely related government procurement operation, the government thereby incurs no responsibility nor any obligation whatsoever, and the fact that the government may have formulated, furnished or in any way supplied the said drawings, specifications or other data is not to be regarded by implication or otherwise, as in any manner licensing the holder or any other person or corporation or conveying any rights or permission to manufacture, use or sell any patented invention that may in any way be related thereto.

Inquiries concerning the technical content of this document should be addressed to the Frank J. Seiler Research Laboratory (AFSC), FJSRL/NC, USAF Academy, CO 80840. Phone AC 303, 472-2655.

This technical report has been reviewed and is approved for publication.



R. CAMERON, DOREY, III, Captain, USAF
Project Scientist



KENNETH E. SIEGENTHALER, Lt Colonel, USAF
Director
Directorate of Chemical Sciences



WILLIAM D. SIURU, JR., Lt Colonel, USAF
Commander

Copies of this report should not be returned unless return is required by security considerations, contractual obligations, or notice on a specific document.

Printed in the United States of America. Qualified requestors may obtain additional copies from the Defense Documentation Center. All others should apply to: National Technical Information Service
6285 Port Royal Road
Springfield, Virginia 22161

FJSRL-TR-81-0005

A LIQUID CHROMATOGRAPHY DETECTOR
FOR
TRANSITION AND RARE-EARTH METAL IONS
BASED ON A CUPRIC ION-SELECTIVE ELECTRODE

By

R. CAMERON DOREY

TECHNICAL REPORT FJSRL-TR-81-0005

MAY 1981

Approved for public release; distribution unlimited.

Directorate of Chemical Sciences
Frank J. Seiler Research Laboratory
Air Force Systems Command
US Air Force Academy, Colorado 80840

UNCLASSIFIED

SECURITY CLASSIFICATION OF THIS PAGE (When Data Entered)

REPORT DOCUMENTATION PAGE		READ INSTRUCTIONS BEFORE COMPLETING FORM									
1. REPORT NUMBER FJSRL-TR-81-0005 ✓	2. GOVT ACCESSION NO. AD-A100455 ADA	3. RECIPIENT'S CATALOG NUMBER									
4. TITLE (and Subtitle) A Liquid Chromatography Detector for Transition and Rare-earth Metal Ions Based on a Cupric Ion-selective Electrode		5. TYPE OF REPORT & PERIOD COVERED									
7. AUTHOR(s) R. Cameron Dorey		6. PERFORMING ORG. REPORT NUMBER									
9. PERFORMING ORGANIZATION NAME AND ADDRESS Frank J. Seiler Research Laboratory (AFSC) USAF Academy, CO 80840		8. CONTRACT OR GRANT NUMBER(s)									
11. CONTROLLING OFFICE NAME AND ADDRESS Frank J. Seiler Research Laboratory (AFSC) USAF Academy, CO 80840		10. PROGRAM ELEMENT, PROJECT, TASK AREA & WORK UNIT NUMBERS 2303-F3-05									
14. MONITORING AGENCY NAME & ADDRESS (if different from Controlling Office)		12. REPORT DATE May 1981									
		13. NUMBER OF PAGES 220									
		15. SECURITY CLASS. (of this report) UNCLASSIFIED									
		15a. DECLASSIFICATION/DOWNGRADING SCHEDULE									
16. DISTRIBUTION STATEMENT (of this Report) Approved for public release; distribution unlimited.											
17. DISTRIBUTION STATEMENT (of the abstract entered in Block 20, if different from Report)											
18. SUPPLEMENTARY NOTES											
19. KEY WORDS (Continue on reverse side if necessary and identify by block number)											
<table border="0"> <tr> <td>Liquid Chromatography</td> <td>Ion-selective Electrode</td> <td rowspan="4">A</td> </tr> <tr> <td>Transition Metal</td> <td>Cu(II)</td> </tr> <tr> <td>Rare Earth</td> <td>Potentiometry</td> </tr> <tr> <td>Lanthanide</td> <td>Flow-through Electrode</td> </tr> </table>			Liquid Chromatography	Ion-selective Electrode	A	Transition Metal	Cu(II)	Rare Earth	Potentiometry	Lanthanide	Flow-through Electrode
Liquid Chromatography	Ion-selective Electrode	A									
Transition Metal	Cu(II)										
Rare Earth	Potentiometry										
Lanthanide	Flow-through Electrode										
20. ABSTRACT (Continue on reverse side if necessary and identify by block number) A potentiometric detector sensitive to many transition and rare earth metal ions has been developed, using a cupric ion-selective electrode. The sample stream is mixed with a stream of copper(II)-ethylene-diaminetetraacetic acid complex (CuEDTA), and metal ions in the eluent displace copper(II) from the complex. The increase in free copper(II) is then measured by the electrode. Background copper(II) level in the CuEDTA stream sets the lower limit of detection of metal ions at approximately 3×10^{-7} M, and the detector response											

DD FORM 1 JAN 73 1473

EDITION OF 1 NOV 65 IS OBSOLETE

UNCLASSIFIED

SECURITY CLASSIFICATION OF THIS PAGE (When Data Entered)

UNCLASSIFIED

SECURITY CLASSIFICATION OF THIS PAGE(When Data Entered)

characteristics require that approximately 1500 μ L flow through the detector to reach steady-state response. This establishes a detection limit of 1.5×10^{-10} mole metal ion. Theoretical response of the detector has been developed and the experimental values agree closely with theory for specific metals over the range 3×10^{-7} M to 10^{-2} M metal ion.

Both transient and steady-state response of the detector to metal ions and some common anions, including halide ions, is shown, and the advantages and limitations of the system are discussed.

UNCLASSIFIED

SECURITY CLASSIFICATION OF THIS PAGE(When Data Entered)

ACKNOWLEDGEMENTS

This work was supported by grants from the National Science Foundation and National Institute of Health. Special thanks are given to the Frank J. Seiler Research Laboratory of the United States Air Force for their aid which was most generously given, and particularly to Donna Weiss and Betty Darcy, who typed this manuscript.

ABSTRACT

A LIQUID CHROMATOGRAPH DETECTOR FOR TRANSITION AND RARE-EARTH METAL IONS BASED ON A CUPRIC ION-SELECTIVE ELECTRODE

by

R. Cameron Dorey

A potentiometric detector sensitive to many transition and rare earth metal ions has been developed, using a cupric ion-selective electrode. The sample stream is mixed with a stream of copper(II)-ethylene-diaminetetraacetic acid complex (CuEDTA), and metal ions in the eluent displace copper(II) from the complex. The increase in free copper(II) is then measured by the electrode.

Background copper(II) level in the CuEDTA stream sets the lower limit of detection of metal ions at approximately 3×10^{-7} M, and the detector response characteristics require that approximately 500 μ L flow through the detector to reach steady-state response. This establishes a detection limit of 1.5×10^{-10} mole metal ion. Theoretical response of the detector has been developed and the experimental values agree closely with theory for specific metals over the range 3×10^{-7} M to 10^{-2} M metal ion.

Both transient and steady-state response of the detector to metal ions and some common anions, including halide ions, is shown, and the advantages and limitations of the system are discussed.

TABLE OF CONTENTS

	<u>Page</u>
I. Introduction	1
A. Overview	1
B. Liquid Chromatography Metal Ion Detectors	4
C. Flow Potentiometry with Ion-selective Electrodes	19
1. Introduction - Ideal Ion-selective Electrodes	19
2. Interferences	20
3. Ionic Activities and Concentrations	23
4. Liquid Junction Potentials	24
5. Streaming Potentials	27
6. Transient Response of Ion-selective Electrodes	31
7. Cupric Ion-selective Electrodes	44
a. Construction	44
b. Behavior in Cu(II) solutions	46
c. Behavior in solutions of Cu(II)-complexing ligands	48
d. Behavior in solutions of other interfering ions	49
e. Application in the determination of other metals	51
II. Equilibrium Theory of the Detector	53
III. Experimental	77
A. Electrochemical Cell	77
B. Electronics	78
C. Flow System Design	87
D. Electrode Sensing Material	96

	<u>Page</u>
E. Flow-through Electrode Design	99
F. CuEDTA Solution Preparation	106
G. Calibration for Metal Response	108
IV. Results and Discussion	109
A. Dip-type Electrodes	109
1. Cu(II) response in KNO_3 background	109
2. Cu(II) response in CuEDTA background	112
3. Potential noise and drift in solutions of constant Cu(II) concentration	115
4. Other metal ion response in KNO_3 background	115
5. Other metal ion response in CuEDTA background	118
B. Flow-through Electrodes	129
1. Cu(II) response in KNO_3 background	129
2. Cu(II) response in CuEDTA background	132
3. Potential noise and drift in solutions of constant Cu(II) concentration	132
4. Dynamic response to changes in Cu(II) concentration	132
C. Assembled Detector System	143
1. Dynamic response to changes in Cu(II) concentration	143
a. Dynamic response to varying sample size	143
b. Peak return to baseline after injections of differing Cu(II) concentration	164
2. Effect of delay coil length (reaction time) on extent of displacement reaction for Ni(II)	165
3. Detector response to various metals	171

	<u>Page</u>
4. Detector response to common anions (excluding halides)	180
5. Detector response to halide ions	180
V. Conclusion	186
Appendix. An Automatic Signal-offset Module	187
A. Introduction	187
B. Functional Description	188
C. Operational Principles	191
D. Application	197
Bibliography	201

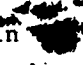
LIST OF FIGURES

	<u>Page</u>
Figure 1. Block Diagram of the Metal Ion Detector	2
Figure 2. Barrier Model of Ion-selective Electrode Dynamic Response (59)	32
Figure 3. Unstirred Diffusion Layer Model of Ion-selective Electrode Dynamic Response (59,61)	35
Figure 4. Schematic Diagram of Multielectrode Model of Ion- selective Electrode Response	38
Figure 5. Theoretical Logarithmic Plots of Dimensionless Uncom- plexed Cu(II) Concentration <u>vs</u> the Dimensionless Total Metal Ion Concentration	61
Figure 6. Theoretical Plots of the Slope of Dimensionless Total Metal Ion Concentration with Respect to Dimensionless Uncomplexed Cu(II) Concentration <u>vs</u> the Dimensionless Total Metal Ion Concentration	64
Figure 7. Theoretical Logarithmic Plots of Dimensionless Uncom- plexed Cu(II) Concentration <u>vs</u> the Dimensionless Total Metal Ion Concentration	67
Figure 8. Theoretical Logarithmic Plots of Dimensionless Uncom- plexed Cu(II) Concentration <u>vs</u> the Dimensionless Total Metal Ion Concentration	69
Figure 9. Theoretical Logarithmic Plots of Dimensionless Uncom- plexed Cu(II) Concentration <u>vs</u> the Dimensionless Total Metal Ion Concentration	72

	<u>Page</u>
Figure 10. Theoretical Logarithmic Plots of Dimensionless Uncomplexed Cu(II) Concentration <u>vs</u> the Dimensionless Total Metal Ion Concentration	75
Figure 11. Schematic Diagram of the Differential Electrometer . . .	80
Figure 12. Schematic Diagram of the Antilog Transducer for Potential to Cu(II) Concentration Conversion	83
Figure 13. Schematic Diagram of the Metal Ion Detector	88
Figure 14. Construction of Room Temperature Potentiometric Cell . .	94
Figure 15. Construction of Flow-through Cupric Ion-selective Electrode	103
Figure 16. Steady-state Response of Dip-type Cupric Ion-selective Electrode to Added Cu(II)	110
Figure 17. Steady-state Response of Dip-type Cupric Ion-selective Electrode to Added Cu(II) in Equimolar CuEDTA	113
Figure 18. Time-dependent Response of Dip-type Cupric Ion-selective Electrode to Various Metal Ion Salt Solutions	116
Figure 19. Time-dependent Displacement of Cu(II) from Equimolar CuEDTA by Various Metal Ions	119
Figure 20. pH Dependence of Kinetics of Zn(II) Displacement of Cu(II) from Equimolar CuEDTA	125
Figure 21. Temperature Dependence of Kinetics of Ni(II) Displacement of Cu(II) from Equimolar CuEDTA	127
Figure 22. Steady-state Response of Flow-through Cupric Ion-selective Electrode to Added Cu(II)	130

	<u>Page</u>
Figure 23. Steady-state Response of Flow-through Cupric Ion-selective Electrode in Equimolar CuEDTA to Added Cu(II).	133
Figure 24. Background Noise and Drift of Flow-through Cupric Ion-selective Electrode	135
Figure 25. Dynamic Response of Flow-through Cupric Ion-selective Electrode	137
Figure 26. Dynamic Detector Response as a Function of Sample Volume	145
Figure 27. Peak Width at Half Height Squared as a Function of Sample Volume Squared for the Detector	148
Figure 28. Model of Liquid Flow Rate and Accumulated Output Volume for Sample Input (Sampling Loop) for the Detector System	157
Figure 29. Detector Peak Height as a Function of Sample Volume . .	162
Figure 30. Steady-state Logarithmic Response of Detector to $\text{Ni}(\text{NO}_3)_2$ Samples	169
Figure 31. Steady-state Logarithmic Response of Detector to Various Metal Ions	172
Figure 32. Dynamic Response of Detector to Potassium Halide Samples	183
Figure 33. Block Diagram of the Automatic Offset Module	189
Figure 34. Schematic Diagram of the Automatic Offset Module	192
Figure 35. Operation of the Automatic Offset Module	198

LIST OF TABLES

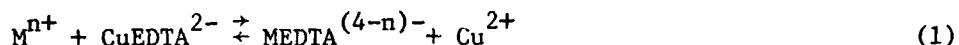
	<u>Page</u>
Table I. Liquid Chromatography Metal Ion Detectors	6
Table II. Components Used in  Circuit in Figure 11 (Electrometer)	82
Table III. Components Used in the Circuit in Figure 12 (Antilog Transducer)	85
Table IV. Apparent Half-reaction Times ($t_{1/2}$) for the Metal Exchange Reactions	122
Table V. Dynamic Concentration Response of Flow through Electrode	140
Table VI. Evaluation of Dispersion Due to the Detector	150
Table VII. Various Measures of Recovery Time for a Detector to the Concentration Function $C = C_0 e^{-t^2/\tau_r}$	166
Table VIII. Recovery Time for the Detector	167
Table IX. Experimental Estimates of the Dimensionless Parameters Governing the CuEDTA-M^{n+} Exchange Reaction	175
Table X. Linear Range of Steady-state Response of Detector for Metal Ions	177
Table XI. Comparison of Experimental and Theoretical Slopes of Metal Ion Response over the "Linear" Range of the Detector	179
Table XII. Steady-state Response of the Detector to Common Anion Salts	181
Table XIII. Components Used in the Circuit in Figure 34 (Automatic Offset Module)	194

I. Introduction

A. Overview

In this report we describe a detector for transition and rare earth metal ions which is applicable to high performance liquid chromatography. The detector is in essence a post-column derivitization flow system which incorporates a chemical reaction system and an ion-selective potentiometric cell to monitor a product (Cu^{2+}) of the reaction. A block diagram of the detector scheme is shown in Figure 1.

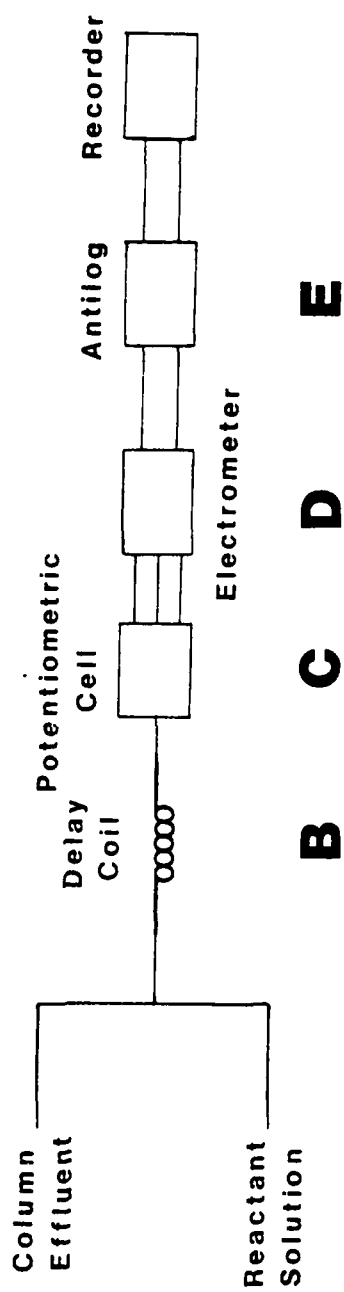
The chemical basis of the detector involves the competition between two metal ions for a fixed amount of ligand which is assumed to form 1:1 complexes with both cations. Specifically, the copper(II)-ethylenediaminetetraacetate (CuEDTA^{2-}) ion is in the reactant solution used in this work, and a metal ion M^{n+} is introduced in the effluent from a chromatographic column. In its simplest form, reaction then proceeds



After the combined stream passes through a delay coil to allow the reaction to achieve equilibrium, the liberated Cu^{2+} is measured with a flow-through cupric ion-selective electrode in a three-electrode potentiometric cell. Finally, the potentiometric readings are translated into units of Cu^{2+} concentration with an electronic antilogarithmic transducer. The concentration of Cu^{2+} at the electrode can then be related to the original concentration of M^{n+} through equilibrium calculations concerning the specific metal ion.

Figure 1. Block Diagram of the Metal Ion Detector.

- A. Typically 0.01 M CuEDTA in 0.1 M KNO_3 , pH adjusted to 4.0, at 25° C, pumped at 1.0 mL/min.
- B. Typically 2.0 m of 0.5mm I.D. Teflon tubing in 75° C water bath plus 0.25 m of 0.5mm I.D. Teflon tubing in room temperature (no external control) water bath.
- C. Comprised of a flow-through cupric ion-selective electrode, saturated calomel reference electrode isolated by a "Thirsty Glass" (porous Vycor) plug, and stainless steel hypodermic needle common electrode.
- D. Dual high impedance input differential electrometer.
- E. Antilogarithmic circuit.



This chemical system is not the only one applicable to the problem, but there were five main reasons for its choice in this work. First, the cupric ion-selective electrode is inexpensive and simple to produce, without elaborate or critical procedure. Second, it is one of the most-studied ion-selective electrodes used, so there is a large volume of literature on its characteristics. Third, EDTA complexes strongly with a very wide spectrum of metal ions, making many ions detectable with this system, and equilibrium constants for its reactions with metal ions under many conditions have been well tabulated. Fourth, the exchange reaction in Equation 1 is rapid enough for many metal ions to be useful in our detector system. Fifth, crystalline $H_2CuEDTA$ can be prepared easily with reproducible stoichiometry, and has very good long-term (months) stability in the solid form.

In this work, we will show the theory governing the detector response in general terms, so that other metal-ligand systems can be used to demonstrate other applications of the principles used here. Construction of the detector components and materials which we made is described, and the experimental dynamic and steady-state response characteristics to metal ions and several anions are discussed in detail.

B. Liquid Chromatography Metal Ion Detectors

On-line detectors for metal ions in liquid chromatography have been developed mainly in the past few years with the advent of high pressure (and high flow rate) chromatographic systems. With traditional gravity fed ion-exchange systems, stationary phase (resin) particles are usually larger than 200 mesh (75 μm diameter) to allow reasonable flow rates to

be attained through the columns. Mass transfer within the resin particles is very slow, so in many cases, solvents are chosen which will elute (or retain) only the species of interest, or elute the individual species very slowly with large eluent volumes between the peaks. The resolution of a detector is unimportant under these circumstances and fraction collecting can be employed.

Alternatively, the flow rate of the eluting solvent can be reduced so that ionic equilibrium is maintained between the interior and exterior of the resin. Here, the time required to analyze eluent fractions after separation can be very small compared to the separation time. Both of these cases minimize the need for real-time analysis of the eluent.

Ion-exchange systems are being developed, however, using high-pressure techniques with pellicular and microparticle ($\sim 10 \mu\text{m}$) stationary phases. For example, Takata and Fujita (1) have obtained near-baseline separation of six transition metal ions on an $8\text{--}11 \mu\text{m}$ cation exchange resin within seven minutes at a flow rate of 1.22 mL/min . This separation used less than 10 mL of solvent, and required a fast continuous coulometric detector to prevent severe post-column degradation of the resolution.

Many different on-line detectors sensitive to more than one metal ion at a time have been demonstrated or proposed. These can be broadly divided into three types: (I) Passive detectors, (II) Interactive detectors, and (III) Reaction detectors. An overview of these detector designs as applied to metal ions as well as detectors relevant to metal ions (although not demonstrated for them) is given in Table I.

Table I. Liquid Chromatography Metal Ion Detectors.

Type of Detector	Principle of Operation	Response Time	Limit of Detection	Dead Volume	Comments	Ref.
Passive	UV absorption	6 sec ^a	2×10^{-7} g Cu(II) ^b	32 μ L (Spectro- photometer flow cell)	Eluent must form UV-absorbing complex with metal	2
	Radiation (β -decay)	36 sec ^{a,c,d}	100 countse, ^d per transit time	200 μ L	Tracer must be added if metal is not normally radioactive	3
	Conductivity	< 1 sec ^{a,c,e}	0.3% change in baseline conduc- tivity; 1.5×10^{-5} M KCl ^g	2 μ L ^{c,e}	Low-conductivity background solu- tion required, i.e., 10^{-5} M KCl ^g	3
Interactive	Swelling of ion- exchange membrane	> 1 min	2×10^{-7} moles M ⁺ 10^{-8} moles M ²⁺ 5×10^{-8} moles M ³⁺ ^b	0.5 mL	Response flow rate dependent	4,5
	Heat of adsorp- tion on ion- exchange membrane	4 sec	7×10^{-5} M Zn(II)	64 μ L	Complicated peak shape	6
	Atomic emission	NA ^f	4×10^{-6} M Na	NA	Emission must occur within narrow spectral band	7

<u>Type of Detector</u>	<u>Principle of Operation</u>	<u>Response Time</u>	<u>Limit of Detection</u>	<u>Dead Volume</u>	<u>Comments</u>	<u>Ref.</u>
	Flame ionization	NA	10^{-13} mole alkali metal	NA	Small linear range, contamination problems	8
	Polarography (DC)	> 3.5 min	10^{-6} M Cd(II)	1 mL	Solution requires degassing, electroactive metal required	9
	Polarography (AC)	> 3.5 min	NA	1.5 mL	No O_2 interference, sensitivity enhanced	10
	Coulometry	3 sec ^a	1.3×10^{-11} moles I^- (used in detection limit study)	15 μ L	Electrolyzed material cannot deposit on electrode	11
	UV-vis absorption of metal-dye complex	6 sec ^a	2×10^{-6} M Ca(II)	32 μ L (spectrophotometer flow cell volume)	Different wavelengths required for different metals	12, 13
Reaction	Chemiluminescence	18 sec ^a	10^{-10} M Cu(II)	100 μ L	Reaction proceeds only above pH 10	14, 15, 16
	Coulometry, ligand exchange	< 1 sec	10^{-7} mole metal ion	< 60 μ L	High limit of detection	17

<u>Type of Detector</u>	<u>Principle of Operation</u>	<u>Response Time</u>	<u>Limit of Detection</u>	<u>Dead Volume</u>	<u>Comments</u>	<u>Ref.</u>
	Conductivity with background suppression	< 1 sec (conductivity cell alone) ^{a,c,e}	10^{-8} to 10^{-9} mole ^b	2 μ L ^{c,e}	Not compatible with metals which form insoluble hydroxides	18
Other (not demonstrated in metal detection)	Ion-selective electrode		10^{-10} mole NO_3^-	5 μ L	Nonspecificity of electrode used in detection of substances	19
	Ion-selective electrode	6 sec (90%) (electrode alone) ^h	10^{-8} g glycine	< 100 μ L ^{b,h}	Responds to substances which complex Cu(II)	20
	Amperometry (metal or carbon electrode)	< 1 sec ^a	10^{-14} equivalents electroactive substance/sec	< 1 μ L	Precise flow control needed (also see polarography, coulometry)	21, 22, 23
	Amperometry (Hg electrode)	< 1 sec ^a	10^{-9} g glutathione	< 0.5 μ L	see above	24, 25

All response times, limits of detection, and dead volumes given in paper referenced unless otherwise noted.

- a. Time required to sweep three void volumes of detector at 1 mL/min flow rate.
- b. Estimated from data given in reference.
- c. From reference on similar detector, but not concerned with metal ions.
- d. Ref. 26.
- e. Ref. 27.
- f. Not available or not applicable.
- g. Ref. 28.
- h. Ref. 29.

Passive detectors. The detectors in this class measure a property inherent in the chromatographic eluent. They do not alter the composition or physical characteristics of the fluid which flows through them.

The primary detector of this type measures the UV absorption of the metal ion in the chromatographic eluent, usually in the form of complexes with the chemical species used to effect elution. Seymour and Fritz (2) describe a high-speed anion-exchange separation of metal ions in 6 M HCl with UV detection at 225 nm in a 32 μ L quartz flow cell. From data given, a detection limit of 2×10^{-7} grams of Cu(II) or Pb(II) can be estimated for 99% transmittance.

Obviously, with this method of detection, the chromatographer is restricted to elution solvents which form highly absorbing complexes with the ions of interest.

Flow-through radiation detectors have also been employed for metal ions (3). These are generally used to qualitatively follow a chromatogram with tracer ions, since only the transactinides (with a few exceptions) are totally radioactive. The added tracers cannot indicate the total amounts of each metal ion present, so fractions must be collected for quantitative data.

One major problem with radiation detectors concerns the principle upon which they operate. Statistically, theoretical error bounds can be calculated according to the number of radioactive disintegrations which are counted from a sample, whether static or flowing. The magnitude of this error decreases as the number of counts (disintegrations) increases. Thus, to improve the precision of counting for a finite size sample in a flowing stream, it has to remain within the detector confines longer.

With a specific flow rate, this is accomplished by increasing the detector volume, which increases the width of the minimum detectable peak (26). This tradeoff of precision vs. time (or in this case, apparent peak width) is common to all methods of analysis (30), of which radiation monitoring is a case.

Flow-through conductivity cells have been utilized (3) in metal ion detection, but ion-exchange mobile phases are generally highly conductive, for example, aqueous HCl (10). This severely limits the sensitivity of this technique, since the conductivity of the solution would be essentially completely determined by the major ions in solution. Sisson, Mode, and Campbell (3) describe conductometric detection of rare earths in α -hydroxybutyric acid, a weak acid, to minimize this problem.

Interactive detectors. Detectors of this type either measure a physical change in the detector itself (through interaction of the active component of the detector with the eluent), or the detector changes the physical or chemical characteristics of the eluent metal ions during the measurement. These detectors are chromatographically more versatile than passive devices in general. They utilize a broader spectrum of analytical methods in order to be more selective or more sensitive to the ions of interest.

Two detectors measure interactions of ions with ion-exchange materials. One, by Gilbert and Dobbs (4), measures longitudinal swelling of an ion-exchange membrane. The detector's active components consist of a cation-exchange membrane stretched over the tip of a linear displacement transducer. This assembly extends into a cup into which the

chromatographic eluent flows. A change in the concentration of any ion in the solution in contact with the membrane causes it to shrink or swell, and this is measured. From the signal-to-noise level for 0.01 M metal solutions, we estimate a lower limit of detection of approximately 10^{-7} moles of divalent cation. The detector has a dead volume of approximately 0.5 mL, so this corresponds to a 2×10^{-4} M solution. The peak height for a 1.0 mL sample is flow rate dependent, since only a fraction of the steady-state response is reached before the peak elutes from the detector. Gradient elution (e.g., with HCl) is not feasible because the detector is sensitive to a change in concentration of any ionic species.

Warren and McKay (6) have proposed a detector for metals which senses the heat of adsorption onto an ion-exchange resin, using a commercial dual thermistor heat of adsorption detector. An effective dead volume is calculated from impulse rise times at 64 μ L. Under optimum conditions, the lower limit of detection for Zn(II) is determined to be 7×10^{-5} M (S/N = 2) with a linear range of 10^3 . No separations are shown using this detector, but an injection of metal ion produces a complicated response consisting of a sharp peak followed by a broader, shallower trough, with a slow final return to baseline.

A number of groups have investigated the use of the various forms of atomic spectroscopy in flames as detector systems for metal ion separation. Atomic emission has been used by Freed (7) for the detection of various metal ions. In this scheme, the effluent of the ion-exchange column is connected directly to the aspirator inlet of a home-made flame emission spectrometer. The optics can be configured without

entrance slits to detect a wider wavelength band for minimum selectivity (50 nm bandpass), or with entrance slits to reject broadband flame emission to achieve lower detection limits (0.8 nm bandpass). A detection limit is given for sodium ion of 4×10^{-6} M with a linear response to 4×10^{-4} M. This narrow linear range would cause several different dilutions to be needed if species of widely different concentrations were to be determined in a sample.

Araki, Suzuki, and Yamada (8) have described a transport type detector for alkali metals and alkaline earths based on the principle of the gas chromatographic flame ionization detector. The system uses a modified automatic fraction collector, which catches each drop of eluent on a platinum wire loop, drives off the solvent, and then evaporates the metal salt into an ionizing flame. A detection limit of 10^{-13} mole of applicable metals is quoted, but the linear range of most metals is only 10^2 , so extreme care must always be taken to prevent contamination of reagents or apparatus. Samples with high concentrations of metal must be greatly diluted before introduction. The authors note a continual baseline drift which they attribute to an unspecified contamination of the system.

Finally, two different types of electrochemical detectors have been used for metals. Blaedel and Todd (9) describe a DC polarographic detector used with a gravity-fed column. The eluent is degassed with N_2 and debubbled after the column but prior to entering a 1 mL flow-through polarographic cell. The response time of this system is very long due to the large volume. It responds to within 10% of steady-state in approximately 3.5 minutes at a flow rate of 1 mL/minute. The system

has a lower limit of detection of approximately 10^{-6} M for Cd(II) (defined as the concentration of sample required to give twice the background current), with similar limits for other transition metal ions. Buchanan and Bacon (10) modified this approach by employing a square-wave polarograph to achieve some selectivity in the case of incomplete resolution of peaks, and to eliminate O_2 interference. In this case, N_2 bubbling is not required. The cell is 1.5 mL in volume, but response time is slightly shorter than Blaedel and Todd's, due to a vertical flow of eluent, with the inlet in close proximity to the mercury capillary.

Several other amperometric detectors have been developed for liquid chromatography, but they have not been demonstrated in metal ion detection. Representatives are discussed in the final section of this review.

Johnson and Larochelle (11) have designed a coulometric flow cell for electroactive metal ions. It consists of a tubular Pt working electrode filled with Pt wire to increase the surface area, a Pt wire coil counter electrode, and a saturated calomel reference electrode. The dead volume of the working electrode is approximately 15 μ L. Oxidation of I^- to I_2 was used to estimate a detection limit of 1.3×10^{-11} moles (2.5×10^{-8} M \times 0.504 mL injection loop). Also, response for I^- is linear over four decades of concentration. The use of the detector was demonstrated in a separation of Fe(III) and Cu(II). 25% HBr was used in the eluent to stabilize the Cu(I) formed.

Reaction Detectors. These react the species of interest chemically with another substance (either mixed with the eluent from a separate

stream or immobilized on a bed through which the eluent passes) before the actual detection of the desired components of the eluent. This type is the most versatile of the three, since detection depends minimally on the chromatographic conditions. Reaction detectors in general have recently been reviewed by Frei and Scholten (31). One disadvantage to most reaction detectors is that most require a delay coil before the detector proper to allow the reaction to proceed. This increases the observed peak broadening.

Fritz and Story (12) use spectrophotometry after a dye stream is mixed with the eluent to form an intensely absorbing metal-dye complex. The dyes can be highly buffered to compensate for any extremes of pH in the eluent stream. The metal-dye complex is strong enough to eliminate interferences from weak complexes in the eluent (e.g., poly-chloro complexes). However, not all of the metal-dye complexes studied have the same optimum wavelength for detection, so a compromise wavelength must be found between sensitivity and generality for a given system. Recently Arguello and Fritz (13) described a variant of this system for metals which complex weakly with the color-forming dyes, such as Ca^{2+} and Mg^{2+} . The eluent is mixed with two streams: (1) dye, and (2) ZnEDTA. Reaction proceeds to form the Zn-dye complex, which is then monitored. The limits of detection for Ca^{2+} and Mg^{2+} can be calculated at approximately $2 \times 10^{-6} \text{ M}$ for 1% absorbance of the incident light (0.004A).

Neary, Seitz, and Hercules (14) have developed a detector based on metal ion catalysis of the chemiluminescent luminol- H_2O_2 reaction. The chromatographic eluent is mixed with an alkaline buffered solution of

luminol and H_2O_2 in a 100 μL light-tight stirred cell. The total light is then measured by a photomultiplier. This detector responds linearly to most metal ions in the concentration range of approximately 10^{-10} to 10^{-7} M , with sensitivity to Co(II) in particular two orders of magnitude below this. Delumyea and Hartkopf (15) also demonstrated a detector based on this reaction at approximately the same time, and they have subsequently shown its applicability for use in acidic and partially nonaqueous chromatographic solvent systems (16) (the chemiluminescence reaction itself proceeds only above pH 10). One difficulty of this type of detection is that the top of the linear range is so low that great care has to be taken to prevent contamination of reagents or apparatus with transition metal ions.

Tanaka and Muto (17) report a coulometric detection system after the eluent has been mixed with a stream of mercury(II)-diethylenetriaminepentaacetate (DTPA) complex. Ligand exchange and reduction of the Hg(II) to Hg^0 occurs in the coulometric cell. The cell is a two-electrode system, with a working electrode of carbon cloth, and an auxiliary electrode of Ag/AgI netting, poised in a flowing stream of 0.5 M KI . Dead volume is less than 60 μL , and the authors state a response time of less than one second. The limit of detection is given as 10^{-7} mole of metal ion, which is high, considering the cell volume.

The last detector for metal ions to be described is actually a complete ion-exchange chromatographic system. Called "ion chromatography" by its inventors Small, Stevens, and Bauman (18), the scheme first separates metal ions on a strong acid cation-exchange resin with HCl eluent, and then replaces the anions with hydroxide by use of a strong

base anion-exchanger. Hydrogen and hydroxide ions combine to form water, and the metal ions are eluted as their hydroxides. Metals are then detected conductometrically in a very low conductance background. Detection limits for metals are not given, but by analogy with data given for chloride ion, they can be estimated at 10^{-8} to 10^{-9} mole. The system has one major drawback - no metals which precipitate as hydroxides can be determined, since they will precipitate within the second column.

Related Detectors. Finally, there have been four electrochemical chromatography detectors described which could be applicable to metal ions, but have not been demonstrated as such.

Shultz and Mathis have used a nitrate ion-selective electrode to determine anions in an ion-exchange column eluent. A flow-through cap is fitted onto the end of an Orion liquid membrane nitrate electrode. They use the non-specificity of the electrode to determine nitrite, phthalate, and perchlorate, and qualitatively observe amino acids and sulfonic acid anions. A lower limit of detection of 10^{-10} mole of nitrate is claimed, with linearity over three orders of magnitude.

Loscombe, Cox, and Dalziel (18) expanded the utility of ion-selective electrode detection by using a cupric ion-selective electrode to detect amino acids from reverse-phase and ion-exchange separations. They combined the column eluent with a 10^{-4} M Cu(II) stream. The amino acids complex Cu(II) and decrease the potential of a flow-through electrode relative to the background without amino acids to complex the free Cu(II). At low amino acid concentrations, potential change is approximately proportional to concentration. This proportionality rolls off above 5 μ g amino acid injected.

Several additional types of amperometric detectors have been described. Kissinger (21) uses a solid platinum, gold, or carbon electrode in a thin-layer cell, with reference and auxiliary electrodes downstream. The total working volume of the thin-layer cell is less than 1 μL . Kissinger claims a lower limit of detection of 10^{-14} equivalents of electroactive substance per second, assuming no noise from the background solution. One drawback of this (or any other amperometric cell) is that very precise flow control is required for quantitative results.

Fenn, Siggia, and Curran (22) expanded this technique for reversibly oxidized and reduced substances by using a "catalytic" four-electrode cell (two working electrodes) to oxidize and reduce the same molecule several times before it leaves the working electrode region. This type of system puts even further restraints on the flow stability of the eluent.

Swartzfager (23) employs pulse and differential pulse voltammetric techniques with a carbon paste working electrode to achieve high sensitivity. He estimates a detection limit of approximately 5×10^{-12} grams of p-aminophenol after chromatographing with this detector.

Rabenstein and Saetre (24) use a static mercury working electrode, in which a channel of mercury contacts the solution from underneath. Again, auxiliary and reference electrodes are placed downstream. The volume in contact with the mercury is the effective dead volume, and this is estimated at less than 0.5 μL . Anodic cleaning pulses are applied between runs to improve reproducibility. The detector has been applied mainly to sulfur-containing compounds, and a lower limit of 10^{-9}

grams of glutathione is quoted. Princeton Applied Research introduced a polarographic detector in 1978 (25) which directs the eluent upwards towards a mercury drop which is renewed once each second. The dead volume of this detector is less than 1 μ L, creating much less peak broadening than the earlier polarographic detectors (9,10).

C. Flow Potentiometry with Ion-Selective Electrodes

1. Introduction - Ideal Ion-Selective Electrodes

Potentiometry with ion-selective electrodes is a common method used to determine the activity of specific ions in solution. The advantages of such electrodes include the properties that they are selective to one or a few ions over many others, and that they are responsive to only the free (uncomplexed) form of the ion in solution, not the total concentration of that ion. Unfortunately, however, electrodes can only be made which are selective to certain ions, and most metals cannot be determined directly with an ion-selective electrode. Because of these characteristics, many methods have been developed for the determination of ion concentrations, either by direct potentiometry, or addition of a reagent which will indirectly set the level of a sensed ion through reaction with the analyte (32).

Ideally, the potential of a cell containing an ion-selective electrode and a suitable reference electrode is proportional to the logarithm of the activity of the ion sensed, according to the equation

$$E = E_k + \frac{2.303 RT}{nF} \log_{10} a_i \quad (2)$$

where E is the cell potential in volts, RT/F is called the "Nernst factor," comprised of the gas constant (R), the Faraday (F) and the

absolute temperature (T , degrees Kelvin), n is the charge (signed) of the sensed ion and a_i is the activity of the sensed ion (33). $E^{o'}$ is a constant term according to the measurement made, and

$$E^{o'} = -E_{\text{ref}}^{o'} + E_j + E_i^{o'} \quad (3)$$

where $E_{\text{ref}}^{o'}$ is the standard potential of the reference electrode (against the hydrogen electrode), E_j is the potential due to any liquid junction in the cell, and $E_i^{o'}$ is the pseudo-formal potential of the ion-selective electrode (34). The coefficient of the $\log a_i$ term is $\frac{0.059}{n}$ at 25°C , but in real functioning electrodes, this value can vary by several percent (35).

If this equation were followed exactly, the cell would have an infinite potential in solutions where ion i was absent. For real electrodes, however, in progressively diluted solutions of ion i , the cell potential approaches a limiting value (36), set by processes such as dissolution equilibrium of the electrode material (37) or response to another ion in solution (38). Adherence to Equation (2) is often observed to much lower activities of the sensed ion when metal buffers (39,40,41) or anion buffers (42) are used. These have a high total concentration of the sensed ion, but low free ion activity.

2. Interferences

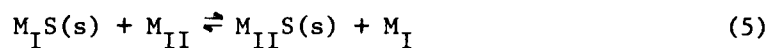
No electrode is truly specific for one ion alone, so the potential of ion-selective electrodes is given by a modified form of Equation (2):

$$E = E^{o'} + \frac{2.303 RT}{nF} \log_{10} \left(a_i + \sum_j K_{ij} (a_j)^m \right) \quad (4)$$

where K_{ij} is a factor ("selectivity coefficient") which describes the

relative influences of ions i and j on the potential of the electrode, a_j is the activity of ion j , and m is the ratio of the charge on ion j to the charge on ion i (43).

For the precipitate-based solid state electrodes (the cupric-ion electrode belongs to this class), the simplest mechanism of interference involves precipitation of a layer of the interfering ion on the surface of the electrode, according to the reaction:



where M_I and M_{II} are the primary and interfering ions, respectively.

If the individual sulfides have solubility products $K_{s(I)}$ and $K_{s(II)}$, then $M_{II} S$ will precipitate on the surface when in solution

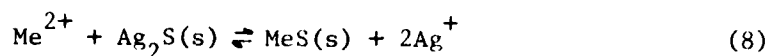
$$\frac{a_{M_{II}}}{a_{M_I}} > \frac{K_{s(II)}}{K_{s(I)}} \quad (6)$$

The potential of the electrode is then determined by the activity of M_{II} in solution (38).

This phenomenon was used by Jensen (44) to produce electrodes for $Cu(II)$, $Pb(II)$, $Cd(II)$, and $Zn(II)$ from a silver wire electrode, made from a silver metal electrode on which Ag_2S was electrolyzed. When the electrode is immersed in water, a small amount of Ag^+ enters solution. If divalent metal ions (Me^{2+}) are added to the solution, the metal sulfide will precipitate when

$$a_{Me^{2+}} > \frac{K_{s(MeS)}}{\left(\frac{1}{4}K_{s(Ag_2S)}\right)^{1/3}} \quad (7)$$

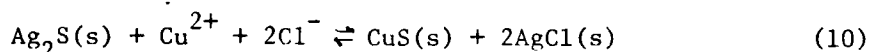
The chemical reaction at the surface is



and the potential of the electrode is

$$E = E_{\text{Ag/Ag}^+}^0 + \frac{RT}{2F} \ln \left(\frac{K_{\text{s(Ag}_2\text{S)}}}{K_{\text{s(MeS)}}} \right) + \frac{RT}{2F} \ln a_{\text{Me}^{2+}} \quad (9)$$

In the case of the cupric-ion electrode, two other mechanisms of interference have been studied. The electrode is made from a mixed silver/copper sulfide (as will be discussed later), and a more complicated variant of the solubility-determined interference occurs when both copper (II) and chloride ions are in solution. The pertinent reaction is:



in which the silver sulfide on the surface is converted to silver chloride and the electrode responds to chloride instead of copper (II). In order to prevent this kind of interference, the following relation must hold (33):

$$a_{\text{Cu}}(a_{\text{Cl}})^2 < \frac{K_{\text{s(Ag}_2\text{S)}}}{\left(K_{\text{s(CuS)}} K_{\text{s(AgCl)}} \right)^2} \quad (11)$$

Interferences caused by precipitation of a second crystalline lattice on the surface of a solid-state electrode can be rectified by the removal of the interfering layer, either physically, by sanding the electrode, or chemically, by immersing the electrode either in a solution which will drive the reaction causing interference far to the

reverse (i.e., a strong solution of M_I in the case of Equation 5, or a solution which will dissolve the interfering layer from the surface (i.e., concentrated ammonia in the case of Equations 10 and 11) (33).

There is also an interference from iron (III), which has been postulated to result from oxidation of the sulfide matrix (45), or oxidation of copper (I) in the electrode to copper (II) (46). This phenomenon does not have any dependence on solubility products of iron and copper sulfides, since it is an oxidation-reduction mechanism, although the electrode component involved is not certain. Iron (III) interference has also been observed with a lead-selective electrode (47), which is constructed of a lead sulfide-silver sulfide coprecipitate, which should arise from an oxidation of the sulfide matrix, since there is no general higher stable oxidation state for lead than Pb(II).

3. Ionic Activities and Concentrations

In the preceding discussion, ionic activities have been used exclusively, since that is the parameter to which an ion-selective electrode responds. However, in many cases, the concentration of an ion in solution is analytically important.

The activity of an ion and its concentration are related by the activity coefficient, γ_i

$$a_i = \gamma_i c_i \quad (12)$$

where c_i is the concentration of ion i in solution. γ_i is a function of the ionic strength of the solution, I

$$I = \frac{1}{2} \sum m_i z_i^2 \quad (13)$$

where m_i and z_i are the molal concentration and unsigned charge of ion i .

One of the most common methods to calculate γ_i for ions in solution is the Davies equation, which states

$$-\log \gamma_{\pm} = Az_+z_- \left(\frac{\sqrt{I}}{1+\sqrt{I}} - 0.2I \right) \quad (14)$$

γ_{\pm} is the mean activity coefficient for ions z_+ and z_- and A is determined by the dielectric constant and temperature of the solvent. For a single ion

$$-\log \gamma_i = Az_i^2 \left(\frac{\sqrt{I}}{1+\sqrt{I}} - 0.2I \right) \quad (15)$$

This equation gives answers accurate to 3% at an ionic strength of 0.1 for 1:1 electrolytes in water (48).

Hence, to a first approximation, ionic activity coefficients will remain constant if the ionic strength of a solution is kept constant with an excess of inert electrolyte. Ionic concentrations will then be directly proportional to activities, and can then be calculated directly from cell potentials, providing that standards are used to calibrate the slope and intercept on a concentration vs cell voltage curve.

4. Liquid Junction Potentials

Another consideration of many potentiometric measurements is the liquid junction potential, a component of $E^{0'}$ in Equation 2. The electrode used as reference must have a stable potential. If this is not possible in the solution to be analyzed, then it is commonly

immersed in a solution which defines its potential, and this solution is connected to the analyte solution through an ion-conducting bridge.

Commonly this bridge is constructed so that the flow of ions between the two solutions is restricted, such as a porous frit, ground-glass fitting, or agar (salt-saturated) filled tube.

The macroscopic boundary between the ion-conducting bridge and the solution it contacts is distinct, however, the microscopic boundary is not distinct. Ions at this junction diffuse outward from their original solution, i.e., at the junction between a KCl salt bridge and a solution containing NaNO_3 , K^+ and Cl^- ions diffuse into the solution and Na^+ and NO_3^- ions diffuse into the salt bridge. Ideally, each kind of ion has a unique mobility in solution, but opposite charges cannot be separated macroscopically. Ions of opposite charge must then diffuse at an average rate to maintain electro-neutrality in any volume.

This situation establishes a potential difference across the junction, comprised of a continuous concentration gradient of ions across the diffusion volume (49). The potential difference is termed the liquid junction potential. It is a function of activities a_i and transference numbers t_i of ionic species i in the transition layers between the two end (homogeneous) solutions (50):

$$E_j = - \frac{RT}{F} \int_{c_i'}^{c_i''} \sum \frac{t_i}{z_i} d \ln a_i \quad (16)$$

where c_i' and c_i'' are the two end solutions.

If one assumes that the liquid junction is comprised of a continuous gradient between the two solutions, Equation 15 can be approximated

by the method of Henderson (50). Two further assumptions are involved: (1) the activity of each ionic species is equal to the concentration of that species, and (2) the mobility of each ion, u_i , is constant throughout the junction. The transference number, t_i , is given by

$$t_i = \frac{c_i u_i}{\alpha \sum c_i'' u_i + (1-\alpha) \sum c_i' u_i} \quad (17)$$

where c_i is the instantaneous concentration of ion i , and α is the volume fraction (mixing fraction) of solution c_i'' in the volume involved. Substitution of Equation 17 into Equation 16 and integration over the total volume of the junction produces

$$E_j = \frac{RT}{F} \frac{\sum (u_i/z_i)(c_i'' - c_i')}{\sum u_i(c_i'' - c_i')} \ln \frac{\sum c_i' u_i}{\sum c_i'' u_i} \quad (18)$$

If ionic mobilities in solution c_i' and c_i'' are assumed to be equal to the ionic mobilities at infinite dilution (λ^0/F , where λ^0 is the limiting ionic conductivity), then

$$E_j = \frac{RT}{F} \frac{(U_{c_i'} - V_{c_i'}) - (U_{c_i''} - V_{c_i''})}{(U_{c_i'} + V_{c_i'}) - (U_{c_i''} + V_{c_i''})} \ln \frac{U_{c_i'} + V_{c_i'}}{U_{c_i''} + V_{c_i''}} \quad (19)$$

where $U = \sum c_+ \lambda_+^0$, $V = \sum c_- \lambda_-^0$, $U' = \sum c_+ \lambda_+^0 |z_+|$, $V' = \sum c_- \lambda_-^0 |z_-|$, and their subscripts in Equation 19 indicate the solutions involved.

If solution c_i'' is saturated KCl at 25°C (as in the case of the saturated calomel electrode), Equation 19 becomes

$$E_j = 0.05916 \frac{U_{c_i'} - V_{c_i'} + 11.6}{U_{c_i'} + V_{c_i'} - 623} \log_{10} \frac{U_{c_i'} + V_{c_i'}}{623} \quad (20)$$

Equation 20 can be solved for 0.1 M KNO_3 vs saturated KCl to simulate the liquid junction potential between a saturated calomel electrode and an 0.1 M KNO_3 solution. In this case, $\lambda_{\text{K}^+}^0 = 73.5$ and $\lambda_{\text{NO}_3^-}^0 = 71.5$ at 25°C (51), and $E_j = 0.0019$ volts.

The Henderson equation gives only a semi-quantitative result for the liquid junction potential, since only homoionic junctions (ions in both solutions are the same) can be calculated exactly, but the values are close to experimental results. The potential across a junction which is not homoionic depends on the method of forming the junction and the resulting interdiffusion characteristics of the two solutions (52). However, the variations of experimental vs calculated potential is very small, within a few millivolts.

5. Streaming Potentials

One aspect of potentiometry in flowing solutions which is not present in static measurements is the streaming potential, a potential difference which is established between two points in a capillary through which an ionic liquid is flowing.

The basis of the streaming potential lies in the fact that ions in solution will adsorb onto the interface of the solution and a solid in contact with it. Ions of a specific charge will preferably adsorb the charge depending on the nature of the surface. A layer of oppositely charged ions will then form just outward of these adsorbed ions, since charges in solution cannot be macroscopically separated. A potential difference is thus established between the surface and the outer ionic layer (the outer layer is actually diffuse, but can be treated as having sharp boundaries), called the electrokinetic, or zeta potential, ζ (53).

When a liquid flows past a surface (as in a capillary), this double layer is disrupted, the outer (counterion) layer being sheared from the surface layer. This produces a current flow in the capillary, proportional to the pressure applied to one end. Helmholtz originally derived the theory for this effect, assuming a rigid double layer, and his derivation was later modified slightly by Smoluchowski. Bikerman later derived equations on the basis of a diffuse double layer.

The streaming potential is derived by the following treatment, assuming a rigid double layer (54): The velocity of a liquid flowing in a capillary varies with the distance from the center of the capillary, x , according to the relation

$$v_x = \frac{P(r^2 - x^2)}{4\eta l} \quad (21)$$

where r is the radius of the capillary, η is the viscosity of the liquid, and l is the length of the capillary. Assuming the outer (moving) part of the double layer to be a distance d from the surface and further that d is small compared to the radius, then the velocity of the moving double layer is

$$v_d = \frac{Prd}{2\eta l} \quad (22)$$

The current produced by the slippage of one side of the double layer against the other is

$$I = 2\pi r v_d \sigma \quad (23)$$

since $2\pi r v_d$ is the area of the layer which moves past a point in unit time, and σ is the charge per unit area. Substituting Equation 22 into Equation 23,

$$I = \frac{P\pi r^2 \sigma d}{\eta l} \quad (24)$$

If Λ is the specific conductance of the salt, the electrical resistance across the tube is

$$R = \frac{1}{\pi r^2 \Lambda} \quad (25)$$

and the streaming potential is given by

$$E_s = IR = \frac{P\sigma d}{\eta \Lambda} \quad (26)$$

According to electrostatics, ζ and σ are related through the relation

$$\zeta = \frac{4\pi\sigma d}{D} \quad (27)$$

where D is the dielectric constant of the liquid, and

$$E_s = \frac{\zeta P D}{4\pi\eta\Lambda} \quad (28)$$

This equation is true regardless of the size of the capillary, since the pressure through the capillary is involved, and the linear flow rate (at any particular distance from the center) is directly proportional to pressure, although the volume flow rate is dependent on both pressure and capillary radius. Thus, for a capillary of radius r ,

$$P = \frac{8F\eta l}{\pi r^4} \quad (29)$$

where F is the volume flow rate of solution, and

$$E_s = \frac{2FD\zeta l}{\pi r^2 \Lambda} \quad (30)$$

Van den Winkel, Mertens, and Massart (55) have demonstrated streaming potentials in ion-selective electrode flow systems, using a fluoride-selective electrode vs a saturated calomel electrode (with flowing liquid-liquid junction) or a chloride-selective electrode (without flowing liquid-liquid junction). They obtained streaming potentials in good agreement with theory, except at very low conductivities ($\lambda \leq 10^{-6} \text{ ohm}^{-1} \text{ cm}^{-1}$), where values of E_s were lower than expected. Even so, with a $5 \times 10^{-5} \text{ M NaCl}$ solution in water, 0.66 mL/min flow rate and a 12 cm long x 0.17 mm diameter capillary, they obtained a streaming potential of 1.35 volt. The phenomenon can therefore be very important.

In our system, however, streaming potentials are negligible. For typical conditions, $F = 0.017 \text{ mL/sec}$, $D = 7.16 \times 10^{-12} \text{ coul}^2/\text{Joule-cm}$, $l = 10 \text{ cm}$, $\zeta = 0.1 \text{ volt}$ (ζ is usually between 0.05 and 0.2 volt (56)), $r = 0.08 \text{ cm}$, and $\lambda = 120.4 \text{ ohm}^{-1} \text{ cm}^{-1}$ (0.1 M KNO_3). E_s can then be calculated to be 5.0×10^{-11} volts. This is insignificant compared to the level of signals important in potentiometry (an error of 0.1 mV corresponds to an error of 0.7% in the reading of the activity of a divalent cation).

Since flow is also restricted across the measuring electrode in our system, a streaming potential can also be calculated for this distance (for electrode geometry, vide infra). As worst-case conditions, assuming a circular cross-section of radius 0.006 cm and length 0.25 cm, $E_s = 4.0 \times 10^{-9}$ volts. Since the flow channel as constructed here actually has a much wider cross-sectional area, E_s is even lower, again insignificant compared to the potentials we measure.

6. Transient Response of Ion-Selective Electrodes

The rate of response of an ion-selective electrode is extremely important when it is to be used in a dynamic situation, such as following the concentration of an ion involved in a reaction (56), or measuring an ion's concentration at a specific point in a flowing stream (57). The time required for an ion-selective electrode to reach a steady-state potential when the activity of the sensed ion is changed can vary from less than one second (58) to several hours (59). This "response time," as it is often called (some authors use the term to denote the time required to attain a certain percentage of the total potential change, i.e., 95%, since the electrode potential approaches the steady-state value asymptotically (60)) depends on the mechanism of electrode response, and thus the type of electrode (59,61), the activity of the sensed ion, both initial and final (61,62), and even the method of measurement of response time (57).

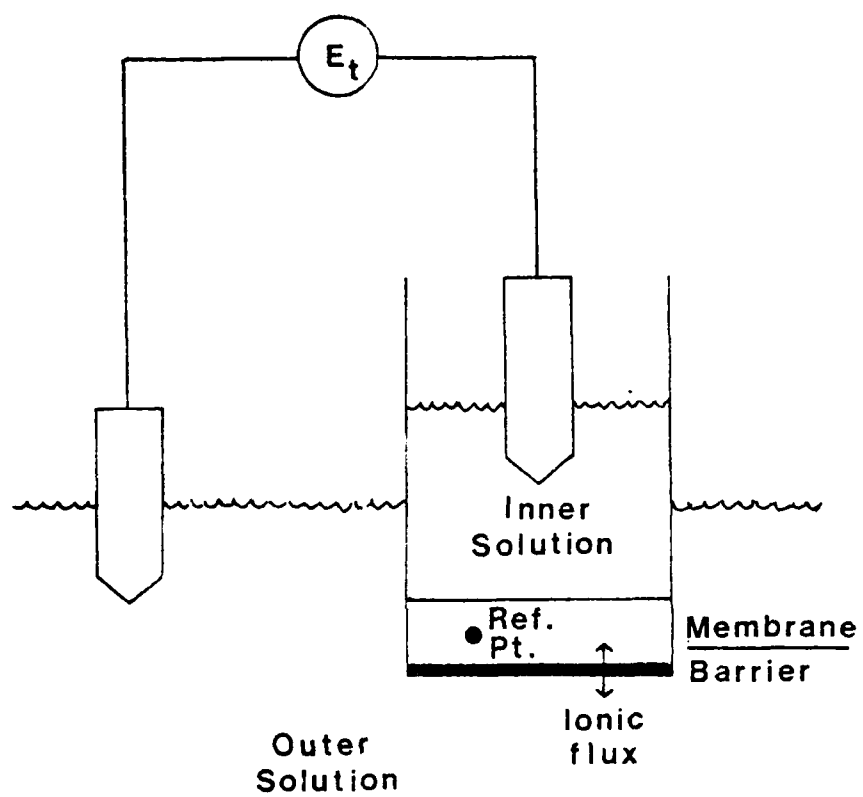
Two main theoretical models have been proposed for the transient response of an ion-selective electrode. They were reviewed by Skatkey (59). The first, initially proposed by Rechnitz and Hamka (63), represents the electrode as a homogeneous membrane with a barrier to ionic transport at the membrane-solution interface (Figure 2). When the concentration of the relevant ions in the membrane and "outer" solution are not identical, an ionic flux exists across the barrier in directions both into and out of the solution. The magnitude of this flux, along with the ionic concentrations in the "outer" solution, determines the measured potential of the cell.

Figure 2. Barrier Model of Ion-selective Electrode Dynamic Response (59).

E_t . Measured potential as a function of time.

Reference point. Imaginary point within the electrode membrane at which the concentration of sensed ion is considered in the model.

A, B. Ideal reference electrodes.



Next, a thin layer behind the barrier inside the membrane is assumed to have a uniform concentration. Therefore the concentration at a reference point in this layer can be used to represent the whole layer. When the ionic concentration in the "outer" solution is changed, the ionic fluxes across the barrier change, and the thin layer (including the reference point) behaves as a capacitor, accumulating charge until the ionic fluxes again reach a steady-state. This leads to a potential-time curve of the form

$$E_t = E_1 + (E_2 - E_1)(1 - e^{-Kt}) \quad (31)$$

where E_t is the potential at time t , E_1 and E_2 are the initial and final potentials, respectively, and K is an empirical rate constant, from the "charging" of the "capacitor."

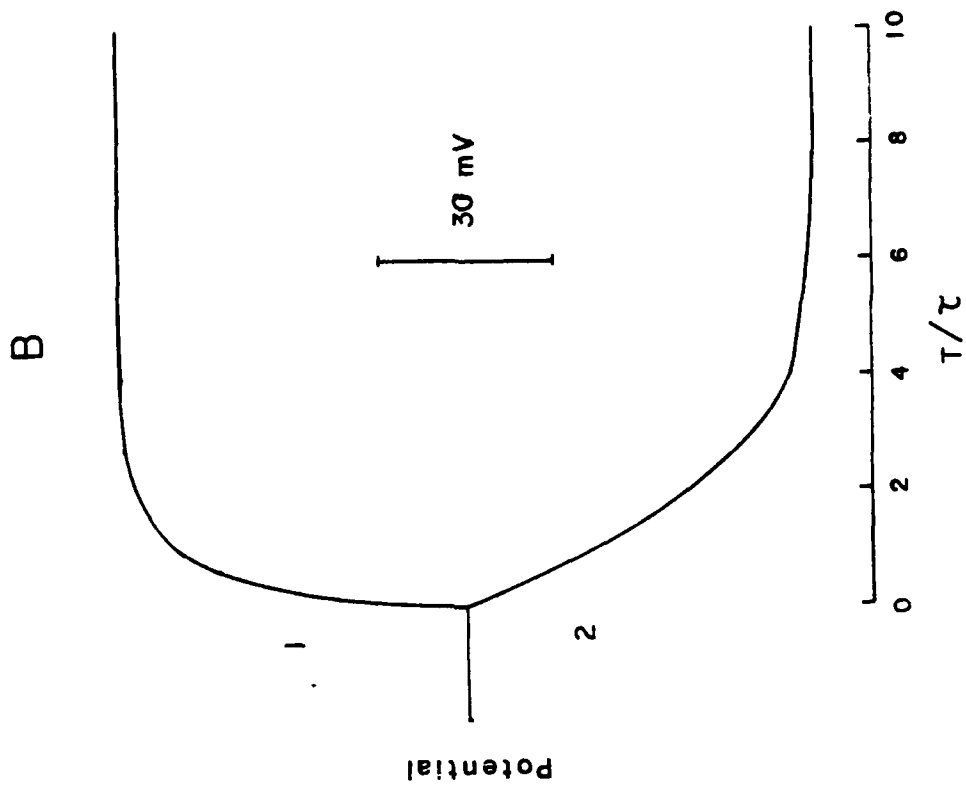
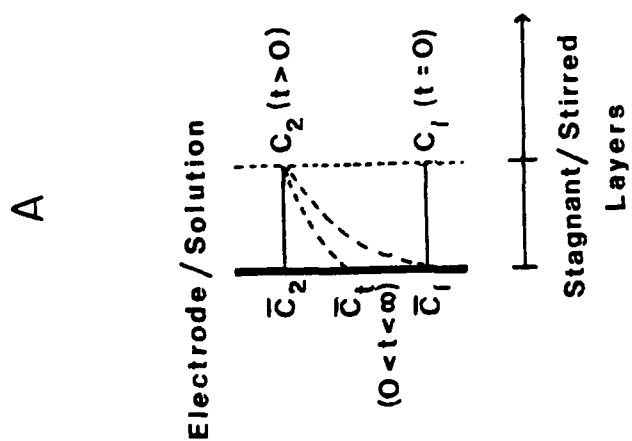
The second model assumes that the electrode responds rapidly to the activity of the sensed ion at the surface, but there is a thin unstirred layer of solution extending from the surface, even though the bulk of the solution may be stirred (Figure 3). Ions in this unstirred layer diffuse according to Fick's first law, and the ionic concentration at the surface of the electrode as a function of time is given by

$$\bar{C}_t = C_1 + (C_2 - C_1)[1 - \exp(-2Dt/L^2)] \quad (32)$$

where \bar{C}_t is the surface concentration at time t , C_1 and C_2 are the initial and final concentrations of the bulk solution, respectively, D is the diffusion coefficient of the ion and L is the thickness of the stagnant layer. The electrode potential as a function of time is then given by the equation

Figure 3. Unstirred Diffusion Layer Model of Ion-selective Electrode Dynamic Response (59,61).

- A. Schematic representation of concentration gradient in unstirred layer.
- C_1 . Initial concentration of sensed ion in solution.
 - C_2 . Concentration of sensed ion in solution after instantaneous change.
 - \bar{C}_1 . Initial concentration of sensed ion at electrode surface.
 - \bar{C}_t . Concentration of sensed ion at electrode surface at time t .
 - \bar{C}_2 . Final (equilibrium) concentration of sensed ion at electrode surface.
- B. Theoretical potential curves as a function of time, calculated with Equation 32, using first-order diffusion coefficient τ ($= -2D/L^2$) and an electrode response of 60 mV/decade cation concentration.
1. Tenfold instantaneous increase in bulk solution sensed cation concentration.
 2. Tenfold instantaneous decrease in bulk solution sensed cation concentration.



$$E_t = E_1 + \frac{RT}{nF} \ln \left\{ 1 + \frac{C_2 - C_1}{C_1} [1 - \exp(-2Dt/L^2)] \right\} \quad (33)$$

This relation explains the phenomenon that the potential of an ion-selective electrode reaches a final (within experimental precision) value more rapidly when the concentration of sensed ion increases than when it decreases. The ionic concentration profile with time has an identical (although inverse) shape whether the concentration increases or decreases, depending only on D and L . However, the logarithmic concentration response characteristic of potentiometry compresses the concentration scale in the increasing direction and expands it in the decreasing direction (61). This phenomenon has been widely found in the literature, but rarely explained (59,61).

Skatkey concluded in his article (59) that fast transients could be approximated with a single exponential or hyperbolic equation, but slow transients required a sum of exponential or hyperbolic terms, demonstrating that more than one process is involved in the transient response mechanism, or that the rate limiting process is not strictly first order.

Lindner et al (64) attempted to explain the transient response of ion-selective electrodes in terms of a "multielectrode" model (Figure 4). Here, the surface of the electrode is divided into a large number of "point electrodes," whose potentials are added in parallel, with all R_n equal. As the bulk activity of the sensed ion changes, the surface concentration does not necessarily uniformly change in time, and "mixed" potentials result. The potential at time t is then represented by

Figure 4. Schematic Diagram of Multielectrode Model of Ion-selective Electrode Response.

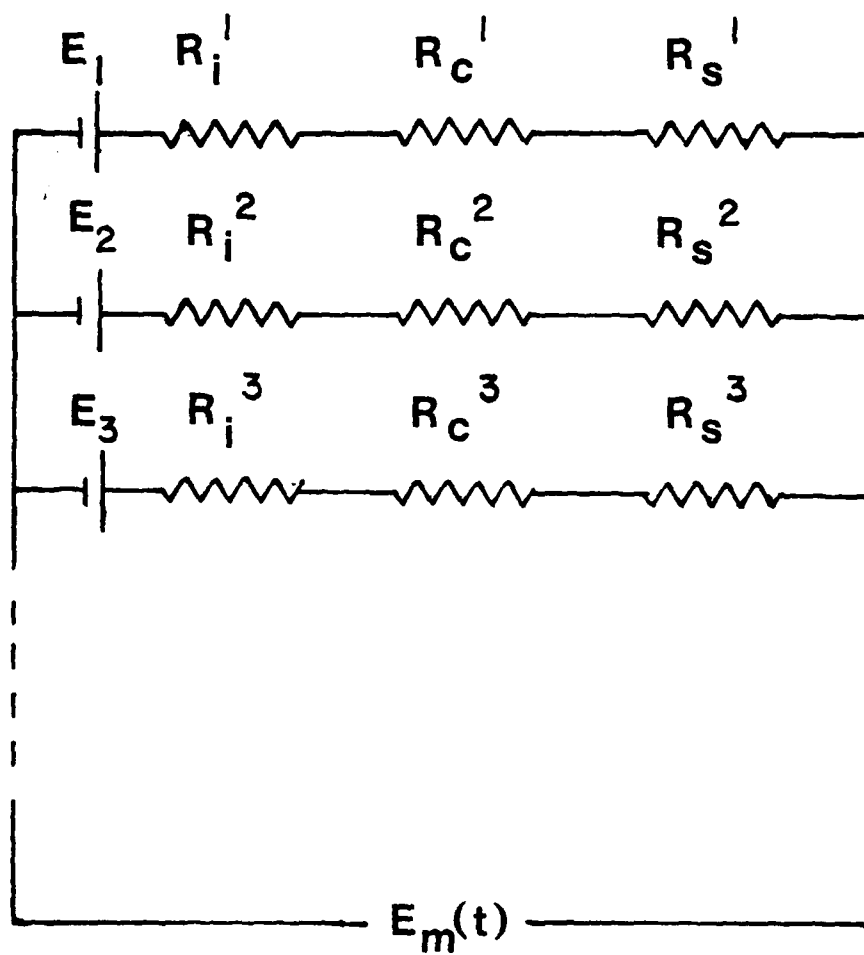
$E_m(t)$. "Mixed electrode" potential at time t .

E_j . Potential of "point" electrode j (defined in text).

R_{ij} . Internal resistance of "point" electrode j .

R_{cj} . Charge transfer resistance of "point" electrode j .

R_{sj} . Resistance of solution around "point" electrode j .



$$E_m(t) = \frac{\sum_{i=1}^n F_i E_i^i}{\sum_{i=1}^n F_i} \quad (34)$$

or

$$-\log a = \frac{\sum_{i=1}^n F_i (-\log a_i)}{\sum_{i=1}^n F_i} \quad (35)$$

where F_i is the area of the point electrode i , E_i^i is the potential of point electrode i , a is the average measured activity of the ion, and a_i is the activity of the ion in contact with point electrode i . No kinetic curves were shown to validate this model, but an iodide-selective electrode was partitioned on its surface and the various sections covered with different iodide solutions. Each separate section was connected to a common reference electrode through a salt bridge. The authors present results of seven different combinations of iodide concentrations on the surface of the electrode as $-(\log a)$ calculated from Equation 35 and the electrode potential obtained. They state that the equation gives a good approximation of the multielectrode potentials. However, if the average activity of iodide on the electrode is computed according to the equation

$$a = \frac{\sum_{i=1}^n F_i a_i}{\sum_{i=1}^n F_i} \quad (36)$$

the activity calculated is closer to the experimentally determined activity in five of the seven cases, casting great doubts on the validity of this particular model.

These theories have been used in the references noted only to describe the electrode potential change after a step change of the bulk solution concentration of the primary sensed ion. Morf (65) has developed an analysis of electrode response for a concentration change of an interfering ion (or any second ion the electrode will respond to). He assumes an inhomogeneous membrane, in which ionic diffusion through the interior is finite (such as in the "energy barrier" model), but there is a surface layer with different properties from the interior. Ionic mobilities in the interior are assumed to be much slower than at the surface. In this model, differential ionic selectivities (K_{ij}) at the surface layer and in the bulk are not necessarily equal. This representation of an electrode allows not only for monotonic potential shifts, but also for overshooting, where the electrode potential rises (or falls) upon a change in the concentration of an ion and settles back to a potential closer to the original electrode potential. The phenomenon of potential overshooting caused by an interferant cannot be explained using a homogeneous membrane model.

Morf shows that when the membrane surface is selective for ion I^+ , while the interior is selective for J^+ , overshooting can occur upon a change in the solution concentration of I^+ . From the original potential, determined by the concentration of I^+ and J^+ in solution, introduction (or removal) of I^+ causes a rapid potential shift determined primarily by I^+ followed by a slower return to a potential again

determined by the concentrations of I^+ , J^+ , and the bulk selectivity coefficient K_{ij} .

Morf uses as examples data previously published where I and J are of the same charge and one ion remains unvariant. However, this model could be expanded to the situation where I and J are of opposite charge, and where the concentrations of both ions change. Transient response of a cupric ion-selective electrode to halide ions has been noted by Midgley (66) (F^- , Cl^-) in the presence of Cu(II), but no explanation was given. Similar transient response to halide ions (F^- , Cl^- , Br^- , I^-) has been found in this work (vide infra) with a constant CuEDTA background.

Response times of ion-selective electrodes have been measured by many methods, and the results obtained can depend on the method used. For example, ion-selective and reference electrodes can be immersed in a vessel filled with stirred solution, and a concentrated solution of the sensed ion or inert electrolyte added. This will respectively increase or decrease the sensed ion's activity (61). Stirring rate has a profound influence on rate of response in this case.

Another procedure used is to remove the ion-selective electrode from a solution of activity a (sensed ion) and place it in a solution of activity b. The two solutions are often unstirred. Very long response times have been observed using this technique (59,67). Parthasarathy et al (67) postulated that the long response times were partially caused by electrostatic charge buildup on the electrode during the transfer process.

Another common method of measuring electrode transients involves spraying a high velocity stream directly at the electrode, at flow rates up to 1000 mL/min (57,60,68). Response times for precipitate-based electrodes measured by this method are commonly below one second. Mertens et al (57) have shown that these times are not necessarily representative of those found under moderate flow conditions, under 10 mL/min, where the linear velocity past the electrode surface was much less. Under these conditions, electrode response times were an order of magnitude or more longer.

All of these experiments point to a marked dependence of the electrode response time on the rate of movement of solution over the surface of the electrode, whether by stirring or forced flow. This points to a stagnant solution layer on the surface of the electrode playing an important part in the transient response, since agitation of the bulk solution will disrupt this stagnant layer and allow the surface concentration of ions to approach the bulk concentration more rapidly.

There are thus several complicating factors in the mechanism of dynamic response of ion-selective electrodes. Many experiments point to solution diffusion-controlled processes being strongly involved, as no doubt they are. But the electrodes themselves must take an active role in their transient response. This has to be assumed to account for the fact that not all electrodes of the same geometry have identical transient response characteristics. Another unsolved problem concerns the fact that response times for concentration jumps involving different initial and final concentration pairs (i.e., $10^{-3} \text{ M} \rightarrow 10^{-2} \text{ M}$

and $10^{-8} \text{ M} \rightarrow 10^{-7} \text{ M}$) can be different by orders of magnitude for the same electrode and sensed ion (59). No model has yet been proposed which can take into effect both the "solution-controlled" and "electrode-controlled" phenomena. Such a model could possibly take into account such things as the semiconductor nature of many electrodes and interfacial phenomena such as chemisorption from solutions, neither phenomenon now being considered in these models.

7. Cupric Ion-Selective Electrode Studies

a. Construction

The cupric ion-selective electrode is one of the most-studied ion-selective electrodes. Although some early electrodes were made using liquid ion-exchangers, such as S-alkyl thioglycolic acids dissolved in water-immiscible solvents (69), the vast majority of cupric ion-selective electrodes are solid-state. The solid-state electrodes are usually based on copper sulfide or a copper-sulfide-silver-sulfide coprecipitate; however, two manufacturers produce electrodes based on copper selenide (Tacussel and Radiometer). By far, most of the literature concerns the sulfide-based electrodes.

Many methods have been used to prepare the sulfide-based electrodes. Copper sulfide precipitates have been imbedded in silicone rubber (70) or epoxy resin (71), or pressed into a ceramic membrane (72). Ceramic membranes of copper sulfide have been described as difficult to prepare; when an internal reference solution was used, the membranes leaked, and they crumbled readily (73). The valence state of copper ions in these electrodes apparently can either be +1, +2, or a mixture of both states.

The majority of the sulfide-based electrodes contain both silver and copper sulfides, usually coprecipitated from homogeneous solution.

One major approach using the mixed copper/silver sulfide involves manually affixing a small amount of the granular precipitate onto the end of a hydrophobized graphite rod. This type of construction has been named the "Selectrode" by its inventors (74). Electrical contact is made through the graphite rod. Electrodes made in this way require a pretreatment procedure of soaking the electroactive surface in KCN or EDTA solutions before initial use. Otherwise, the sensitivity and limit of detection are poor.

Cupric ion-selective electrodes have also been prepared by depositing copper sulfide onto a silver sulfide surface. Anfalt and Jagner (75) first precipitated silver sulfide on the surface of a silver rod, and added $\text{Cu}(\text{NO}_3)_2$ to the solution to coat the surface with copper sulfide. Van de Leest (76) vapor deposited copper atoms onto the surface of a silver sulfide pellet, and then heated the pellet in an atmosphere saturated with sulfur vapor. Both of these techniques have been demonstrated, but nothing further on electrodes prepared in this manner has appeared in the literature.

The Orion commercial electrode and many laboratory-prepared electrodes are constructed from a pressed disk of coprecipitated copper/silver sulfide. Electrical contact to the electrode can be made either through a conventional internal reference electrode, directly to the electrode surface through a silver or copper powder, or via silver or gold-containing epoxy (62,77).

Heyne et al (73,78) carried out a thorough study of the preparation of pressed silver/copper sulfide electrodes. The solid was prepared by precipitation by addition of a copper nitrate/silver nitrate solution to an excess of sodium sulfide, hydrogen sulfide, and by precipitation from homogeneous solution with thioacetamide, varying the copper:silver ratio and the metal:sulfide ratio, and varying the absolute ionic strengths of the solutions to be mixed. They analyzed the resulting precipitates by X-ray diffraction and concluded that the electrodes with the most mechanical strength and best electrochemical response (lowest limit of detection, Nernstian slope, shortest response time) contained the ternary compounds jalpaite ($\text{Ag}_{1.5}\text{Cu}_{0.5}\text{S}$) and mckinstryite ($\text{Ag}_{1.2}\text{Cu}_{0.8}\text{S}$) and very little Ag_2S , CuS or Cu_2S . They presented a detailed procedure for preparation of these electrodes, and emphasized that the best results occurred when the precipitation step was performed under nitrogen instead of air. This experimental detail was not mentioned in studies by other researchers, but should serve to help eliminate the formation of hydroxides and sulfates in the electrodes. Copper (II) sulfate has been found in preparations of electrode material which were exposed to humid air for long periods (> 2 weeks).

b. Behavior in Cu(II) solutions

The sensitivity and detection limit of cupric ion-selective electrodes depends on the method of calibration used by the researcher. If dilute Cu(II) solutions in water are used as standards, the electrode is not responsive below approximately 10^{-9} M Cu(II) (36). This limit of detection cannot be explained on the basis of the solubility of CuS or

Cu_2S in the electrode material, since dissolution should only play a part in solutions below 10^{-13} M (78). However, the electrode material has been shown to adsorb Cu(II) ions from submicromolar solutions onto its surface (36) and in other cases corrode, raising the Cu(II) concentration in solutions containing complexing ligands (79).

The behavior of the electrode in Cu(II) buffer solutions is quite different. These buffer solutions contain a high total concentration of Cu(II) ($\sim 10^{-2}\text{ M}$), most of which is complexed by a ligand, e.g., EDTA, NTA (80), Trien, or Tetren (79). By varying the solution pH and the Cu(II) :ligand ratio, the free Cu(II) activity can be fixed at very low levels. Electrodes will respond with Nernstian slopes to levels as low as 10^{-18} M free Cu(II) in buffer solutions of Trien or Tetren (81). In these solutions, dissolution of the electrode would make almost no change in the free Cu(II) concentration, since the total Cu(II) concentration is large ($> 10^9$) compared to that which could arise from electrode dissolution.

There is one other major difference between the electrode's response in Cu(II) buffered and unbuffered solutions. In unbuffered solutions, the electrode requires at least one hour to achieve steady-state when immersed in 10^{-8} M Cu(II) (36). In buffered solutions, stable potentials were obtained within five minutes at free Cu(II) concentrations below 10^{-9} M (81).

One caution must be applied in the use of Cu(II) buffers for calibration of cupric ion-selective electrodes. Several groups have found that the potential of the electrode in solutions with an excess of EDTA or NTA over Cu(II) is higher than that calculated from

equilibrium formation constants of the complexes (79,82,83). It has been postulated that the reason for this may be the negative charge of the CuEDTA and CuNTA complexes, since ligands which form positively charged complexes with Cu(II) (i.e., Trien and Tetren) do not show this behavior (79). Trien and Tetren have thus been proposed as the basis for Cu(II) calibration buffers (79). Jyo et al (84) have proposed a "ligand interference preventative buffer" to mask the effects of such complexing agents. The buffer consists of a high concentration of Trien buffered with nitric acid so that it preferentially complexes Cu(II) to establish the electrode potential. They show almost no (< 1 mV) influence of 10^{-3} M EDTA or NTA on the potential of an electrode in this buffer with 10^{-4} M Cu(II) added.

c. Behavior in solutions of Cu(II)-complexing ligands

In addition to selectivity for metal ions other than Cu(II), as predicted from Equation 6, the electrode responds to a number of ions. First, it will respond to Cu(II)-complexing ions without any Cu(II) (other than that which arises from electrode dissolution) present in solution. This is different from the case stated above, where there was a small amount of free Cu(II) present from dissociation of Cu(II)-ligand complexes.

Several authors have studied the electrode response to complexing agents as a function of solution pH (79,83,85,86), or concentration of the ligand (86). The potentials may or may not be identical to potentials with Cu(II) present, depending on the ligand used (79,83). The fact that EDTA and NTA give identical responses whether or not Cu(II) is present in solution suggests that the electrode potential depends

only on the free ligand concentration in these cases. This has been used to explain the anomalous behavior of the electrode in CuEDTA and CuNTA buffers, and titrations of Cu(II) with EDTA, where potentials past the endpoint (excess EDTA) do not agree with theory (79).

The response of the electrode to Cu(II)-complexing ligands was the basis for a study of titrations of metals other than Cu(II) with these ligands (85). One observation Olsen et al made was that potentials were unsteady or required long times to reach a steady-state value at low pH. This effect disappeared in high pH solutions (absolute pH ranges were not specified).

d. Behavior in solutions of other interfering ions

An interference of Fe(III) on the potential of the cupric ion-selective electrode has been previously mentioned. As stated, this does not appear to come from a solubility mechanism, but oxidation of one of the components of the electrode by Fe(III) (45,46). The application of a cupric ion-selective electrode for the determination of Fe(III) using this interference has been discussed by Fung and Fung (87). The analytical slope was 25 mV/decade [Fe(III)], whereas the theoretical Nernstian response for a trivalent cation (Equation 7) is 19.7 mV/decade.

Halide ions also have a profound interference on a cupric ion-selective electrode, and the mechanism of this interference is not well understood. As discussed earlier, a film of silver chloride can form on the surface of an electrode at high Cu(II) and chloride concentrations (Equations 10 and 11) which will make the electrode nonresponsive to Cu(II) (33). Crombie, Moody, and Thomas (88) reexamined this

phenomenon for the points at which Cu(II) and chloride ions affect the potential equally and found that these points follow the more complicated equation:

$$\log [\text{Cu}^{2+}] - 2.8 \log [\text{Cl}^{-}] = 2.7 \quad (37)$$

They suggested that chloro-complexes of Cu(II) might be implicated in this phenomenon, but gave no firm explanation. They also noted that the response of a fouled electrode is not Nernstian with respect to chloride, which they attribute to the formation of an imperfect layer of silver chloride on the surface.

There are other phenomena which occur at high levels of chloride and low levels of Cu(II), well below that needed to form the silver chloride layer on the surface of the electrode. High levels of chloride increase the slope of the response to Cu(II) (89,90). Slopes up to 50 mV/decade [Cu(II)] were found in solutions with high ($\geq 0.5 \text{ M}$) levels of NaCl or KCl as background electrolyte. This effect was not found when solutions of CuCl_2 were tested in varying concentrations of KNO_3 as background electrolyte (90), so the authors concluded that the excess high chloride concentration was the cause, not any ionic strength phenomenon, but they offered no explanation for the results.

Midgley (66) studied the interference of chloride on the cupric ion-selective electrode by injecting a small amount of saturated KCl into solutions of CuSO_4 at various concentrations. He found shifts in potential greater than those which could be explained by ionic strength changes caused by adding the KCl or complex formation (i.e., CuCl^+). He also discounted the possibility of reduction of Cu(II) to Cu(I) due to the high redox potential of the solutions involved. He

found similar, although smaller, effects when NaF was injected into CuSO_4 solutions. At low Cu(II) concentrations, injections of KCl or NaF gave a transient shift to lower potentials (apparent lower concentrations of Cu(II)) and in most cases a drift to higher potentials. It was not stated whether the electrode assumed the initial potential after the drift subsided. No explanation was given for this response.

e. Application in the determination of other metals

The cupric ion-selective electrode is obviously suitable for the titration of Cu(II) with a ligand which forms a strong complex, such as EDTA or Trien. It has also been used for the titration of other metals which form EDTA complexes. Other than the case mentioned previously (85), the procedure involves addition of a small amount of CuEDTA to a solution of the metal to be titrated. Some of the EDTA will complex with the analyte, freeing Cu(II). As EDTA is added to the solution during the titration, the levels of both the free analyte metal and free Cu(II) will decrease. When the total EDTA concentration exceeds the total concentration of the analyte metal and Cu(II), there will be a sharp decrease in the free Cu(II) level, similar to the endpoint of a titration of Cu(II) alone with EDTA. The magnitude of this endpoint break depends on the conditional stability constants of both the analyte metal-EDTA complex and the CuEDTA complex (92). Conditions (pH, buffer used, ligand used) can be varied to provide sensitivity or selectivity as needed. Both ions which form a weaker metal-ligand complex than Cu(II) (46,91,92,93,94) and a stronger metal-ligand complex (95,96) can be determined in this way. Calcium, which forms

relatively very weak complexes with EDTA, can be determined in this way, when the solution is adjusted to pH 9 (92).

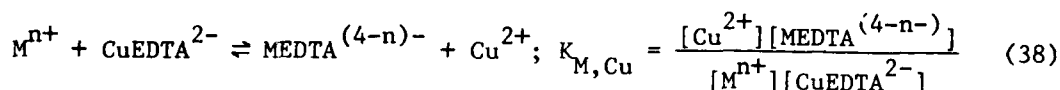
Van der Meer et al (97,98) have discussed the theory of the more general case, where Cu(II) and a second metal are both titrated with a ligand, including back-titrations of excess ligand in a ligand-metal ion mixture with Cu(II). In their study, they included the effect of non-zero selectivity coefficients for metals other than Cu(II) with the cupric ion-selective electrode. It was found that metals which form weaker complexes with the titrant ligand than Cu(II) could be sometimes determined separately, with a second endpoint for the total metal ion (including Cu(II)) concentration. Heijne et al (46) could find only the combined metal ion endpoint, however, for mixtures of Cu(II) with metals which formed stronger complexes with the titrant ligand.

The cupric ion-selective electrode is thus seen to be very useful in analysis for metals other than Cu(II), when these metals can be made to influence free Cu(II) concentration in solution in some way.

Finally, van der Linden and Oostervink (99) have designed a flow-through cupric-ion electrode similar to the one constructed in this work, where the flowing stream passes over a face of the electrode. They show a detailed picture of the electrode, but give few dimensional details. Also, they state that the electrode reaches 90% of steady-state response for Cu(II) injection in 6 seconds, but give no data on experimental conditions, so this cannot be used for comparison with other flow-through electrodes.

II. Equilibrium Theory of the Detector

The basic rationale of the detector is given in Chapter I.A., in which it is stated that the response to a metal ion M^{n+} is governed in the simplest case by the chemical reaction



where $K_{M,Cu}$ is the equilibrium constant for the reaction. In this elementary case, the concentration of Cu^{2+} at the sensor depends only on the initial amounts of M^{n+} and $CuEDTA^{2-}$ and the absolute strengths of the two complexes involved. This, however, only presents a part of the problem.

This section will treat the chemical system involved in the detector in detail, taking into consideration nonideal situations, such as competing reactions and nonstoichiometry of the $CuEDTA$ used as a reactant. Using reasonable simplifying assumptions, we will derive a general master equation relating the analyte (M^{n+}) to the sensed product (Cu^{2+}), so that it can be applied directly to similar soluble chemical systems.

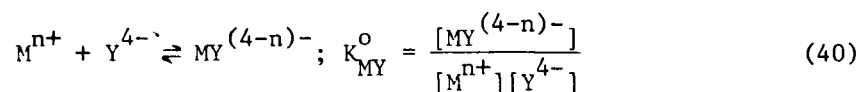
The equation for the formation of a 1:1 M-X complex with the corresponding formation constant is



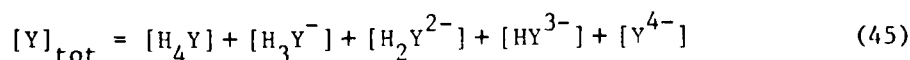
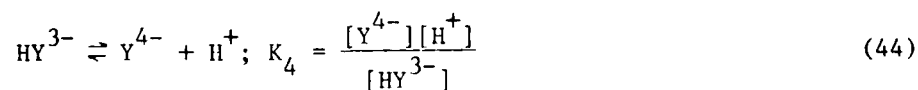
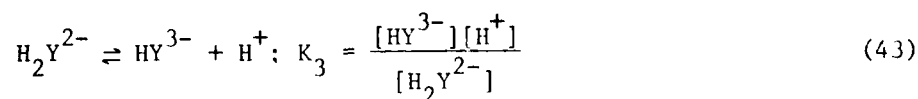
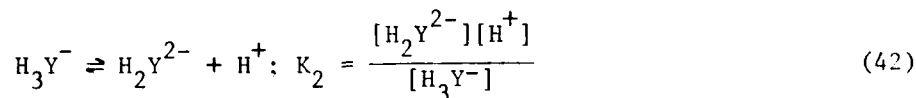
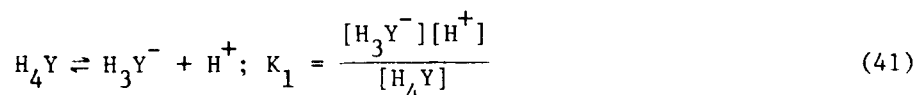
This relation holds true for all cases where the three species are the only ones present in solution.

Ethylenediaminetetraacetic acid (EDTA) is a tetraprotic acid. The fully ionized form (EDTA^{4-} or Y^{4-}) is capable of coordinating metal ions at six different points, forming a very stable 1:1 complex $\text{MY}^{(4-n)-}$. This complex strongly predominates over any protonated ($\text{MHY}^{(3-n)-}$) or hydrolyzed ($\text{MOHY}^{(5-n)-}$) except in highly acidic or alkaline solutions (100), so we can ignore all but the $\text{MY}^{(4-n)-}$ form in our treatment. Also, although crystalline compounds of the form $\text{M}_{(1)}\text{M}_{(2)}\text{Y}$ have been prepared, all stable EDTA complexes in solution contain only one metal ion apiece (101), although mixed-metal chelates have been proposed as intermediates in many EDTA-exchange mechanistic studies (102,104a).

If the $\text{MY}^{(4-n)-}$ complex is considered the only one present in solution, this is analogous to the reaction



The fraction of Y in the totally ionized form can be calculated from the pH of the solution and the successive dissociation constants of the protonated species, thusly:



where $[Y]_{\text{tot}}$ is the concentration of all forms of EDTA. If θ is defined as the fraction of Y as Y^{4-} , then

$$\theta = \frac{K_1 K_2 K_3 K_4}{K_1 K_2 K_3 K_4 + K_1 K_2 K_3 [H^+] + K_1 K_2 [H^+]^2 + K_1 [H^+]^3 + [H^+]^4} \quad (46)$$

$$[Y^{4-}] = \theta [Y]_{\text{tot}} \quad (47)$$

It follows, then, that the pH-dependent ("conditional") stability constant for the reaction of M^{n+} with EDTA is

$$K'_{MY} = \theta K_{MY}^0 \quad (48)$$

In the same way, M is not always present as the reactive form, M^{n+} . At high pH (the value varies for different metals), the polyhydroxides MOH , $M(OH)_2$, $M(OH)_3$ (charges have been omitted for simplicity), etc. can form, or in the presence of an excess of a second ligand Z, the complexes MZ , MZ_2 , etc., can be present in significant amounts. The fraction ϕ of metal available as M^{n+} to complex with Y can be calculated using the amounts of interfering ligands in the solutions and the formation constants and stoichiometries of the individual M-ligand reactions. Taking the treatment in Equation 48 one step farther, then

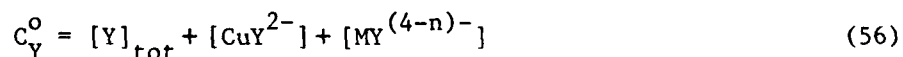
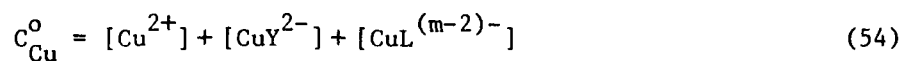
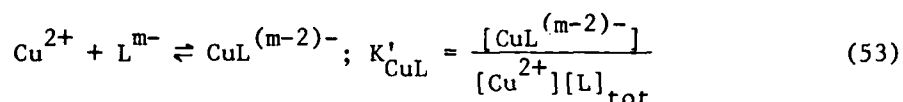
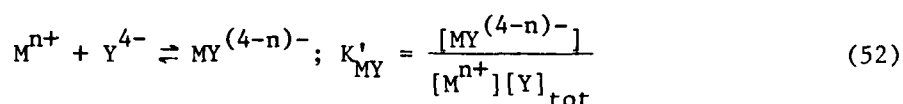
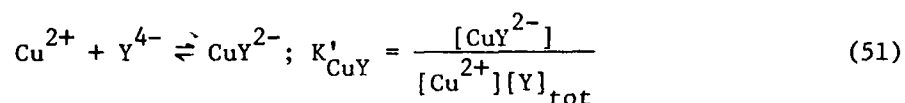
$$[M^{n+}] = \phi [M]_{\text{tot}} \quad (49)$$

$$K'_{MY} = \phi \theta [M]_{\text{tot}} \quad (50)$$

Any M-complexing ligands will serve to lower the concentration of free M^{n+} and also lower the conditional formation constant for the MY complex, K'_{MY} . For our purposes, the second effect is the important one for the analyte metal ion M^{n+} . In the same manner, a second ligand

which complexes Cu^{2+} will lower both the solution concentration of Cu^{2+} and K_{CuY} . The following derivation will include the presence of such ligands, but since the pH can be adjusted to prevent hydrolysis of Cu^{2+} and other interfering ligands can be excluded from solution, consideration of such substances on the detector response will be deferred to the end of this section.

The chemical system we are considering involves, then, a metal ion M^{n+} , EDTA(Y), Cu^{2+} , and a Cu^{2+} -complexing ligand L (as stated before, M^{n+} -complexing ligands affect primarily K_{MY} , so they need not be specifically included). At equilibrium (the time frame to reach equilibrium is treated in Chapter IV.B.5), it can be described fully by the following seven equations:



where C_{Cu}^0 , C_Y^0 , C_M^0 , and C_L^0 are the total concentrations of the respective species in all combinations and $[Y]_{tot}$, $[M]_{tot}$, and $[L]_{tot}$ are the concentrations of the free ligands in all ionized forms.

A singular equilibrium solution can be found for any combination of values of the above parameters. However, evaluation of every individual case leads to a spectrum of redundant solutions. For this reason, we have transformed the measurable variables into dimensionless parameters, relating each quantity to C_{Cu}^0 or K'_{CuY} . The parameters used are:

$$\bar{c} = [Cu^{2+}]/C_{Cu}^0 \quad (58)$$

$$\alpha = C_M^0/C_{Cu}^0 \quad (59)$$

$$f = C_Y^0/C_{Cu}^0 \quad (60)$$

$$\beta = K'_{MY}/K'_{CuY} \quad (61)$$

$$\beta^* = K'_{CuY} \cdot C_{Cu}^0 \quad (62)$$

$$\delta = K'_{CuL}/K'_{CuY} \quad (63)$$

$$\Delta = C_L^0/C_{Cu}^0 \quad (64)$$

To simulate a solution highly buffered with a Cu^{2+} -complexing ligand (i.e., phthalate or THAM), we can assume that C_L^0 is in great excess over C_{Cu}^0 . In this case, we can state

$$[L]_{tot} \approx C_L^0 \text{ if } C_L^0 \gg C_{Cu}^0 \quad (65)$$

since only an insignificant amount of L can be in the CuL complex.

Equations 51 to 57 can then all be combined for a solution in terms of $[\text{Cu}^{2+}]$, and the dimensionless parameters defined in Equations 58 to 64 can be substituted for the terms in this master equation. This treatment results in an equation cubic in terms of \bar{c} , the fraction of total copper which is uncomplexed. The equation contains, in addition to \bar{c} , only parameters dealing with the total amounts of each species and formation constants of the complexes involved, again all relative to C_{Cu}^0 and K'_{CuY} :

$$\begin{aligned} &\bar{c}^3\{\beta^*(1-\beta)[1+(\Delta\delta\beta^*)^2] - 2\beta\beta^*(\Delta\delta\beta^*)\} + \bar{c}^2\{\beta\beta^*(1+\Delta\delta\beta^*)(a-f+2) + \\ &\beta^*(f-1) - \beta[1+(\Delta\delta\beta^*)^2] + \Delta\delta\beta^*(1-2\beta) + 1\} + \\ &\bar{c}\{\beta\beta^*(f-1-\alpha) + 2\beta(1+\Delta\delta\beta^*) - 1 - \beta\} = 0 \end{aligned} \quad (66)$$

For any combination of parameters in the above equation, a real positive root can be found for \bar{c} . Equilibrium response curves can be calculated by setting β , β^* , Δ , δ , and f constant, varying α , and solving the equation for \bar{c} . With this treatment, sigmoidal curves result, with \bar{c} approaching a specific value set by the values of the fixed parameters at very low values of α , and approaching 1.0 at high values of α . This type of curve is expected, since the amount of Cu^{2+} in the system cannot be lowered below the value without any other metal ion added, and when large amounts of metal ions are added, eventually all Cu^{2+} will be liberated.

Competing ligands (represented by $\Delta\delta$) will be discussed only at the end of this section, since they can only diminish the sensitivity of the detector (vide infra). Thus, setting $\Delta\delta$ equal to zero gives the more manageable equation

$$\begin{aligned} & \bar{c}^3\{\beta^*(1-\beta) + \bar{c}^2\{\beta\beta^*(\alpha+2-f) + \beta^*(f-1) - \beta+1\} + \\ & \bar{c}\{\beta\beta^*(f-1-\alpha) + 2\beta-1\} - \beta = 0 \end{aligned} \quad (67)$$

As will be seen, the most important case for our purposes occurs when f is exactly equal to one, and Equation 67 further reduces to

$$\bar{c}^3\{\beta^*(1-\beta)\} + \bar{c}^2\{\beta\beta^*(\alpha+1) - \beta+1\} + \bar{c}\{\beta(2-\beta^*\alpha) - 1\} - \beta = 0 \quad (68)$$

The theoretical response curves were calculated on a Data General Corporation Nova II minicomputer with 32K bytes of core memory using the Data General BASIC language.

We first attempted to evaluate the equations in their original form with an exact general cubic equation solution. Numerical errors in our case on the Nova II (due to the limited precision of the BASIC software and the wide dynamic range between the parameters involved) were very serious. We subsequently rearranged the equations into forms in which α could be back-calculated from \bar{c} , i.e., for Equation 67:

$$\alpha = \frac{\bar{c}^3\{\beta^*(1-\beta)\} + \bar{c}^2\{\beta\beta^*(f-2) + \beta(2-f) - 1\} + \bar{c}\{\beta\beta^*(1-f) - 2\beta-1\} + \beta}{\bar{c}(\bar{c}-1)\beta\beta^*} \quad (69)$$

this form proved to be tractable with the Nova II, and all the succeeding theoretical response curves were constructed by calculating or $d(\log \alpha)/d(\log \bar{c})$ from \bar{c} .

The curves were then plotted on a Hewlett-Packard Model 7001 X-Y recorder using an OLIS 3600 general-purpose interface built specifically for the Nova computer and an assembly language plotting program developed in our laboratory.

Because of the logarithmic response of an ion-selective electrode to sensed-ion concentration, a logical representation of the detector

response is shown in a plot of $\log \bar{c}$ vs $\log \alpha$. This form gives a realistic picture of the sensitivity of the detector, since the measured potential noise is not a function of the sensed ion concentration.

Figure 5 is a plot of $\log \bar{c}$ vs $\log \alpha$ calculated with Equation 67 for the case $f = 1.0$ ($C_{Cu}^0 = C_Y^0$) and $\beta^* = 10^{10}$. We have varied β from 10^3 to 10^{-6} . These values simulate the experimental conditions used in our detector, i.e., an 0.01 M solution of CuEDTA at a pH of 4.0. The concentration of CuEDTA was selected for detection of metals in the micromolar range (when $[CuEDTA] = 10^{-2}$, an $\alpha = 10^{-5} \equiv 10^{-7}$ M metal ion, whereas with $[CuEDTA] = 1.0$, $\alpha = 10^{-5} \equiv 10^{-5}$ M metal ion), and the pH was selected as a compromise between prevention of metal ion hydrolysis (greater at high pH), acceleration of the ligand exchange kinetics (often faster at lower pH in this region (56,100-104), and the strength of the metal-EDTA complexes (generally greater at higher pH in this region (106)).

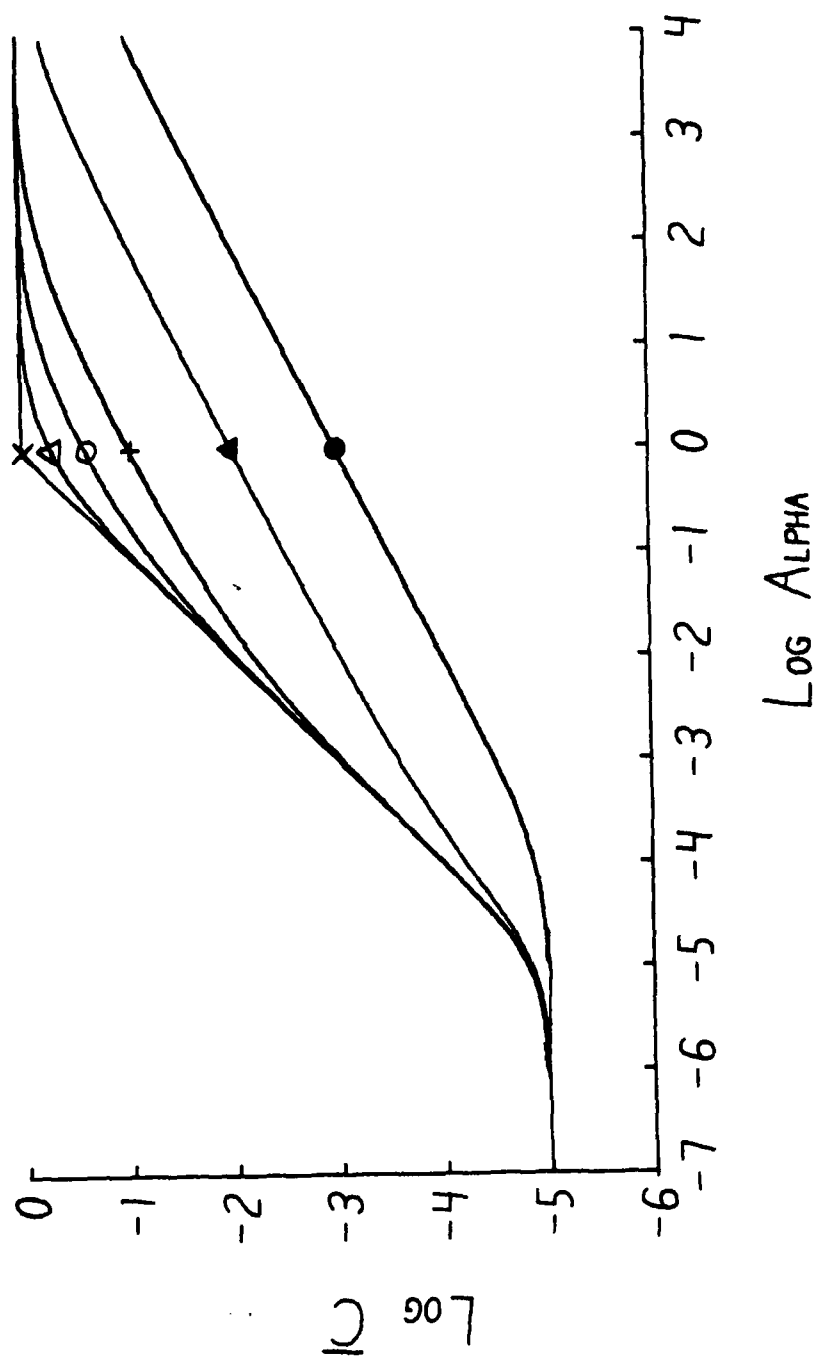
The figure shows that at values of α approaching zero, \bar{c} approaches a level set only by β^* , or the normalized strength of the CuEDTA complex. At low but finite α , the magnitude of \bar{c} is largely independent of β (the relative strength of the metal-EDTA complex). Here, the perturbation of the original $Cu + EDTA \rightleftharpoons CuEDTA$ equilibrium is small, and essentially complete displacement of Cu(II) occurs.

As α increases, however, the rise of \bar{c} becomes increasingly dependent on β . The uppermost curve, calculated for $\beta = 10^3$, shows essentially total displacement of Cu(II) over the entire length of the curve. A sharp break occurs at $\log \alpha = 0$ ($\alpha = 1.0$), since the limiting value for $\log \bar{c}$ is zero (all Cu(II) is displaced from the EDTA

Figure 5. Theoretical Logarithmic Plots of Dimensionless Uncomplexed Cu(II) Concentration vs the Dimensionless Total Metal Ion Concentration.

All plots were computed from Equation 67 with $\beta^* = 10^{10}$ and $f = 1.0000$

- A. $\beta = 10^3$ (\times).
- B. $\beta = 1.0$ (Δ).
- C. $\beta = 0.1$ (\circ).
- D. $\beta = 0.01$ ($+$).
- E. $\beta = 10^{-4}$ (\blacktriangle).
- F. $\beta = 10^{-6}$ (\bullet).



complex). At this point, \bar{c} is approximately 0.999. As β decreases, the curves fall from this line, showing decreased Cu(II) displacement for fixed values of α .

The slope of the curve $\log \alpha$ vs $\log \bar{c}$ predicts the uncertainty in determining $\log \alpha$ assuming a constant uncertainty in $\log \bar{c}$, or in this case, a constant uncertainty in the measured electrode potential. This is mathematically equivalent to the relative uncertainty in α ($\Delta\alpha/\alpha$) arising from a constant relative uncertainty in \bar{c} ($\Delta\bar{c}/\bar{c}$) as can be shown:

$$\frac{d(\ln\alpha)}{dx} = \frac{1}{\alpha} \frac{d\alpha}{dx} \quad (70)$$

$$\frac{d(\ln\bar{c})}{dx} = \frac{1}{\bar{c}} \frac{d\bar{c}}{dx} \quad (71)$$

$$\frac{d(\ln\alpha)}{d(\ln\bar{c})} = \frac{d\alpha/\alpha}{d\bar{c}/\bar{c}} \quad (72)$$

where x is a dummy variable used only for the derivation.

Since α is the ratio C_M^0/C_{Cu}^0 , this describes the relative uncertainty in the concentration of the metal of interest assuming a specific uncertainty in the measured electrode potential.

Figure 6 is a plot of $d(\log\alpha)/d(\log \bar{c})$ vs α for the same conditions as Figure 5. The function $d(\log\alpha)/d(\log \bar{c})$ is the inverse slope of the curves plotted in Figure 5, since in an analytical situation, α will be determined from \bar{c} .

The figure shows that the highest possible precision in the determination of α is found under conditions such that Cu(II) is totally displaced from the complex (high β or moderate β and low α), as would be expected. At extremely low values of α , precision is degraded

Figure 6. Theoretical Plots of the Slope of Dimensionless Total Metal Ion Concentration with Respect to Dimensionless Uncomplexed Cu(II) Concentration vs the Dimensionless Total Metal Ion Concentration.

All plots were computed from Equation 67 with $\beta^* = 10^{10}$ and $f = 1.0000$.

A. $\beta = 10^3$ (\times).

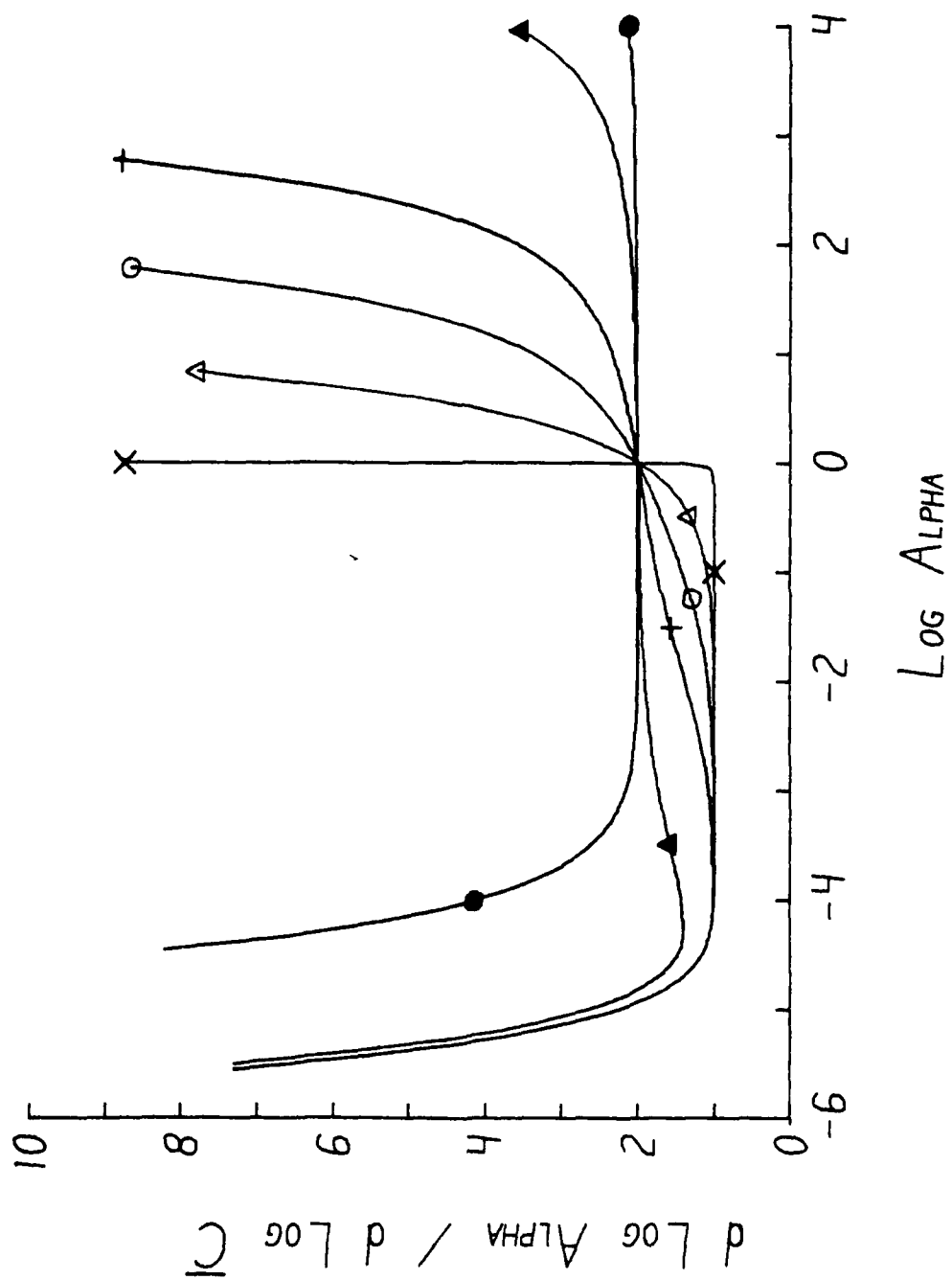
B. $\beta = 1.0$ (Δ).

C. $\beta = 0.1$ (\circ).

D. $\beta = 0.01$ ($+$).

E. $\beta = 10^{-4}$ (\blacktriangle).

F. $\beta = 10^{-6}$ (\bullet).



because the background level of \bar{c} is higher than the amount added by the introduction of the second metal.

Values of β lower than that needed to cause total displacement of Cu(II) yields slightly degraded precision at low α , but do not exhibit the sharp break at $\log \alpha = 0$.

The highest values of α shown in Figures 5 and 6 are not realized experimentally in the detector, due to solubility limits of the metal ions (C_{Cu}^0 in the detector is 0.01 M, so $\alpha = 10^4$ is equivalent to 100 M metal ion), but if C_{Cu}^0 were lowered and the pH adjusted to keep constant, response at high values of α might be possible.

Figure 7 is another plot of $\log \bar{c}$ vs $\log \alpha$, this time using a fixed β of 0.01 and f of 1.0, but varying β^* from 10^6 to 10^{12} . This represents the case in which the absolute metal-complex strengths were varied, but their strengths relative to each other remained constant. This type of situation can occur when the pH of the solution with a multiionizing ligand is changed, varying θ in Equation 46, and K'_{MY} in Equation 48. If the pH is raised enough so that one metal hydrolyzes, β will also change, according to Equations 49 and 50, or when the ligand is changed with the metal ions remaining the same, since similar ligands (e.g., EDTA and trans-1,2 cyclohexanediaminetetraacetic acid (CyDTA)) have approximately the same relative formation constants for metal ion pairs.

By varying β^* , the response at the lower end of the $\log \alpha$ range is affected, since residual \bar{c} is again determined only by β^* , reaching a limiting value of $1/\beta^*$ as α approaches zero.

Figure 8 expands the model to include the condition of f not equal to unity. In this figure, β and β^* are fixed at 10 and 10^8 , respectively,

Figure 7. Theoretical Logarithmic Plots of Dimensionless Uncomplexed Cu(II) Concentration vs the Dimensionless Total Metal Ion Concentration.

All plots were computed from Equation 67 with $\beta = 0.01$ and $f = 1.0000$.

- A. $\beta^* = 10^6$ (Δ).
- B. $\beta^* = 10^8$ (\circ).
- C. $\beta^* = 10^9$ (\times).
- D. $\beta^* = 10^{10}$ (\blacktriangle).
- E. $\beta^* = 10^{12}$ (\bullet).

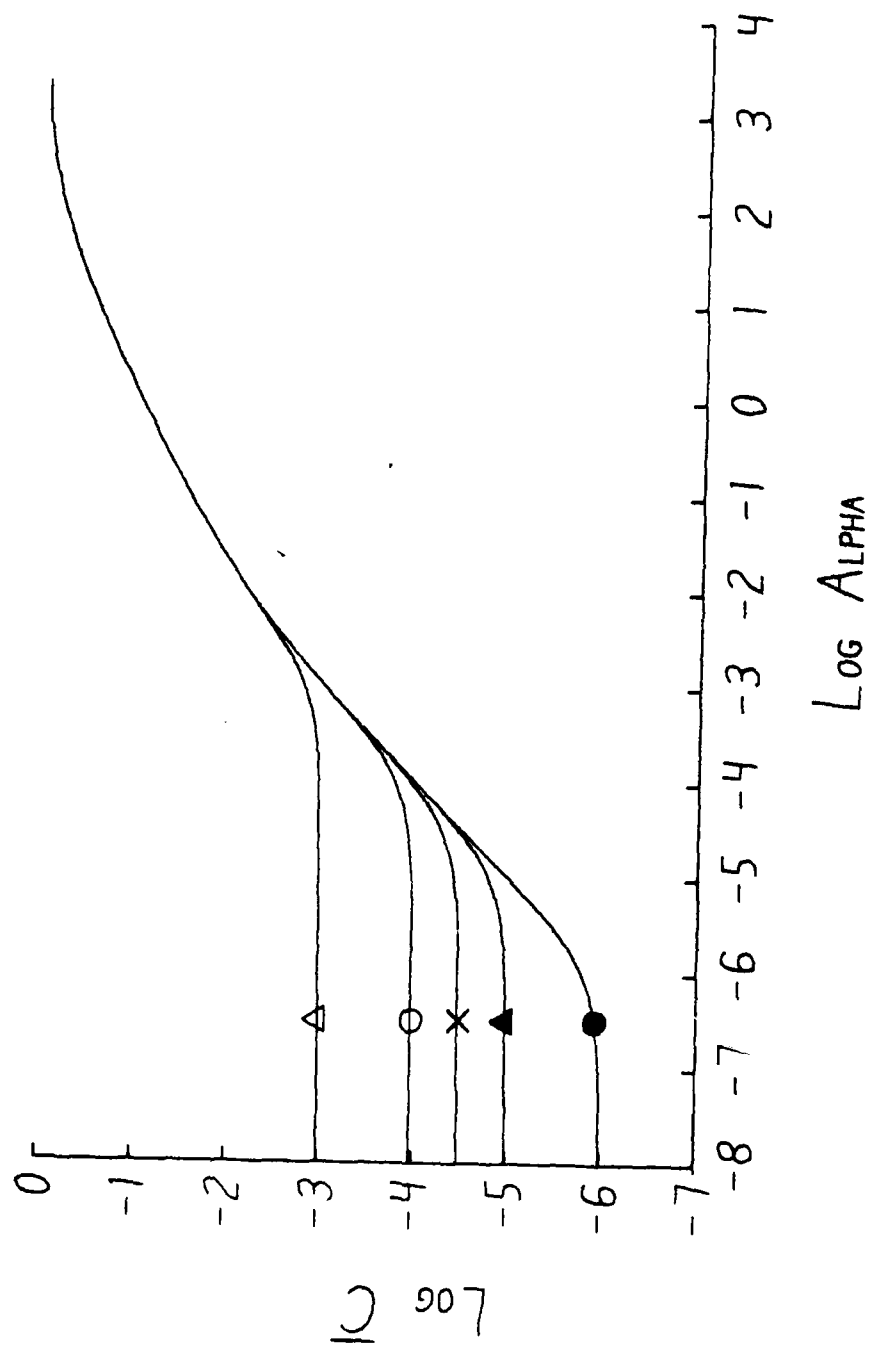
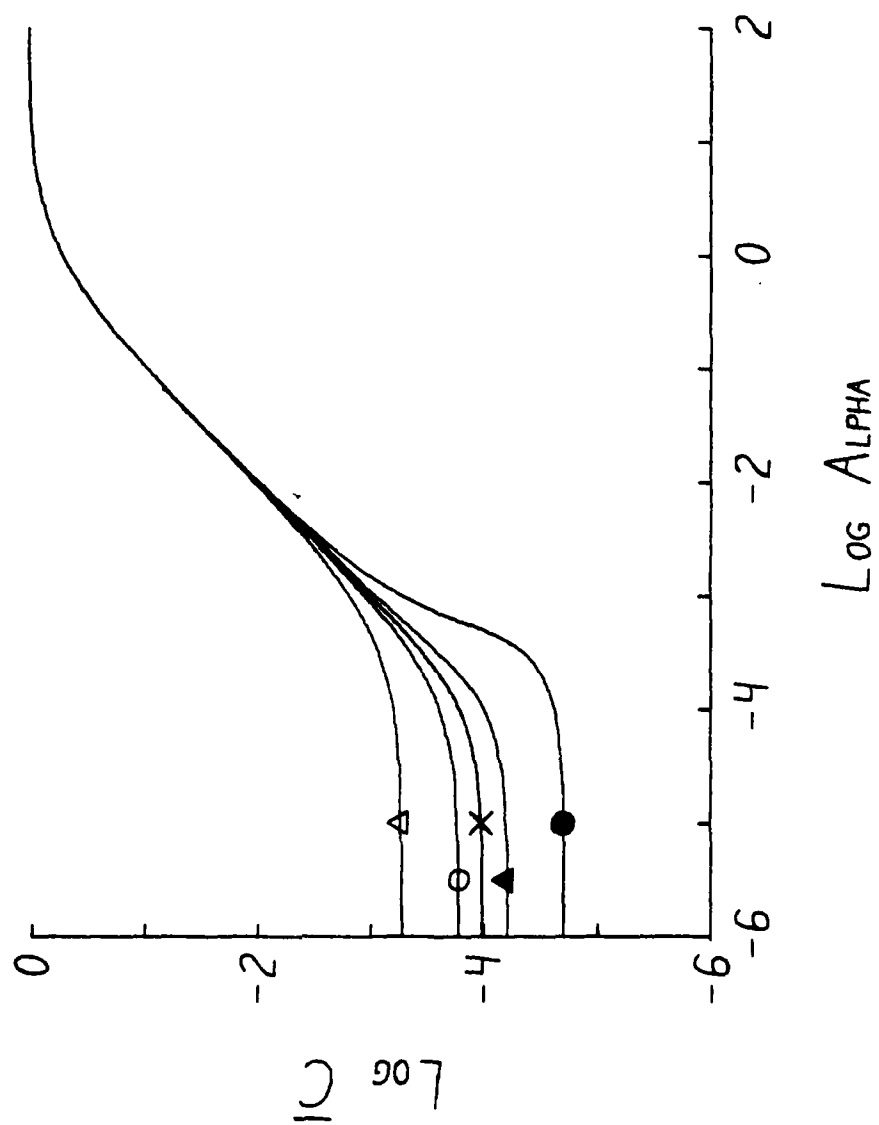


Figure 8. Theoretical Logarithmic Plots of Dimensionless Uncomplexed Cu(II) Concentration vs the Dimensionless Total Metal Ion Concentration.

All plots were computed from Equation 67 with $\beta = 1.0$ and $\beta^* = 10^8$.

- A. $f = 0.9995$ (Δ).
- B. $f = 0.9999$ (\circ).
- C. $f = 1.0000$ (\times).
- D. $f = 1.0001$ (\blacktriangle).
- E. $f = 1.0005$ (\bullet).



and f is varied from 0.9995 to 1.0005. Calculations with variable f simulate the case where the Cu(II):EDTA ratio in the complex is not exactly unity. This situation can occur from adsorption of either component onto the surface of the precipitated CuEDTA when it is prepared (vide infra).

At a value of f greater than 1, the curve is distorted to where $\log \bar{c}$ is lower than the case of f equal to 1. The slope of the curve is greater than 1 over a short range, where the excess ligand is being titrated by the addition of the second metal, and gradually merges into the curve of f equal to 1.

When f is less than 1, the response to addition of metal ions is suppressed at low α , since the limiting value of $\log \bar{c}$ is higher than for f equal to 1, due to the excess of free Cu(II). This restricts the utility of the system for measuring low levels of metals.

The implications of the condition of excess free Cu(II) are shown in Figure 9. In the upper curve $\beta = 1.0$, $\beta^* = 10^{10}$ and $f = 0.9999$. In the lower curve, $\beta = 1.0$, $\beta^* = 10^8$, and $f = 1.0$. Using this example, the limiting values of $\log \bar{c}$ for the two cases are within 0.01, indistinguishable in a potentiometric experiment. If f equal to 1 were assumed, giving the lower curve from the limiting $\log \bar{c}$ value, and the upper curve were the actual analytical function, a positive error of 0.3 log unit could result in determining $\log \alpha$ from $\log \bar{c}$, or a 100% positive error in the value of α . Thus, at even very low imbalances in the Cu(II):EDTA ratio, f needs to be incorporated into the analytical equation.

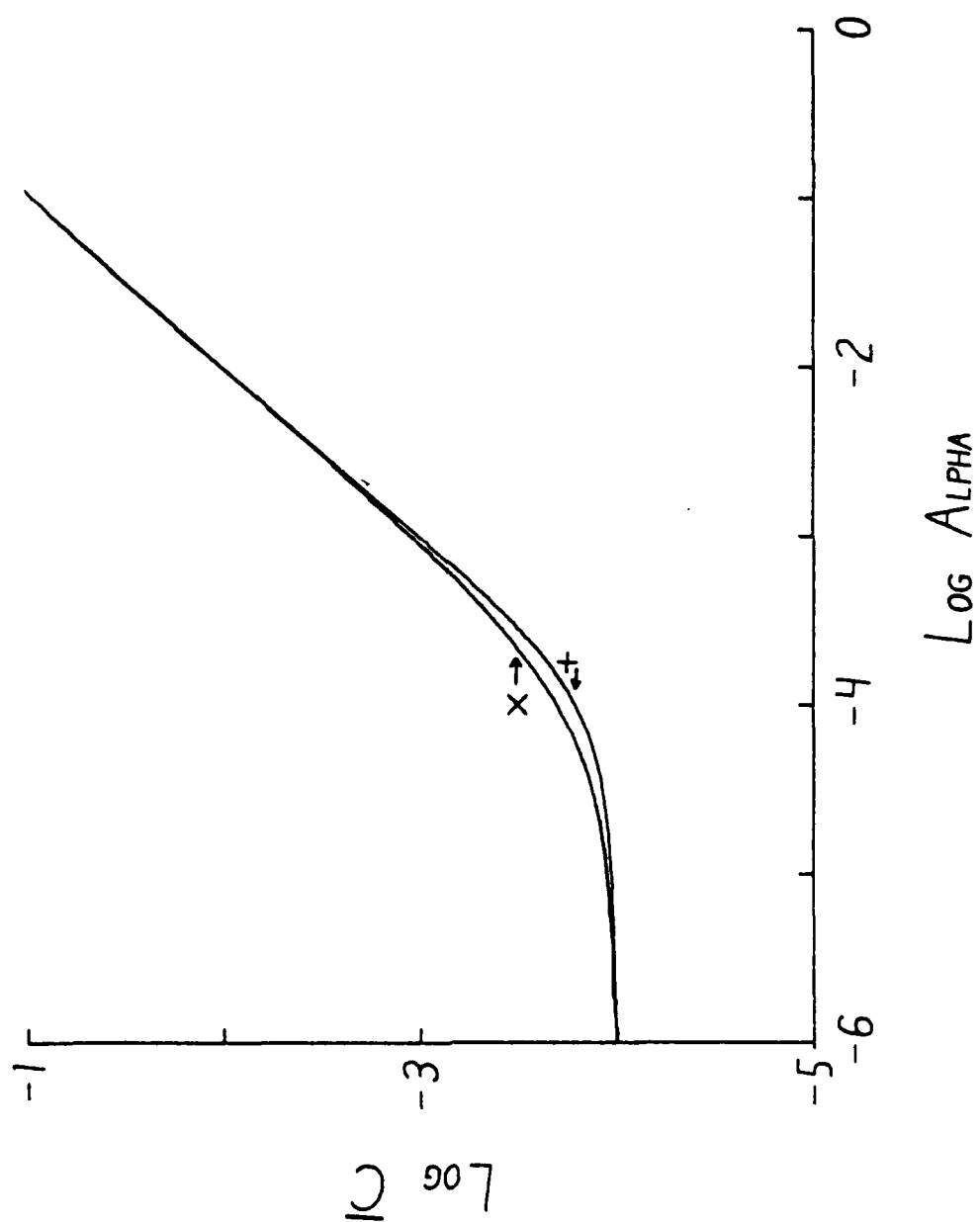
Also, in Figure 9, all curves with $f = 0.9999$ and β^* greater than 10^{10} are identical (within 0.01 log unit in the values of $\log \bar{c}$), so no information can be obtained about the strength of the CuEDTA complex

Figure 9. Theoretical Logarithmic Plots of Dimensionless Uncomplexed Cu(II) Concentration vs Dimensionless Total Metal Ion Concentration.

All plots were computed from Equation 67 with $\beta = 1.0$.

A. $\beta^* = 10^{10}$, $f = 0.9999$ (\times).

B. $\beta^* = 10^8$, $f = 1.0000$ ($+$).



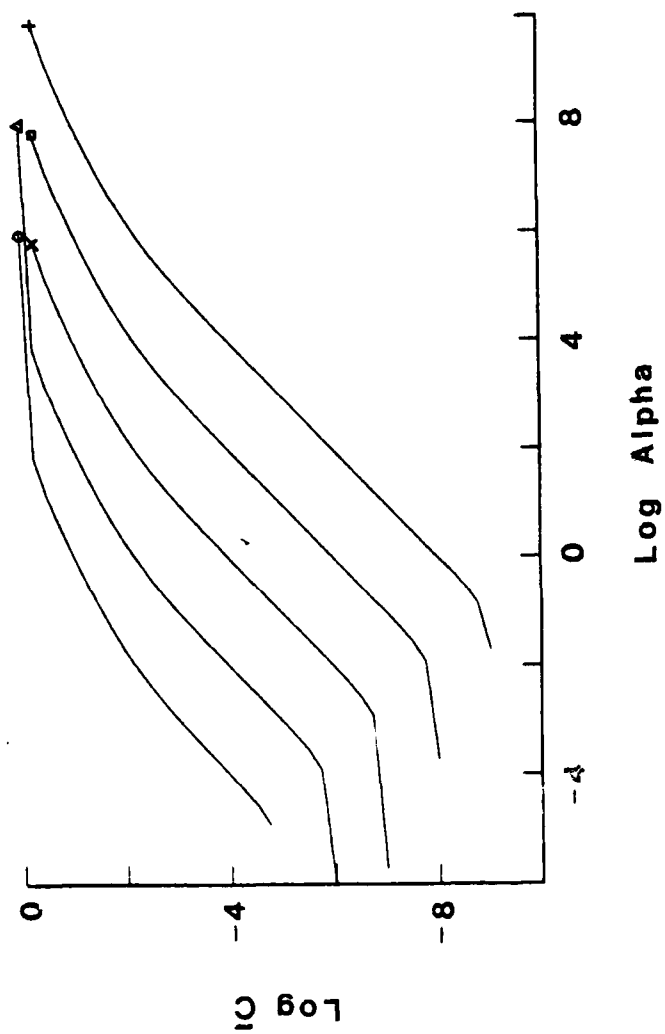
except that it is greater than or equal to 10^{10} . If an extremely low detection limit is not mandatory, then a small amount of excess Cu(II) can be added to the CuEDTA solution to fix the response function, provided that $1/\beta^*$ is less than one percent of $1-f$.

Finally, Figure 10 takes into account the complete Equation 65, with $\Delta\delta$ not equal to zero. This is the case where a second ligand is introduced which complexes with Cu(II), such as many pH-buffering ions will. The figure was constructed for the case $f = 1.0$, $\beta = 0.01$, $\beta^* = 10^{10}$, and $\Delta\delta$ is varied from zero to 10^{-4} (with 1M potassium biphthalate as the second ligand at pH4 for buffering, $\Delta\delta$ would be approximately 10^{-6}). It clearly shows that adding a second ligand lowers the Cu(II) concentration at a specific level of M^{n+} , and extends the "linear" segment of the curve, as is intuitively expected. However, the sensitivity of the system at low levels of M^{n+} is greatly reduced, damaging the utility of the detector. The larger $\Delta\delta$ used, the more sensitive the actual measurement device at lower Cu(II) levels would be needed. Therefore, unless sensitivity is not a problem (as might be the case with very strongly complexing ligands and coulometric detection), the introduction of a second ligand in the system should be avoided.

Figure 10. Theoretical Logarithmic Plots of Dimensionless Uncomplexed Cu(II) Concentration vs the Dimensionless Total Metal Ion Concentration.

All plots were computed from Equation 66 with $\beta = 0.01$, $\beta^* = 10^{10}$, and $f = 1.0000$.

- A. $\Delta\delta = 0.0$ (o).
- B. $\Delta\delta = 10^{-10}$ (Δ).
- C. $\Delta\delta = 10^{-8}$ (\times).
- D. $\Delta\delta = 10^{-6}$ (\square).
- E. $\Delta\delta = 10^{-4}$ (+).

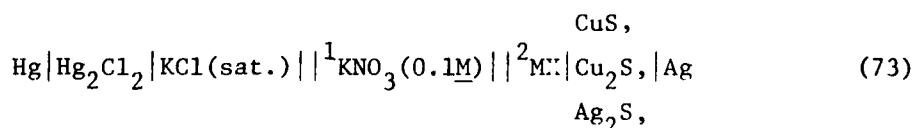


III. Experimental

A. Electrochemical Cell

The potentiometric cell used in this work contains a saturated calomel electrode (SCE) and a cupric-ion selective electrode. The SCE was separated from the analyte solution by immersing it in a tube filled with 0.1 M KNO_3 solution and connected to the analyte solution via a plug of unfused Vycor glass ("Thirsty Glass," Corning Glass Works). This arrangement was used to prevent chloride leakage into the analyte solution in experiments in which a dip-type electrode was used, and to prevent any unknown effects in the ceramic frit of the SCE such as a precipitate forming and blocking the frit (vide infra).

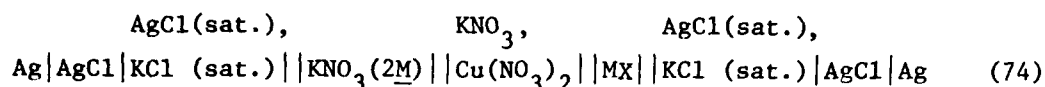
The cell can be depicted diagrammatically as follows:



Liquid junction 1 is the porous ceramic frit of the SCE, and liquid junction 2 is the Vycor plug, which acts as an ion-exchange membrane, allowing negligible mixing of solutions on either side of the membrane while maintaining a low resistance electrical path. The solution designated MX is the analyte solution, containing KNO_3 , CuEDTA, and sometimes other cations and anions.

As discussed previously, liquid junction potentials exist at any ion-conducting interface between two solutions which are not identical. By using solutions of constant composition on either side of liquid

junction 1, the liquid junction potential is kept constant, and can be compensated for electrically. Johansson and Edstrom (106) have measured the potential between two double junction reference electrodes with various bridge filling solutions and an analyte solution between the electrodes containing KNO_3 and varying concentrations of $\text{Cu}(\text{NO}_3)_2$. Their cell was configured



where the concentrations of KNO_3 and $\text{Cu}(\text{NO}_3)_2$ in the center compartment were varied, and MX was either KNO_3 (1M), NaNO_3 (1M), KCl (sat.), or Orion 90-00-02 filling solution (0.7 M KCl , 1.5 M KNO_3 , and small amounts of NaNO_3 and AgNO_3). When the ionic strength of the center compartment was kept at 0.3 M with KNO_3 , the bridge solutions (MX) containing KNO_3 or KCl gave essentially invariant junction potentials. In the case of KNO_3 , since the two bridges contain the same ions indifferent concentrations, this shows that the influence of small (< 0.01 M) amounts of $\text{Cu}(\text{NO}_3)_2$ in a much stronger solution of KNO_3 do not seriously affect the liquid junction potential against KNO_3 solutions. This property enables us to use the reference electrode with liquid junction in our system.

B. Electronics

Potentiometric measurements were made with a homemade electrometer, consisting of an instrumentation amplifier with a fixed gain of 10 and an inverting amplifier with switchable gain of 0.3, 1.0, 3.0 and 10.0. The electrometer thus has a switchable overall gain of 3.0, 10.0, 30 and 100. A diagram is given in Figure 11 and parts are listed in Table

II. The instrumentation amplifier is a common subtractor (107) with a variable offset built into one arm. The circuit has been used previously in the measuring circuit of an electrochemical pH-stat by Adams, Betso and Carr (108). The Analog Devices 515J amplifiers are FET-operational amplifiers, with an input impedance of 10^{13} ohms, and the Burr-Brown 3142 operational amplifier was selected for its very low voltage noise specifications. This configuration allows two high-impedance electrodes to be used for measurement and reference, and requires a third low-impedance contact to the solution, which was accomplished in this work by a stainless-steel hypodermic needle.

The signal was then fed to an inverting low-pass filter with a time constant (RC) of approximately 1 sec. This was used to filter out 60 Hz pickup in the flow system which was transmitted to the electrodes and any other high-frequency noise which arose before the filter.

For measurements of electrode potentials, the signal from the proceeding circuits was fed directly into a Perkin-Elmer Model 56 recorder. We converted electrode potentials directly to copper (II) concentrations with an antilog transducer constructed in the laboratory. The transducer is shown schematically in Figure 12, and components are given in Table III. The heart of the transducer is an Analog Devices Model 752N Logarithmic Transconductor. The 752N is designed to take the antilog of an input voltage according to the transfer function

$$e_o = I_{\text{ref}} R_f (10^{-e_{\text{in}}/K}) \pm E_{\text{os}} \quad (75)$$

Figure 11. Schematic Diagram of the Differential Electrometer.

For Component values and types, see Table II.

A. Instrumentation amplifier, gain = 10.

B. Inverting amplifier, gain = 0.3, 1.0, 3.0, 10.

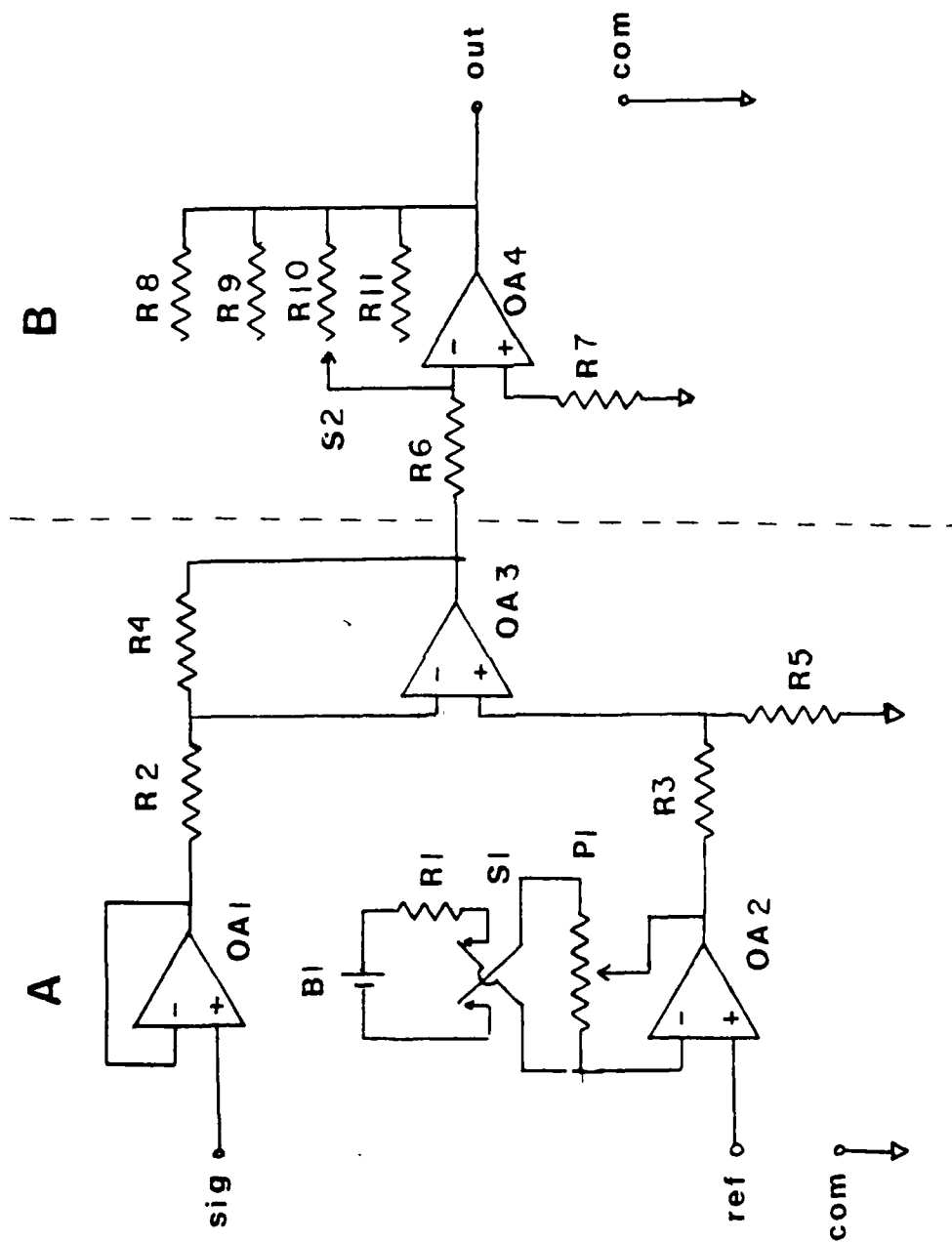


Table II. Components Used in the Circuit in Figure 11.

Resistors:

All fixed resistors are metal film, 1/4 W, 1% tolerance.

R1 - 80.6 K Ω .

R2, R3, R6, R7, R9 - 10 K Ω .

R4, R5, R11 - 100 K Ω .

R8 - 3.01 K Ω .

R10 - 30.1 K Ω .

P1 - 10 K Ω , ten-turn potentiometer, 0.5% linearity.

Switches:

S1 - Double-pole, double-throw toggle.

S2 - Single-pole, four-position rotary.

Battery:

B1 - Two mercury cells, each 1.35 V in series.

Operational Amplifiers:

OA1, OA2 - 515J Electrometer FET-input (Analog Devices).

OA3, OA4 - 3142 General purpose, low drift (Burr-Brown).

Figure 12. Schematic Diagram of the Antilog Transducer for Potential to Cu(II) Concentration Conversion.

For component types and values, see Table III.

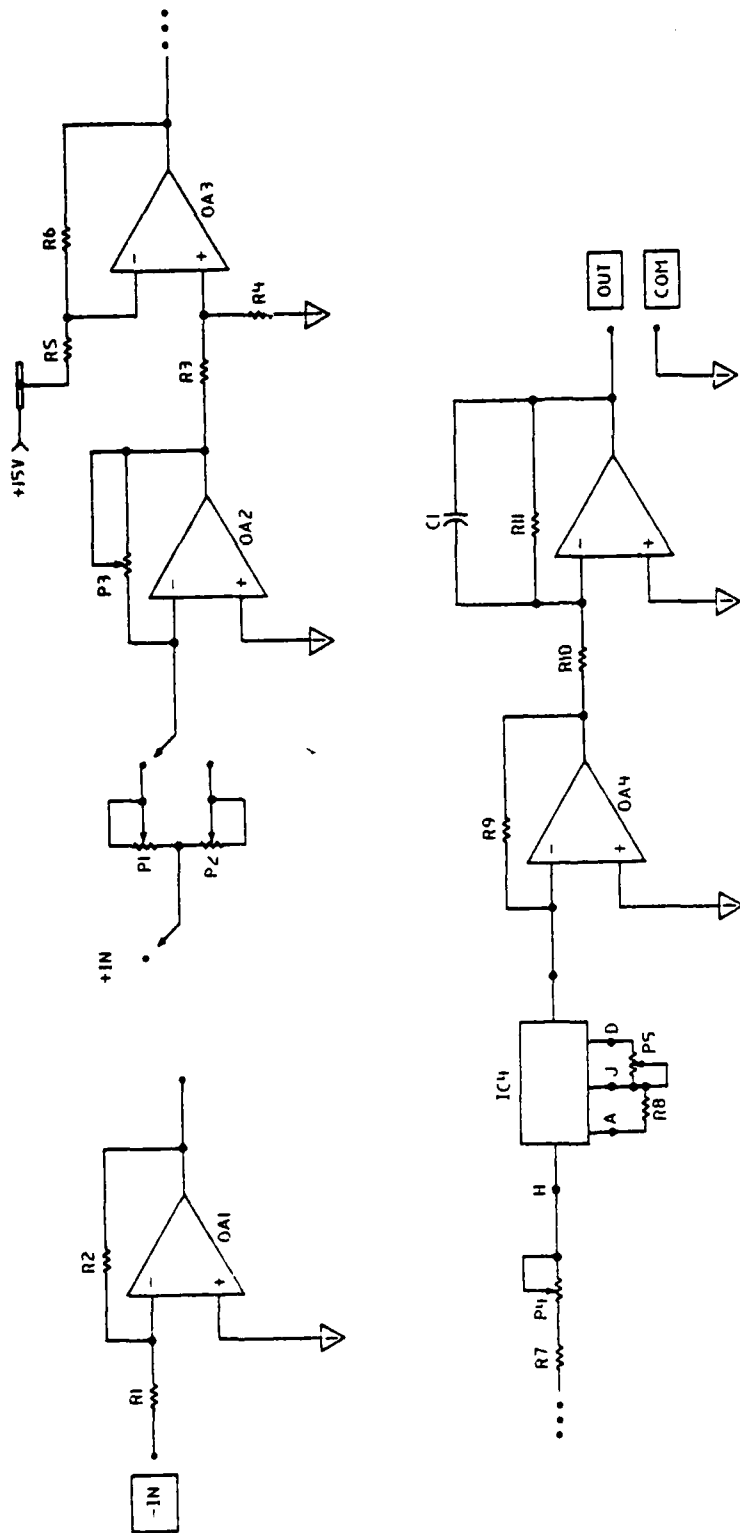


Table III. Components Used in the Circuit in Figure 12.

Resistors:

All fixed resistors are metal film, 1/4 W, 1% tolerance.

R1, R2 - 200 K Ω .

R3, R6 - 20 K Ω .

R4, R5 - 600 K Ω .

R7 - 585 Ω .

R8 - 26.1 K Ω .

R9 - 10 K Ω .

R10, R11 - 220 K Ω .

P1 - 100 K Ω , ten-turn potentiometer, 0.5% linearity.

P2 - 10 K Ω , ten-turn potentiometer, 0.5% linearity.

P3 - 50 K Ω , 22-turn trimpot.

P4 - 1 K Ω , 22-turn trimpot.

P5 - 2 K Ω , 22-turn trimpot.

Capacitor:

C1 - 0.5 μ F Tantalum, 10% tolerance.

Switches:

S1, S2 - Single-pole, double-throw toggle.

Integrated Circuits:

OA1, OA2, OA3, OA5 - LM741CN General purpose operational amplifier (National Semiconductor).

OA4 - 3342 FET-input operational amplifier (Burr-Brown)

IC1-752N Logarithmic Transconductor (Analog Devices)

where

$$-2 \leq e_{in}/K \leq 2 \quad (76)$$

so that four decades of output (approximately 1 mV to 10 V) can be obtained. In Figure 10, I_{ref} is set by R8 and P5, K is set by P4, R_F is R9 (on OA4), and E_{os} is determined by the trim resistor on OA4 (not pictured).

The circuit in Figure 12 was designed to permit maximum flexibility in the input signal requirements. The 752N has a monotonic input slope ($-e_{in}/K$) requirement, so OA1 is an inverter amplifier with a gain of -1, which can be switched in or out. This allows the user to provide either positive or negative input voltages. The electrometer we used has variable gain, because ion-selective electrodes do not always have a perfectly Nernstian slope (34). This necessitates that the exponential component of the transfer function ($-e_{in}/K$) be variable in order to accept different electrodes. Amplifier OA2 is an inverter with a gain of $-P3/P1$ (or P2). P3 is set at approximately 25 K Ω , and P1 or P2 can be varied to produce a gain of -0.25 to -25. The 752N is adjusted by P4 to have a scale factor K of 250 mV/decade. Thus, OA2 can be adjusted to accept input voltages of 10 mV/decade to 1 V/decade. The potentiometers were placed in the input stage of OA2 to permit direct setting of the decade sensitivity from the dial, as this is inversely proportional to the gain of OA2, and thus proportional to P1 (or P2) if the feedback resistor (P3) remains constant.

The transfer function of the 752N is followed only when Equation 75 is satisfied. For K equal to 250 mV/decade, this requires that e_{in} is between -0.5 V and +0.5 V. The transfer function of OA3 is (109):

$$e_o = \frac{R4}{R5} \left(\frac{R5 + R6}{R3 + R4} \right) e_{in}(+) - \frac{R6}{R5} e_{in}(-) \quad (77)$$

With the resistor values in Table 3 and $e_{in}(-)$ equal to +15 V, a constant 0.5 V is subtracted from the input signal (which is gained by +1). This enables us to use the full input range to the 752N.

OA4 is a current to voltage converter which is required when using the 752N in the antilog mode.

OA5 is a single-pole inverting filter with a time constant (RC) of 1 sec to eliminate high frequency noise on the output of the instrument.

The transducer is calibrated straightforwardly, in sequence from OA1 to OA5. Using reference voltage source (Analog Devices AD2700L) as the input, the output of the device is within 1.5% of theoretical output from zero to 10 volts (four decades of output).

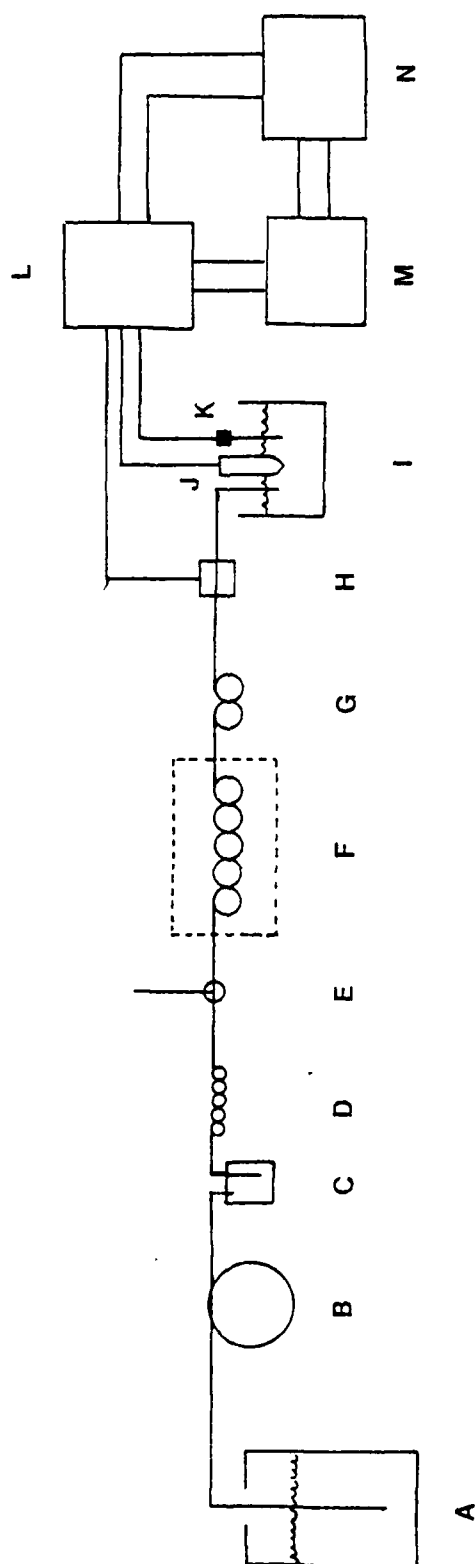
C. Flow System Design

The detector is a flow reactor system in which the chromatographic eluent is mixed with a solution of CuEDTA. The combined stream flows through a delay coil and the free Cu(II) released by the ligand exchange reaction is monitored with a flow-through cupric-ion selective electrode. The electrode measures free Cu(II) released after a known time interval after the liquid flows through a delay coil of fixed volume at a specific flow rate. The two parameters (delay coil volume, flow rate) are adjusted to allow the reaction to proceed to steady-state, so that the response to metal ions can follow the theory derived in the preceding section.

A schematic diagram of the detector is shown in Figure 13. The components which are placed before the point at which the CuEDTA stream is mixed with the chromatographic eluent are: (1) reservoir of CuEDTA,

Figure 13. Schematic Diagram of the Metal Ion Detector.

- A. Reservoir of Reactant Solution, typically 0.01 M CuEDTA in 0.1 M KNO_3 , pH 4.0.
- B. Peristaltic pump, flow rate variable from 0.25 mL/min to 4.0 mL/min.
- C. Drop decoupler, for details, see text.
- D. Flow restrictor, 1 m of 0.3 mm I.D. Teflon tubing.
- E. Column effluent junction, low volume "tee" connector.
- F. Heated delay coil, 2 m of 0.5 mm I.D. Teflon tubing inside 75°C water bath.
- G. Room temperature delay coil, 0.5 m of 0.5 mm I.D. Teflon tubing inside room temperature water bath.
- H. Flow-through cupric ion-selective electrode, for details of construction, see text.
- I. Waste reservoir, 1400 mL capacity, also used for room temperature water bath and as conducting medium for potentiometric cell.
- J. Saturated calomel reference electrode, immersed in 0.1 M KNO_3 and electrically connected to waste reservoir by disk (3 mm dia. x 3 mm thick) of "Thirsty glass" (porous Vycor).
- K. Common electrode, stainless steel hypodermic needle.
- L. Differential electrometer, for details, see text.
- M. Antilogarithmic Transducer, for details, see text.
- N. Two-pen strip-chart recorder, for cell potential and/or concentration measurements.



(2) pump, (3) drop decoupler (vide infra), and (4) flow restrictor.

After the stream and chromatographic eluent are mixed come the following elements: (1) delay coil (heated bath), (2) delay coil (room temperature bath), (3) flow-through cupric ion-selective electrode, (4) tube to waste reservoir, (5) waste reservoir, (6) reference electrode, and (7) ground electrode. The potential between the measuring (cupric ion) and reference electrodes is measured with a laboratory-built electrometer, and the potential is converted to free Cu(II) concentration with a laboratory-built antilog transducer whose slope (volts input/decade output) can be varied continuously from 10 mV/decade to 1 V/decade (see Electronics).

The reagent reservoir is a Pyrex flask or bottle loosely covered to exclude dust. Solutions are prepared as discussed later. All tubing except the pump tubing is Teflon (0.5 mm I.D. x 1.5 mm O.D., from Altex Scientific, Inc., Berkeley, CA 94710, and Bolab, Inc., Derry, NH 03038), which is interconnected with 1/4 x 20 threaded male, female, and tee connectors (Altex). The pump was constructed in our laboratory from a peristaltic pumphead (Cole-Parmer "Masterflex" No. 7013, Chicago, IL 60648) with 0.76 mm I.D. x 4.1 mm O.D. Tygon pump tubing (Cole-Parmer). The pumphead is turned by a 200 steps-per-revolution stepping motor (Rapid-Syn Model 34D-9106A, Santa Fe Springs, CA) which is controlled by a UPDN-1 driver (Rapid-Syn) and powered by two single-ended DC power supplies (Lambda Model LMEE28, 28 volts and LMH3P6, 0 to 5 volts adjustable, Melville, NY). The pumping rate is controlled by means of an external potentiometer on the UPDN-1 driver.

After the pump, the flowing solution enters a drop decoupler in which it drips from the Teflon tubing into a stoppered Pyrex test tube. The stopper had to be wired onto the test tube because of pressure buildup inside. The solution exits from the bottom of the test tube through another length of Teflon tubing. The test tube is angled approximately 60° near the top so that the solution entering does not splash into the solution at the bottom of the tube, entraining air. Any trapped air will escape from the solution inside tubing further downstream. Any bubbles which form interrupt the electrical circuit between the measuring and reference electrodes and drive the electrometer output to saturation. This effect can be seen with aqueous solutions at room temperature, but is especially annoying with aqueous solutions at elevated temperatures, where the solubility of most gases is lower, or with aqueous-alcohol solutions at any temperature, where the solubility of gases in mixed solvents and anomalies therein have to be taken into consideration (110).

The drop decoupler performs two distinct functions. First, it isolates the potentiometric system from the peristaltic pump electrically by introducing an air gap between the two elements. As discussed by Zipper, Fleet, and Perone (111), transient electrostatic charge is built up in the solution pumped by a peristaltic pump by the continuous squeezing and releasing of the pump tubing. The air gap prevents this charge from reaching the electrodes. Without this isolation, fluctuations synchronous with the pumphead rotation in the measured potential of several millivolts were observed.

Second, the drop decoupler acts as a fluid capacitor when followed by a flow restrictor (1 m of 0.3 mm I.D. Teflon tubing) to form a pulse dampener for flow surges from the pump. This is necessary to produce a constant ratio of CuEDTA to chromatographic eluent when the two streams are mixed. A steady flow past the cupric-ion electrode also makes it less crucial for the electrode to be absolutely flow-insensitive. (For a discussion of flow-sensitivity of electrodes, see Flow-through Electrode Design.)

The drop decoupler will still dampen flow pulses with both inlet and exit tubes contacting the internal solution, but the lack of electrical isolation still allows the electrostatic potential fluctuations to pass, which can seriously degrade the detector baseline.

After the flow restrictor (described above), the CuEDTA stream is mixed with the chromatographic eluent in a Tee-connector (Altex model 200-22, 0.8 mm bore). The two streams enter opposing (180°) channels for efficient mixing, and the combined stream exits mutually perpendicular to the other two arms.

The CuEDTA-eluent mixture flows through a delay coil 2.5 m long x 0.5 mm I.D. This tubing has an internal volume of approximately 0.5 mL, and thus represents a reaction time of 30 seconds with a 1 mL/minute combined flow rate. The delay coil is immersed in a rectangular eight liter water bath. A Haake Model FE Constant Temperature Circulator (Saddle Brook, NJ 07662) circulates water through a stainless steel coil inside the bath for heating, and a Bodine Model V10R Stirrer (Chicago, IL) is used to stir the bath.

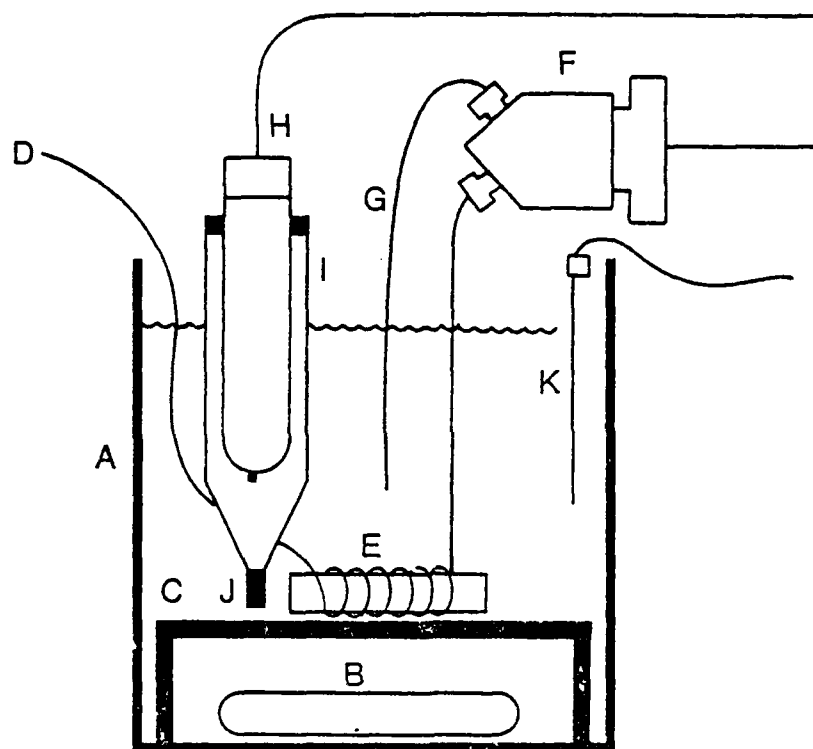
After the combined stream exits the heated delay coil, it enters a shorter (0.5 m length x 0.5 mm I.D.) delay coil in a stirred room temperature (no temperature regulation) bath. This second delay coil allows the reaction to continue longer and ensures that the measuring electrode will be contacting a solution at room temperature, so that possible thermal drifts and changing Nernstian slope caused by measuring Cu(II) in an elevated temperature solution are eliminated. Figure 14 shows the room temperature segment of the detector.

The second delay coil feeds into the cupric ion-selective electrode. This is a flow-through electrode designed in this laboratory, and will be described in detail later. An exit tube leads from the electrode to a 1400 mL Pyrex beaker which is constantly stirred magnetically and contains at least 600 mL of solution at all times. When the beaker fills, excess solution is siphoned off and discarded. The solution in the beaker acts first as a heat sink for the second delay coil, and second provides an electrically conductive medium for the reference and ground electrodes.

The reference electrode assembly consists of a Fisher Model 13-639-63, saturated calomel electrode (SCE) with ceramic plug liquid junction immersed in a tube filled with 0.1 M KNO_3 which is terminated with a small plug (0.6 mm length x 0.6 mm diameter) of "Thirsty Glass," as described in the preceding section. The SCE is isolated from the analyte solution for two reasons. First, we have observed erratic response when using a cupric ion-selective electrode and an SCE in solutions of CuEDTA buffered with potassium biphthalate (KHP). When the SCE is immersed in the above solution for a few hours, the measured

Figure 14. Construction of Room Temperature Potentiometric Cell.

- A. Reservoir, 1400 mL beaker.
- B. Teflon- coated stirring magnet.
- C. Vented ceramic platform, for liquid circulation.
- D. Exit point of heated delay coil.
- E. Room temperature delay coil, 0.5 m of 0.5 mm I.D. tubing.
- F. Flow-through cupric ion-selective electrode, for details, see text.
- G. Exit tube to waste (1400 mL beaker).
- H. Saturated calomel reference electrode.
- I. Reservoir of 0.1 M KNO_3 for reference electrode.
- J. "Thirsty glass" (porous Vycor) electrical junction, between reference electrode reservoir and waste reservoir.
- K. Ground electrode, stainless steel hypodermic needle.



potential drifts randomly, and the effect gets progressively worse with time. When the SCE is removed to a flask of deionized water for an hour and placed back in the CuEDTA/KHP solution, the drift disappears. We postulate that KHP is precipitating in or at the outside edge of the ceramic junction, since the inner electrode solution is saturated KCl (~ 4.6 M) and this flows out through the plug. If the flow is blocked partially, it would seriously affect the liquid junction potential across the plug in incalculable ways. We also did not know if any other components of the analyte were incompatible with the SCE.

The second reason for isolating the SCE from the analyte occurs when using a dip-type electrode in a stirred beaker. The isolation prevents any chloride ion from flowing into the analyte, as chloride can cause an interference in a cupric-ion electrode. In order to make conditions identical for flowing and batch experiments, an isolated SCE is used in both cases.

The "common" electrode needed for the electrometer is a stainless steel hypodermic needle placed in the beaker. The type of electrode used here is noncritical, since both the measuring and reference electrodes are referred to its potential, and this common-mode potential is cancelled out by the electrometer circuitry. For this reason, this simple third connection proved to be adequate.

D. Electrode Sensing Material

We made the electrode material of a mixed copper-silver sulfide, following the general recommendations of Heijne and van der Linden (78). All chemicals we used were reagent grade, and deionized water

was used in all solutions. We performed all work up to drying of the final precipitate in a glove bag with constant N_2 flow.

We first prepared 50 mL of each of two solutions, one 0.67 M in $AgNO_3$ (Drake Brothers, Menomonee Falls, WI 53051) and 0.33 M in $Cu(NO_3)_2$ (J.T. Baker Chemical Co., Phillipsburg, NJ 08865), and the other 1.5 M in Na_2S (Mallenkrodt Chemical Works, St. Louis, MO 65160). In some early work, solids contained in the bottle of $Cu(NO_3)_2$ used would not dissolve completely in deionized water, and electrodes made using this $Cu(NO_3)_2$ did not behave reproducibly.

The solution of Na_2S contained suspended particles, assumed to be insoluble heavy metal sulfides. To prevent contamination of the electrode material by these particles, we filtered the solution at room temperature through Whatman No. 40 filter paper (Clifton, NJ 07014) before further use.

We stirred the solutions in 250 mL beakers on a magnetic stirrer for at least thirty minutes before further manipulation to remove oxygen. Electrodes made from degassed solutions have a lower limit of $Cu(II)$ response and show less effect of air oxidation in use than those made from air-saturated solutions (78).

Plastic bags filled with ice were then placed around the solution vessels to cool them to approximately $10^{\circ}C$ as stirring continued. The mixed $AgNO_3/Cu(NO_3)_2$ solution was then drawn into a 50 mL volumetric pipet, and added to the 50 mL of sulfide solution at a rate of approximately one drop per second. During this time, the sulfide solution was stirred magnetically just below the point of splashing onto the side of the beaker. The ice bag was kept around the side to prevent heating by

the reaction. A black precipitate formed immediately upon mixing of the reactant solutions, and as addition of the $\text{AgNO}_3/\text{Cu}(\text{NO}_3)_2$ continued, the power applied to the magnetic stirrer had to be increased, since the suspension thickened. If the temperature of the black suspension exceeded 15°C , addition was halted until the temperature again dropped to 10°C .

The suspension was stirred and heated at 70°C for thirty minutes after addition of the $\text{AgNO}_3/\text{Cu}(\text{NO}_3)_2$ solution ended. The precipitate was then allowed to settle and cool to room temperature (ca. 3 hours). The yellow supernatant was then poured off. A 100 mL volume of water at room temperature was then added and stirred, and the precipitate allowed to settle (5 min). The supernatant was again poured off. In this manner, the precipitate was washed with consecutive 100 mL volumes of room temperature water (a second time), hot ($80\text{--}90^\circ\text{C}$) water, room temperature water, room temperature 0.1 M HNO_3 , room temperature water, and room temperature acetone. Although CS_2 was recommended by Thompson and Rechnitz for a final rinse (77), it was not used in this work because it seemed to have no beneficial effect and had been reported elsewhere to degrade the membrane material (78). All supernatants were clear, and the precipitate showed no visual change until the addition of the acetone, when the particles began to move around rapidly in the solvent.

After the last wash, the precipitate was poured onto a watch glass and nitrogen was passed directly over the surface of the solid to dry it. After two hours, the precipitate was placed in a 60 mL capped amber glass bottle.

We did not grind and sieve the finished electrode material, since we have found that grinding it in a mortar and pestle aggregates the precipitate, making it hard to sieve. We found no loss in performance (transient response, calibration curves) or physical properties (hardness, ability to polish to a smooth surface) of the electrodes prepared from unsieved vs. sieved material, in contrast to Thompson and Rechnitz (77) who said that the two types gave identical electrochemical response, but the sieved material produced electrodes which were easier to polish.

E. Flow-through Electrode Design

We studied two basic designs of flow-through electrodes, the first in which the sample stream passes through a hole in the electrode pellet, as suggested by Thompson and Rechnitz (77), and the second in which the analyte stream flows past a flat surface of the electrode pellet, contained in a removable cap fitted around the pellet.

To make flow-through electrodes of the first kind, we used the following procedure: A pellet 1.3 cm in diameter containing from 0.5 to 1.5 g of electrode material was pressed at 75,000 to 100,000 p.s.i. for 20 minutes or longer. Pressures and times of pressing were found not to be critical within these limits. We roughened the surfaces of the pellet with 400-600 grit emery cloth with water as a lubricant. We then roughened approximately 1 cm on the end of a copper wire with sandpaper and affixed this end to the circumference of the pellet with silver-impregnated conductive epoxy (E-solder #3017, Acme Chemicals and Insulation Co., New Haven, CT 06505). The assembly was then placed in an oven overnight at 100°C. We then cast the pellet and wire into the

center of a disk of polyester coating resin (#199-0150, Triarco Arts and Crafts, Inc., Wheeling, IL 60090) formed by a glass tube 2.5 cm diameter by 2.5 cm thick, with the flat faces of the pellet roughly parallel to those of the resin disk. This was allowed to set for at least 24 hours. The glass tube was then broken off, and the flat surfaces sanded to remove incompletely cured resin.

The flat faces of the disk were then tapped at their centers for Altex-type connectors (1/4 x 20 thread), and a hole drilled between the two taps through the pellet. We prepared a variety of electrodes, whose channel diameters ranged from 0.3 to 1.5 mm. They were polished by repeatedly drawing through a string coated with a 0.05 μ m alumina slurry (Fisher "Gamal," Itasca, IL 60143).

We judged the roughness of the channel through the electrode pellet by observing the magnitude of a shift in potential when the flow rate through the electrode was changed, or by "flow noise," potential fluctuations synchronous with flow pulses from the pump used.

Some authors (77,106) have stressed the importance of polishing a pressed-precipitate electrode in order to achieve fast response and stability under conditions of changing flow rate. Rough electrode surfaces can be so sensitive to changes in flow rate across them, that pump pulses can cause fluctuations on electrode potential. Others (62,82,88,112) mention polishing of the electrode as part of their procedure without further explanation. We have found that a smooth electrode surface is essential for a steady (non-fluctuating) potential under constant Cu(II) concentration flow.

It was possible to produce quiet and fast electrodes with a channel through the pellet, but they could not be consistently made. During drilling and polishing of the channel, the pellet often separated from the resin disk. This could be seen as a white ring spreading across the pellet surface from the channel during polishing, and resulted in an electrode with flow noise and flow-related baseline shifts. The resin could not be made to seal back to the pellet by heating to the softening point, and the electrode had to be discarded.

Epoxies which would adhere to the electrode pellet were tried in place of the casting resin, but electrodes made in this way did not respond to Cu(II). This approach was abandoned.

To make electrodes of the second type (liquid flow past a flat surface), we first pressed a similar pellet of electrode material, and sanded all edges. A 1 cm length of copper wire was again roughened and formed into a tight loop. This wire was then affixed to the center of one of the flat sides with silver-impregnated epoxy (E-solder #3021). This pellet was then placed on a glass plate in the center of a 1.5 cm hole in a Teflon disk 0.3 cm in height. Polyester casting resin was then poured over the pellet and allowed to cure overnight.

The next day the assembly was removed from the mold and the side of the casting opposite the wire ground to the pellet's surface wetted with 600-grit emery cloth. The other flat surface of the resin was ground parallel to this side with a flat grinding attachment on a Dremel Moto-tool. We then polished the exposed surface of the electrode pellet with 0.3 μm and 0.05 μm alumina (Micropolish, Buehler, and Gamal, grade B, Fisher) on a soft paper mat until no further

improvement of smoothness or flatness of the electrode was apparent upon further polishing.

The electrode cap is shown in Figure 15. It consists of two main elements: (1) the body, which contains the channels for liquid flow and defines the active area of the electrode pellet, and (2) a threaded insert to press the electrode onto the body of the cap and ensure mechanical sealing of the electrode surface to the body of the cap.

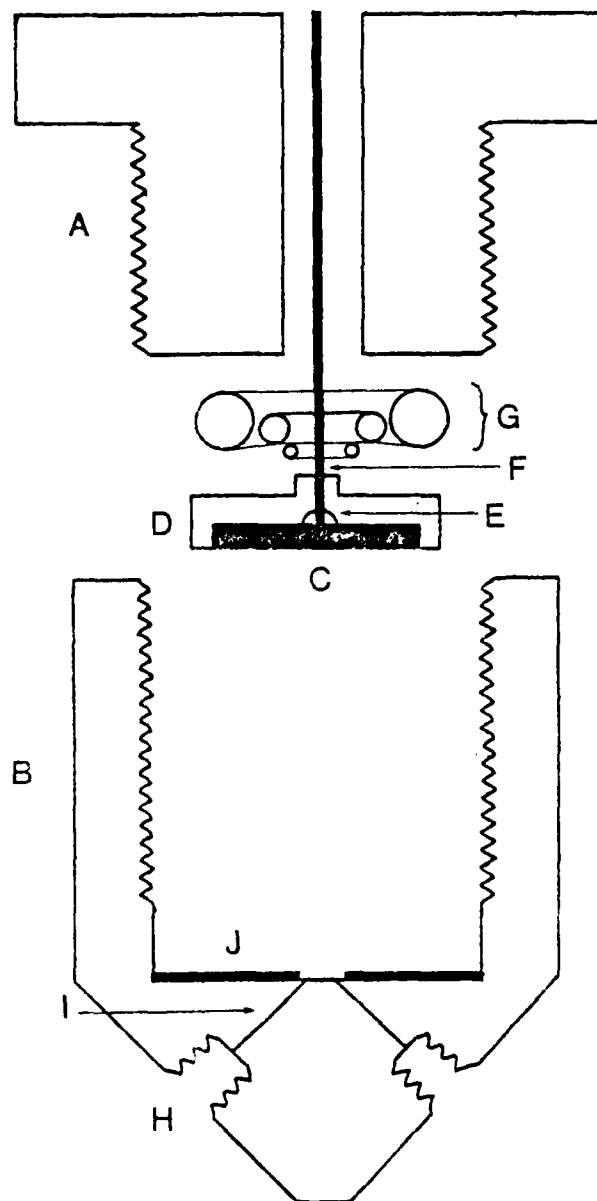
The body was made from a nylon rod 2.5 cm in diameter and 3 cm long. One end was cut at a 45° angle to the axis on two opposite sides. The newly cut faces were tapped for Altex-type connectors along a diameter of the rod. Channels 0.03 cm in diameter were then drilled from the center of these taps to intersect on the axis of the rod. A 1.9 cm diameter threaded hole was tapped from the opposite end, which extends slightly past the point at which the two channels intersect. The bottom of this hole was ground flat so that the surface shows two holes less than 0.25 cm apart.

On this surface is placed a Teflon gasket 0.008 cm thick and 1.9 cm in diameter with a 0.32 cm hole in the center. This hole defines the wetted surface of the electrode. For this reason the gasket must be flexible and compressible enough to mold to the electrode surface and nylon cap under moderate pressure.

If the electrode surface and gasket do not seal without gaps at the exact edge of the hole, then some liquid will be trapped between the two surfaces. This trapped liquid "activates" the electrode surface it contacts, and the potential of the electrode depends on the Cu(II) concentration both in this volume and in the hole in the gasket. Since

Figure 15. Construction of Flow-through Cupric Ion-selective Electrode.

- A. Threaded insert, nylon, 3 cm long.
- B. Body of electrode cap, nylon, 3 cm long x 2.5 cm diameter.
- C. Electrode pellet, 1.3 cm diameter x 1-2 mm thick, for preparation, see text.
- D. Polyester casting resin support, for preparation, see text.
- E. Conductive epoxy, silver-filled.
- F. Insulated copper wire.
- G. "O"-ring assembly, consisting of three "o"-rings: $3/16 \times 1/16$ in. (O.D. x cross-section), $1/4 \times 1/16$ in., and $3/8 \times 1/8$ in.
- H. Tapped hole, to fit Altex connector, $1/4 \times 20$ thread.
- I. Solution flow channel, 0.3 mm diameter.
- J. Teflon gasket, 0.08 mm thick, 1.9 cm. diameter, with 0.32 cm hole in center, for preparation, see text.



the trapped liquid is not flushed from the electrode surface, the transient response of the electrode is severely degraded.

To facilitate sealing of the inside edge of the gasket to the membrane, we press the gasket in a circular die 1.9 cm in diameter with a taper of approximately 0.005 cm towards the center. This makes the center of the gasket slightly thicker than the periphery. Thus, when the flat electrode surface is pressed against the gasket, the first contact is at the edge of the hole. This makes a more reproducible seal between the electrode and gasket than using an unpressed gasket. Each gasket is used once only, because the pressure between the electrode and cap tends to flatten the gasket.

The insert for the back of the electrode is threaded to fit the body, the bottom is flattened, and the top is hexed. There is a 0.6 cm diameter hole along the axis through which the wire extends to the electrode pellet.

There are three O-rings ($3/16 \times 1/16$, $1/4 \times 1/16$, $3/8 \times 1/8$ in. (I.D. \times C/S) between the electrode in the resin disk and the insert. These three O-rings serve to compensate for the top and bottom of the electrode disk not being parallel. Silicone grease is applied to the bottom of the insert to allow the O-rings to slip along the surface and evenly distribute the pressure applied in screwing the insert into the body of the electrode cap.

One great advantage to this type of flow-through electrode is the fact that it can be assembled and disassembled repeatedly. Different electrode pellets or gaskets can be used interchangeably. There is generally a maximum of thirty minutes before a freshly polished

electrode settles to a steady-state potential (± 0.1 mV) at 10^{-6} M free Cu^{2+} activity. Electrodes which have been disassembled and reassembled without repolishing generally reach this steady-state potential within five minutes.

F. CuEDTA Solution Preparation

Since the magnitude of the detector response depends on both the initial and final concentrations of free Cu(II) in solution, a precise method of regulating the background free Cu(II) is imperative.

To prepare a solution of CuEDTA with a reproducible composition, we prepared crystalline $\text{CuH}_2\text{EDTA} \cdot \text{H}_2\text{O}$, modifying slightly the method of Kirschner (113). We first prepared 500 mL of 0.52 M $\text{CuSO}_4 \cdot \text{H}_2\text{O}$ (Fisher Certified Reagent) in deionized water. To this we added 0.25 moles of ethylenediaminetetraacetic acid (EDTA, "Baker Analyzed" Reagent) in approximately eight aliquots over the course of an hour. During this addition, the solution was heated to 90°C and stirred on a Corning heated magnetic stirrer. After approximately the first half of the EDTA was added, crystals precipitated from solution and would not redissolve. This contradicts Kirschner's results (113), as he reported that all material went into solution.

Because of the solubility problem, a 4% excess of CuSO_4 was used. It is much more soluble in strongly acidic solution than free EDTA, so any excess CuSO_4 can be washed off of the final preparation, whereas excess EDTA is incorporated into the precipitate, disturbing the apparent stoichiometry of the complex.

After the final addition of EDTA, the reaction mixture was stirred at 90°C for one hour. Heat was then turned off, and the solution was stirred overnight.

We then filtered the solution through Fisher Qualitative filter paper in an 11 cm Buchner funnel, applying suction. The precipitate was then washed in the funnel with two 500 mL volumes of deionized water and dried at 80°C overnight.

Assuming that the only material in the precipitate was either CuEDTA, free $\text{Cu}(\text{NO}_3)_2$, or H_4EDTA , the preparation was determined to be within 0.01% of a 1:1 (Cu:EDTA) stoichiometry using a cupric-ion selective electrode (vide infra).

The solution of CuEDTA used in the detector was prepared by dissolving 0.01 mole of $\text{CuH}_2\text{EDTA} \cdot \text{H}_2\text{O}$ (MW = 371.62) and 0.10 mole of KNO_3 in approximately 900 mL of deionized water, adjusting the pH to 4.00 with KOH and HNO_3 , and diluting to 1.0 L in a volumetric flask. Before the final pH adjustment, we added solid KOH to expedite the dissolution of the CuEDTA. KNO_3 was used in the solution to fix ionic strength so that we could assume constant activity coefficients for Cu(II) ions.

This solution was degassed by bubbling with helium through a glass frit between five and ten minutes. This was important to prevent formation of bubbles in the flow system which would interrupt the electrical continuity between the measuring and reference electrodes. This technique has recently been proposed as a method for preventing bubble formation in HPLC solvents (110), especially when using partially aqueous solvents, since the solubility of most gases in water is much lower than in organic solvents.

G. Calibration for metal response

When calibrating the detector response for metals, a pumping-depulsing system identical to the pump system in the detector and a sampling valve with a 5 mL loop was placed before the junction with the detector stream. This arrangement allows a plug sample of metal ion solution up to 5 mL in volume to be injected and the spreading and dilution arising from the detector studied. The background solution (constantly pumped) was 0.1 M KNO_3 , and all metal ion calibration solutions were prepared in this background. All metal ion calibration solutions were prepared from 0.1 M stock solutions (in 0.1 M KNO_3) by serial dilution using a single 5 mL class A pipet and 50 mL class A volumetric flask. Between preparation and use, the solutions were stored in glass stoppered 50 mL volumetric flasks. Solutions were prepared with the following metal ion concentrations (M): 10^{-2} , 3×10^{-3} , 10^{-3} , 3×10^{-4} , 10^{-4} , 3×10^{-5} , 10^{-5} , 3×10^{-6} , 10^{-6} , and 3×10^{-7} .

IV. Results and Discussion

A. Dip-type Electrodes

1. Cu(II) response in KNO_3 background.

The cupric ion-selective electrodes produced in this laboratory were first tested for their response in Cu(II) solutions as dip-type electrodes. This was done to confirm that electrodes made from the preparation used have a Nernstian response to Cu(II) concentration. An electrode was immersed in 200 mL of 0.1 M KNO_3 and 10^{-7} M $\text{Cu}(\text{NO}_3)_2$ with isolated saturated calomel reference and inert ground electrodes as was previously described, and varying amounts of 0.1 M $\text{Cu}(\text{NO}_3)_2$ were added until the solution was approximately 0.01 M in $\text{Cu}(\text{NO}_3)_2$. The data are plotted in Figure 16 as steady-state electrode potential above the original potential against the logarithm of the added molar $\text{Cu}(\text{NO}_3)_2$ concentration.

The slope of the plot is 29.4 ± 0.08 mV/decade $[\text{Cu}(\text{NO}_3)_2]$ at room temperature. This compares favorably with the theoretical Nernst slope of 29.6 mV/decade $[\text{Cu}(\text{NO}_3)_2]$ at 25°C (Equation 1). Response was linear, and the electrode potential settled quickly. Less than 10 seconds were required for the electrode potential to approach within 1 mV of steady-state when the bulk concentration changed from 10^{-7} to 3×10^{-7} M $\text{Cu}(\text{NO}_3)_2$ and this time was reduced to less than 5 seconds for a 3×10^{-3} to 10^{-2} M $\text{Cu}(\text{NO}_3)_2$ concentration jump.

Figure 16. Steady-state Response of Dip-type Cupric Ion-selective Electrode to Added Cu(II).

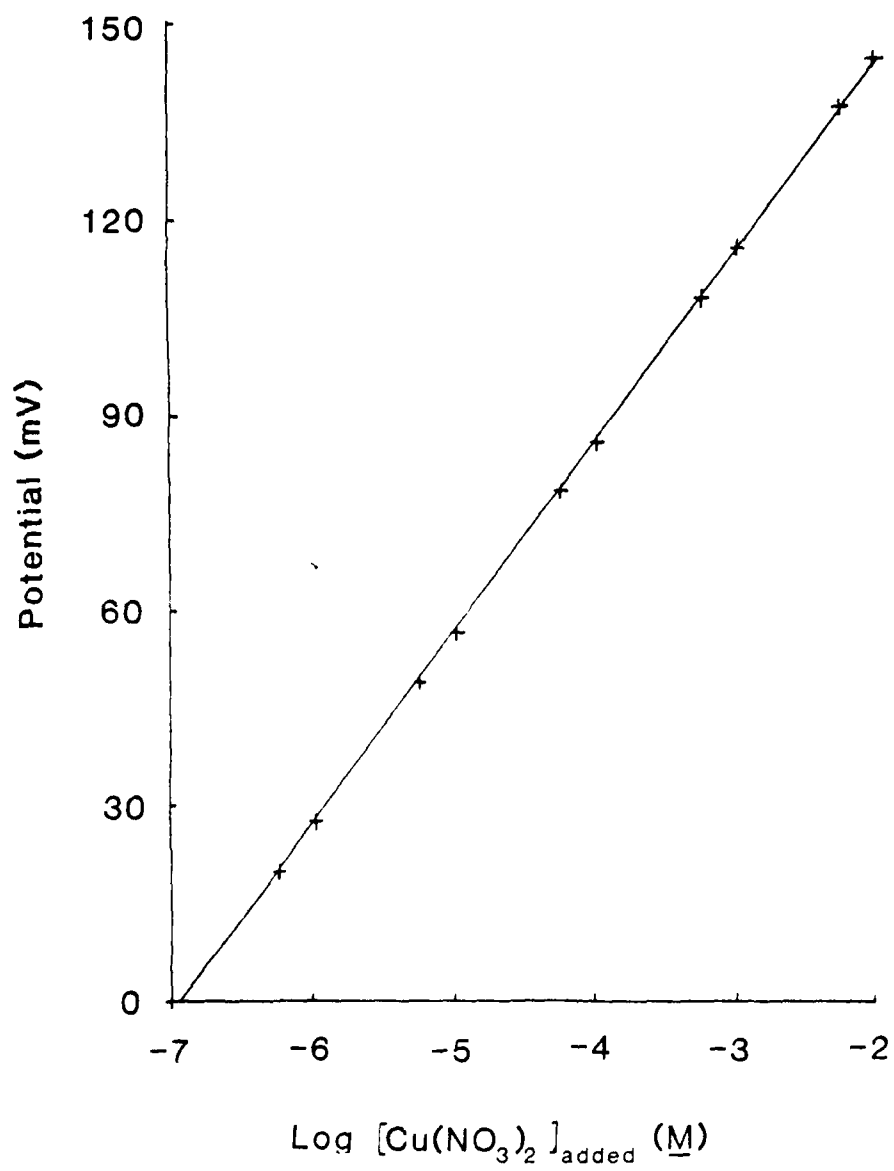
Ion-selective electrode was constructed as described in text. Potentiometric cell consisted of cupric ion-selective electrode, isolated saturated calomel reference electrode (see text), and stainless steel needle common electrode (Figure 14). Potentials plotted are the total change in cell potential from potential in initial solution, 10^{-7} M $\text{Cu}(\text{NO}_3)_2$ in 0.1 M KNO_3 , 25°C. $\text{Cu}(\text{NO}_3)_2$ was successively added to concentrations shown (corrected for dilution).

Linear least-squares analysis:

Slope = 29.36 ± 0.08 mV/decade $[\text{Cu}(\text{II})]$.

Correlation coefficient = 0.99998.

Student's "t" = 419.



2. Cu(II) response in CuEDTA background.

The electrode was then immersed in 200 mL of 0.1 M KNO_3 and 0.01 M CuEDTA solution (prepared as above) which was adjusted to pH 4.00 with KOH and HNO_3 . $\text{Cu}(\text{NO}_3)_2$ was added to the solution as before, and the results are shown in Figure 17. As can be seen, the response is slightly distorted at low $\text{Cu}(\text{NO}_3)_2$ levels. We postulate that this is due to the residual level of free Cu(II) in the original CuEDTA. If 10^{-6} M Cu(II) is assumed to exist in solution prior to addition, the plot of potential above background vs total Cu(II) is linear, with a slope of 30.7 ± 0.09 mV/decade [Cu(II)] at room temperature. The slight difference between this slope and the slope of Figure 16 is due to the fact that measurements were made on different days and at slightly different temperatures.. Imprecision in the slope of a calibration course of this magnitude is not unusual for ion-selective electrode systems (see Table IX, Section IV.C.3).

It is very reasonable to assume that the amount of free Cu(II) found is due to CuEDTA dissociation, since it compares well to the value calculated from literature values of K_{CuEDTA} and the acid dissociation constants of EDTA. In 0.1 M KNO_3 , $\log K_{\text{CuEDTA}}$ has been calculated to be 18.80 (115) and the pKa's (stepwise dissociation constants) for EDTA have been found to be 2.0, 2.67, 6.16, and 10.26 (106). Using these values in Equations 46-48, we calculate a residual free Cu(II) concentration of 69×10^{-7} M under the above conditions. A free Cu(II) level of 10^{-6} M, then, points to a stoichiometry of the prepared solid CuEDTA complex of less than 1.0001:1 (Cu:EDTA).

Figure 17. Steady-state Response of Dip-type Cupric Ion-selective Electrode to Added Cu(II) in Equimolar CuEDTA.

Ion-selective electrode, potentiometric cell, and potential measurements are the same type as in Figure 16. The initial solution was 0.01 M CuEDTA in 0.1 M KNO₃, pH adjusted to 4.0 with HNO₃ and KOH, 25°C. For preparation of CuEDTA, see text.

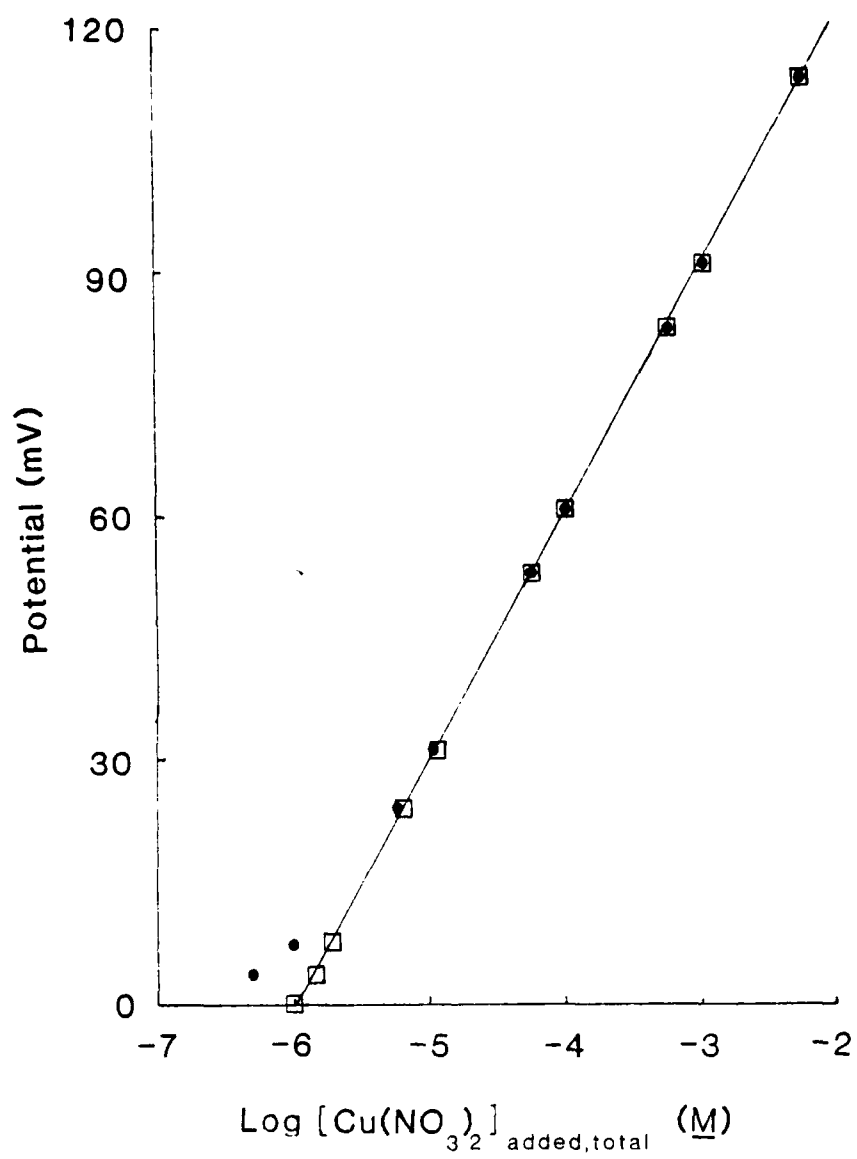
- A. Concentration of Cu(II) added as Cu(NO₃)₂ (•).
- B. Total concentration of Cu(II), assuming 10⁻⁶ M Cu(II) in initial solution (see text) (□).

Linear least-squares analysis:

Slope = 30.56 ± 0.09 mV/decade[Cu(II)].

Correlation coefficient = 0.99998.

Student's "t" = 412.



3. Potential noise and drift in solutions of constant Cu(II) concentration.

The cell potential using well-polished cupric ion electrodes showed a drift of less than 1 mV over several hours (SCE reference electrode) in unthermostatted solutions containing $\text{Cu}(\text{NO}_3)_2$ solutions at 10^{-6} M or higher concentrations. (The temperature coefficient of the cell potential for a cell containing a SCE and cupric ion electrode of this type has been found to be $0.92 \text{ mV}/^\circ\text{C}$ (116)). The potential was independent of stirring rate from rest (unstirred solution) to several hundred RPM with a magnetic stirrer.

However, the instantaneous cell potential oscillated about the average potential at the same frequency as the rotation of the magnetic stirring bar in solution. Unfiltered, the oscillation amounted to as much as 20 mV peak-to-peak. Because of this, in all recorded measurements we used a 1 sec time constant low-pass filter between the electrometer and recorder. This lowered the observed oscillations below 5 mV peak-to-peak.

4. Other metal ion response in KNO_3 background.

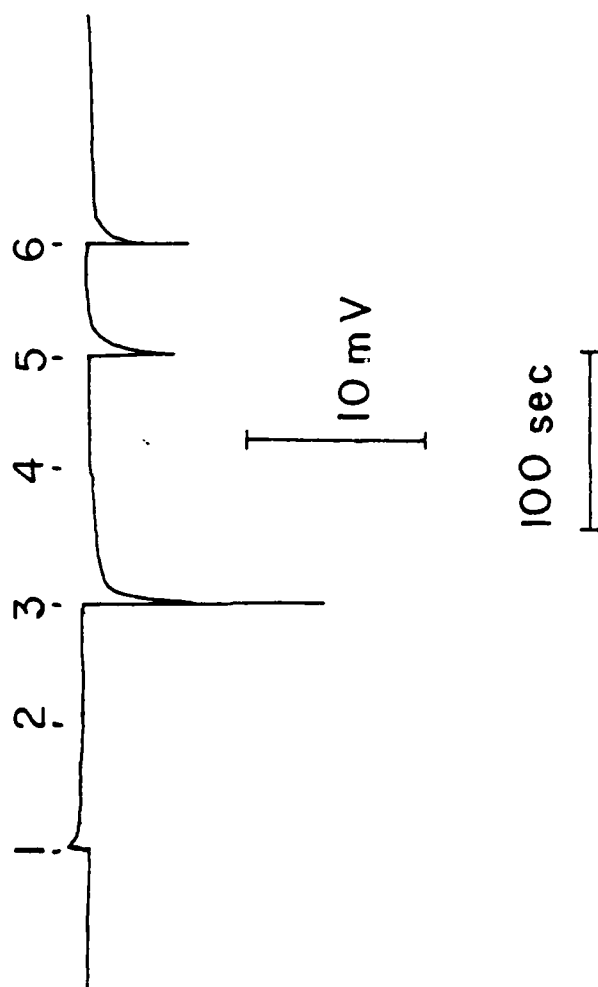
The electrode was immersed in 200 mL of 10^{-7} M $\text{Cu}(\text{NO}_3)_2$ and 0.1 M KNO_3 . We introduced 20 mL of 0.01 M solutions of the following salts successively into the solution: $\text{Zn}(\text{NO}_3)_2$, $\text{Co}(\text{NO}_3)_2$, NiCl_2 , $\text{Ca}(\text{NO}_3)_2$, CdCl_2 , and MnCl_2 . A potential vs time trace of the experiment is given in Figure 18. Introduction of the metal nitrates effects negligible change in the potential observed, demonstrating the selectivity of the electrode for Cu(II) over these other metals, but introduction of the metal chlorides causes a significant transient potential spike in the

Figure 18. Time-dependent Response of Dip-type Cupric Ion-selective Electrode to Various Metal Ion Salt Solutions.

Ion-selective electrode and potentiometric cell are the same as in Figure 16. The initial solution was 10^{-7} M $\text{Cu}(\text{NO}_3)_2$ in 0.1 M KNO_3 . Trace is the cell potential as a function of time.

10^{-3} M metal salt solutions were added at the following points:

1. $\text{Zn}(\text{NO}_3)_2$.
2. $\text{Co}(\text{NO}_3)_2$.
3. NiCl_2 .
4. $\text{Ca}(\text{NO}_3)_2$.
5. CdCl_2 .
6. MnCl_2 .



direction of decreased Cu(II) concentration, although the steady-state potential is changed less than 1 mV. This agrees with Midgeley's observations of sharp transients upon exposing a cupric ion electrode to potassium chloride (76).

5. Other metal ion response in CuEDTA background.

Since, as indicated above, most metals do not influence the potential of the cupric ion electrode, any change in electrode potential upon introduction of a metal salt into a CuEDTA solution must come from Cu(II) displaced from the complex.

We introduced various metal ion solutions into CuEDTA solution to demonstrate the response of the electrode under these conditions. Figure 19 is a series of traces of metal ion injections into CuEDTA at room temperature and pH 4.0. This figure shows both the dynamic and steady-state potential response for injections of $\text{Cu}(\text{NO}_3)_2$, $\text{Pb}(\text{NO}_3)_2$, CdCl_2 , $\text{Co}(\text{NO}_3)_2$, and MnCl_2 as representative of the metal ions the detector is useful for. In the cases of CdCl_2 and MnCl_2 , the sharp negative transients due to addition of chloride ion are evident. The magnitudes of the steady-state responses are results of the various formation constants for the MEDTA complexes and the Cu(II) in the original solution. In these studies, we used CuEDTA prepared by titration of $\text{Cu}(\text{NO}_3)_2$ with EDTA and subsequent pH adjustment. Control of the stoichiometry was not as precise as when crystalline CuEDTA was employed.

The displacement of Cu(II) by Mn(II) in Figure 19 is significant in terms of the applicability of the electrode to detection different metal ions. The ratio of the formation constants of MnEDTA to CuEDTA

Figure 19. Time-dependent Displacement of Cu(II) from Equimolar CuEDTA by Various Metal Ions.

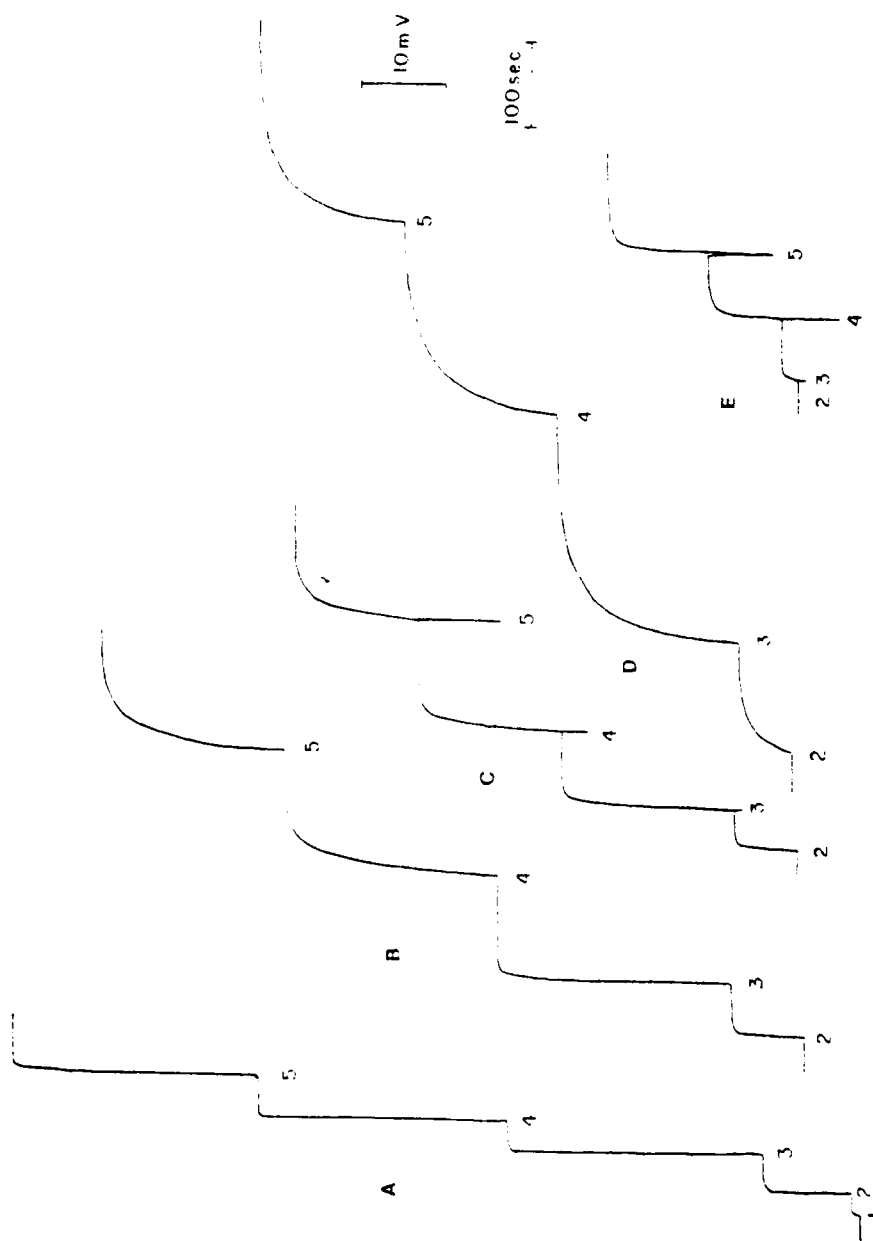
Ion-selective electrode and potentiometric cell are the same as in Figure 16. The initial solution was 0.01 M CuEDTA (titrated to equivalence point) in 0.1 M KNO₃, pH adjusted to 4.0 with HNO₃ and KOH, 25°C. Traces shown are cell potential as functions of time due to Cu(II) liberated from CuEDTA. Absolute cell potentials are offset for display purposes.

Solutions added:

- A. Cu(NO₃)₂.
- B. Pb(NO₃)₂.
- C. CdCl₂.
- D. Co(NO₃)₂.
- E. MnCl₂.

Concentrations of solutions added at points of addition:

- 1. 10⁻⁶ M.
- 2. 10⁻⁵ M.
- 3. 10⁻⁴ M.
- 4. 10⁻³ M.
- 5. 10⁻² M.



(β , Equation 61) is approximately 10^{-5} (115). As can be seen, injection of 10^{-4} M MnCl_2 is easily detected. Thus, detection of most of the transition row metals is thermodynamically feasible with this detector system.

The first trace in Figure 19 is not displacement of Cu(II) from the CuEDTA complex, but addition of $\text{Cu}(\text{NO}_3)_2$. This shows that the electrode response is much faster (< 5 seconds for 97% response, within 0.5 mV of steady-state potential) than the displacement rate of metals into the CuEDTA complex. Thus, the cupric ion electrode is appropriate for a kinetic study of this type. This is a very fast cupric ion electrode based on previous reports; the time needed to reach steady-state is controlled by the time constant of the low-pass filter.

Of the reports in the literature dealing with ligand exchange kinetics between Cu(II) and a second metal ion (100-105), only two deal with the second metal reacting with CuEDTA (100a, 104). The metals involved are Pb(II) and Ni(II), both of which form an EDTA complex of approximately the same strength as Cu(II). This points out a significant advantage of using an ion-selective electrode in studying EDTA displacement from CuEDTA - namely, many metals can be studied, since very small increases in the free Cu(II) concentration can be seen. This is not possible using spectrophotometry with many metals, as Bydalek and Margerum did with Ni(II), since the CuEDTA spectrum can mask any absorbance from free Cu(II) (104).

We did not attempt any detailed kinetic studies, because our interest was in finding conditions for fast exchange reactions for the detector. In Table IV, we have listed the times to half-reaction

Table IV. Apparent Half-reaction Times ($t_{1/2}$) for the Metal Exchange Reactions^a

[M] injected (M)	$t_{1/2}$ for the following metal ions (sec)							
	Pb(II) ^b	Cd(II) ^b	Co(II) ^b	Mn(II) ^b	Zn(II) ^c	Zn(II) ^d	Zn(II) ^e	Ni(II) ^f Ni(II) ^g
10^{-5}	-	-	-	-	60	12	3	300 5
10^{-4}	3	4	22	-	80	24	2	160 10
10^{-3}	10	5	18	-	30	22	3	140 15
10^{-2}	12	8	15	6	-	10	4	- -

a. $t_{1/2}$ is defined as the time required for the electrode potential to reach a point 9 mV below steady-state, where $[\text{Cu(II)}] = \frac{1}{2}[\text{Cu(II)}]_{\text{equilibrium}}$.

b. Conditions as in Figure 19.

c. Conditions as in Figure 20A (pH = 6).

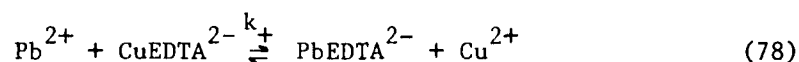
d. Conditions as in Figure 20B (pH = 5).

e. Conditions as in Figure 20C (pH = 4).

f. Conditions as in Figure 21A (Temp = 45°C).

g. Conditions as in Figure 21B (Temp = 75°C).

($t_{1/2}$) of the exchange of EDTA with the metals in the figures in this section. These are the points after injection of a metal ion that the free Cu(II) concentration was half the final (equilibrium) free Cu(II) concentration when the electrode potential remained constant. The data and trends with pH and concentration of metal ion are in qualitative agreement with the literature, as follows. For the reaction between Pb(II) and CuEDTA,



k_+ is a sum of three rate expressions, and varies inversely with [Pb(II)] below 10^{-2} M. At 10^{-3} M Pb(II), pH 4, $k_+ = 1.4 \text{ sec}^{-1} \text{ M}^{-2}$. This corresponds to a $t_{1/2}$ of 49 sec for a 10^{-3} M Pb(II) injection into a 0.01 M CuEDTA, since CuEDTA is in excess, and this is thus a pseudo-first order reaction (117) where

$$[\text{CuEDTA}]k_+ = \frac{0.693}{t_{1/2}} \quad (79)$$

The value of $t_{1/2}$ is not in good agreement with our data. However, Tanaka et al. (100a) studied the system in strong acetate buffer and had to make massive corrections for the buffer's complexing ability.

Our data indicate an inverse dependence of the reaction rate with increasing concentrations of Pb(II), Zn(II), and Cd(II) (see Figures 19 and 20). As was stated, Tanaka et al. found this for Pb(II) (100a), and they concluded in subsequent papers that the mechanism of reactions of CdEDTA and ZnEDTA with Cu(II) was analogous, so we can expect to see such a trend with these metals also. Ligand exchange with these metals is thought to be a two-step process, with one complex dissociating

before the second forms. It is possible that the formation of a transitory three-body complex, M-EDTA-Cu can slow the exchange reaction, if the complex has some appreciable stability. This has been found to be the case for the exchange of CyDTA between Cd(II) and Pb(II) or Cu(II) (104a).

The acid catalysis of the exchange of EDTA between Zn(II) and Cu(II) is shown in Figure 20, where the pH is varied from 6.0 to 4.0. The reaction is decidedly faster at lower pH within the limits of this study. In addition, at pH 6, a precipitate forms upon injection of 10^{-3} M $\text{Zn}(\text{NO}_3)_2$. This sets an upper limit on the allowable Zn(II) concentration at high pH.

The disadvantage of lowering the pH is the fact that the residual Cu(II) level is raised. This raises the detection limit for metals, according to Equation 48 and Figure 20. Therefore, a compromise must be reached between residual Cu(II) level and metal displacement kinetics. We believe that a pH of 4.0 is this optimum, since metal ions in the micromolar range can be seen, and the reaction proceeds at a sufficient rate to be useful for our detector.

In Figure 21, the effect of temperature on the kinetics of Ni(II) displacement of Cu(II) from EDTA at pH 4.0 is shown. This reaction is not pH-dependent (104), so that lowering the pH will not lead to a more favorable kinetic situation. Because of the sluggishness of the reaction at low temperature, the solution must be heated to at least 75°C to allow the reaction to proceed to completion within a reasonable time.

These experiments demonstrated that the detector system is applicable to detection of metal ions in concentrations below 10^{-5} M. They

Figure 20. pH Dependence of Kinetics of Zn(II) Displacement of Cu(II) from Equimolar CuEDTA.

Ion-selective electrode, potentiometric cell, initial solution (except pH), and type of traces shown are the same as in Figure 19.

- A. Solution adjusted to pH 6.0, phosphate buffer.
- B. Solution adjusted to pH 5.0, phosphate buffer.
- C. Solution adjusted to pH 4.0, phosphate buffer.

Concentrations of $\text{Zn}(\text{NO}_3)_2$ solutions added at points of addition:

- 1. 10^{-5} M.
- 2. 10^{-4} M.
- 3. 10^{-3} M.
- 4. 10^{-2} M.

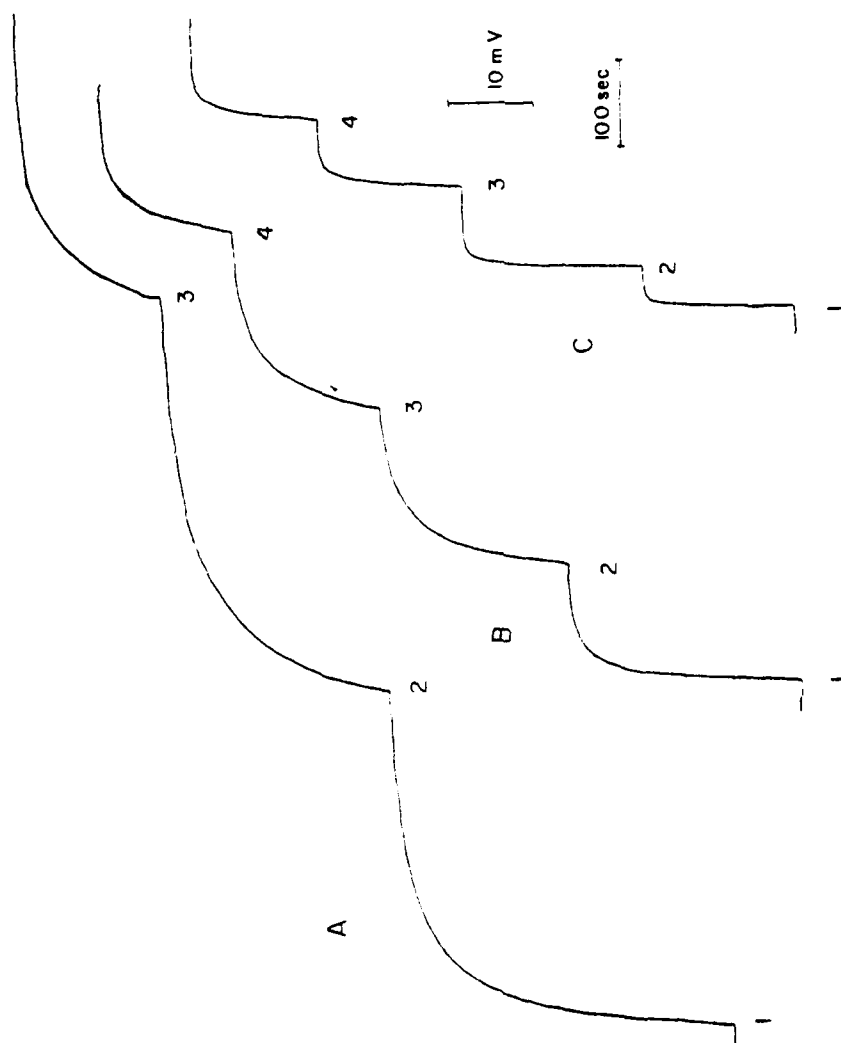


Figure 21. Temperature Dependence of Kinetics of Ni(II) Displacement of Cu(II) from Equimolar CuEDTA.

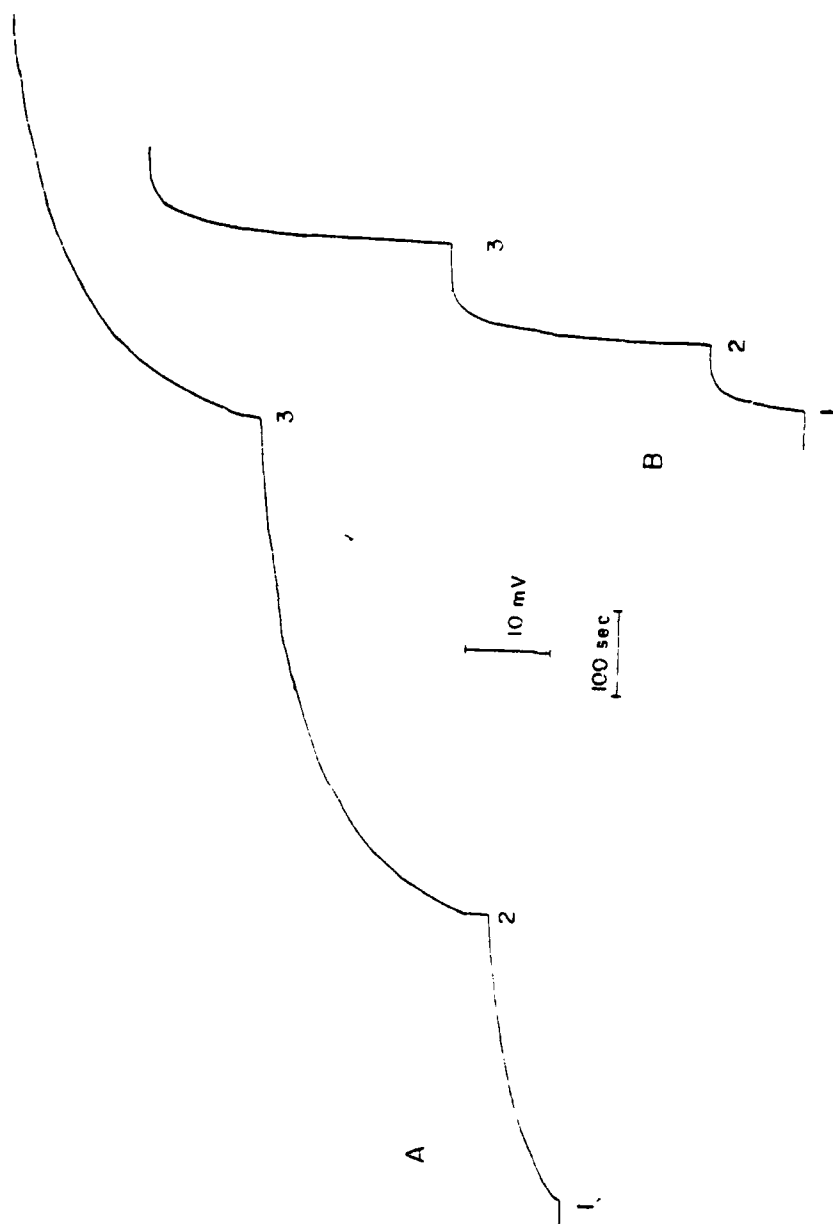
Ion-selective electrode, potentiometric cell, initial solution (except temperature), and type of traces shown are the same as in Figure 19.

A. Solution 45°C.

B. Solution 75°C.

Concentrations of $\text{Ni}(\text{NO}_3)_2$ solutions added at points of addition:

1. 10^{-5} M.
2. 10^{-4} M.
3. 10^{-3} M.



also showed that a pH of 4.0 or below and temperature of over 75°C are required for acceptable chemical kinetics for some of the slower species.

Metals were tested for compatibility with the chemical system used in the detector by dissolving 10^{-3} M metal salt in water and injecting the solution into 0.01 M CuEDTA at pH 4.0 and 75°C. Displacement of Cu(II) was followed by a dip-type cupric ion electrode. Polyvalent metal salts which either would not dissolve in deionized water or precipitated upon introduction into CuEDTA included $\text{Tl}(\text{NO}_3)_3$, $\text{Bi}(\text{NO}_3)_3$, $\text{Tl}(\text{S})_4)_2$, $\text{Zr}(\text{SO}_4)_2$, SnCl_2 , $\text{In}(\text{NO}_3)_3$, and $\text{Th}(\text{NO}_3)_4$. According to solubility constants in the literature, SnCl_2 , $\text{Tl}(\text{NO}_3)_3$, and $\text{In}(\text{NO}_3)_3$ should be soluble at pH 4, but we did not find this to be the case. In addition, $\text{Th}(\text{NO}_3)_4$ precipitated upon addition to 0.01 M CuEDTA, pH 4, although it was soluble in 0.1 M KNO_3 (pH not adjusted).

B. Flow-through Electrodes

1. Cu(II) response in KNO_3 background.

As before, the flow-through electrodes were first tested for Cu(II) response in KNO_3 background. We passed a 10^{-6} M $\text{Cu}(\text{NO}_3)_2$ and 0.1 M KNO_3 solution over the electrode surface, and varying concentrations of $\text{Cu}(\text{NO}_3)_2$ were introduced into the flowing stream with a sampling valve and 5 mL sample loop. The steady-state potentials were then recorded and a plot of steady-state potential vs $\log [\text{Cu(II)}]$ added is shown in Figure 22 for the concentration range of 10^{-6} to 10^{-2} M $\text{Cu}(\text{NO}_3)_2$. Again the plot is linear, with a slope close to the theoretical Nernst slope.

Figure 22. Steady-state Response of Flow-through Cupric Ion-selective Electrode to Added Cu(II).

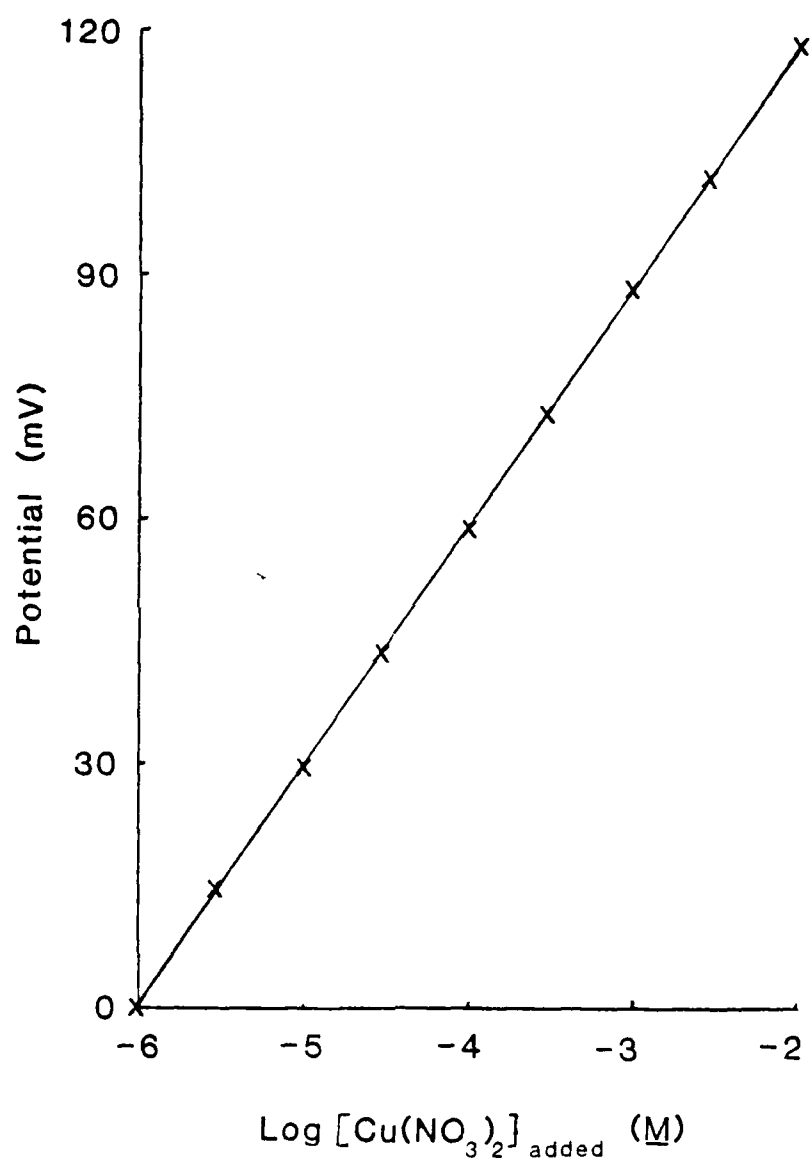
Flow system and flow-through electrode (Figure 15) were constructed as described in text. Potentiometric cell consisted of flow-through cupric ion-selective electrode, isolated saturated calomel reference electrode (see text), and stainless steel needle common electrode. Potentials plotted are the differences in cell potential from initial conditions, 10^{-6} M $\text{Cu}(\text{NO}_3)_2$ in 0.1 M KNO_3 , 25°C. Samples were solutions of $\text{Cu}(\text{NO}_3)_2$ at concentrations shown in 0.1 M KNO_3 . Flow rate was 1.0 mL/min.

Linear least-squares analysis:

Slope = 29.5 ± 0.14 mV/decade[Cu(II)].

Correlation coefficient = 0.99992.

Student's "t" = 211.



2. Cu(II) response on CuEDTA background.

The flow-through electrodes were tested for response to $\text{Cu}(\text{NO}_3)_2$ added to 0.01 M CuEDTA at pH 4.0. A plot of steady-state potential vs. added $[\text{Cu}(\text{NO}_3)_2]$ is shown in Figure 23. The linearized plot assumes 1.6×10^{-6} M Cu(II) present in the original CuEDTA solution. This again is reasonable for the conditions involved and point to a Cu:EDTA ratio of less than 1.0001:1 in the prepared solid.

3. Potential noise and drift in solutions of constant Cu(II) concentration.

The background noise and drift of the final version of the flow potentiometric system is shown in Figure 24. The flowing solution was again 0.1 M KNO_3 + 0.01 M CuEDTA, with the pH adjusted to 4.0. Short term noise is less than 0.1 mV peak-to-peak, and the drift of the average potential over one hour is less than 0.15 mV. Thompson and Rechnitz (77) have shown that flow-through electrodes with rough surfaces exhibit a shift in potential when the flow rate of solution past the electrode is changed. In Figure 24B, the initial flow rate of solution is 2.0 mL/min. At point X (spike added), the flow rate was changed to 0.5 mL/min. The long-term change in potential for a four-fold change in flow rate is less than the inherent noise of the system. This shows that the electrode surface can be made smooth and "clean" enough to give potentials and noise levels essentially independent of flow rate.

4. Dynamic response to changes in Cu(II) concentration.

Time-dependent response of the flow-through electrode to an increase and decrease of Cu(II) concentration is shown in Figure 25.

Figure 23. Steady-state Response of Flow-through Cupric Ion-selective Electrode in Equimolar CuEDTA to Added Cu(II).

Flow system, flow-through ion-selective electrode, potentiometric cell, and potential measurements are the same as in Figure 22. The original solution was 0.01 M CuEDTA (prepared as in text) in 0.1 M KNO₃, adjusted to pH 4.0 with KOH and HNO₃. Samples were solutions as above with added Cu(NO₃)₂. Flow rate was 1.0 mL/min.

- A. Concentration of Cu(II) as added Cu(NO₃)₂ (+).
- B. Concentration of Cu(II), assuming 1.6×10^{-6} M Cu(II) in original solution (see text) (☐).

Linear least-squares analysis:

Slope = 29.7 ± 0.18 mV/decade[Cu(II)].

Correlation Coefficient = 0.99987.

Student's "t" = 163.

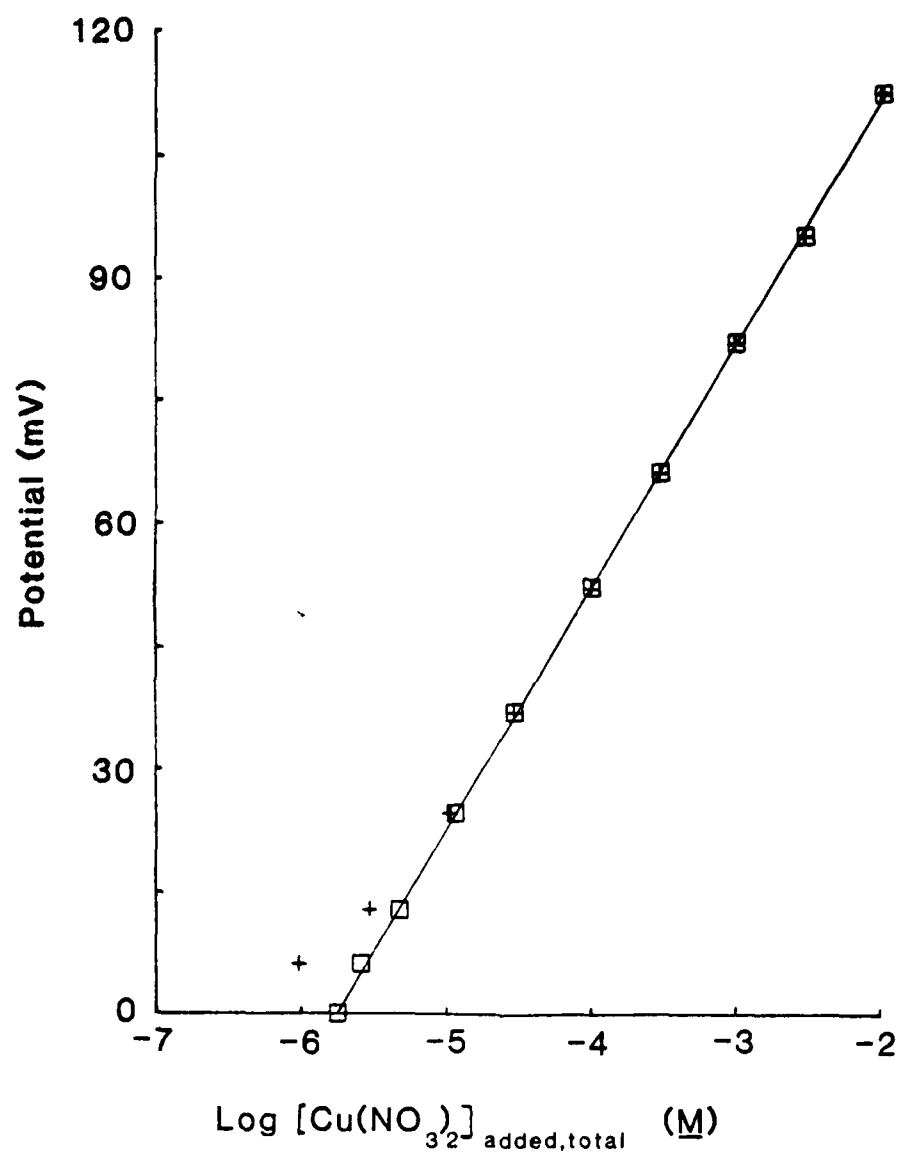


Figure 24. Background Noise and Drift of Flow-through Cupric Ion-selective Electrode.

Flow system, flow-through ion-selective electrode, potentiometric cell, and flowing solution are the same as in Figure 23. No samples were introduced. Traces are cell potentials as functions of time.

A. Flow rate 2.0 mL/min.

B. Initial flow rate 2.0 mL/min, at point X, changed to 0.5 mL/min.

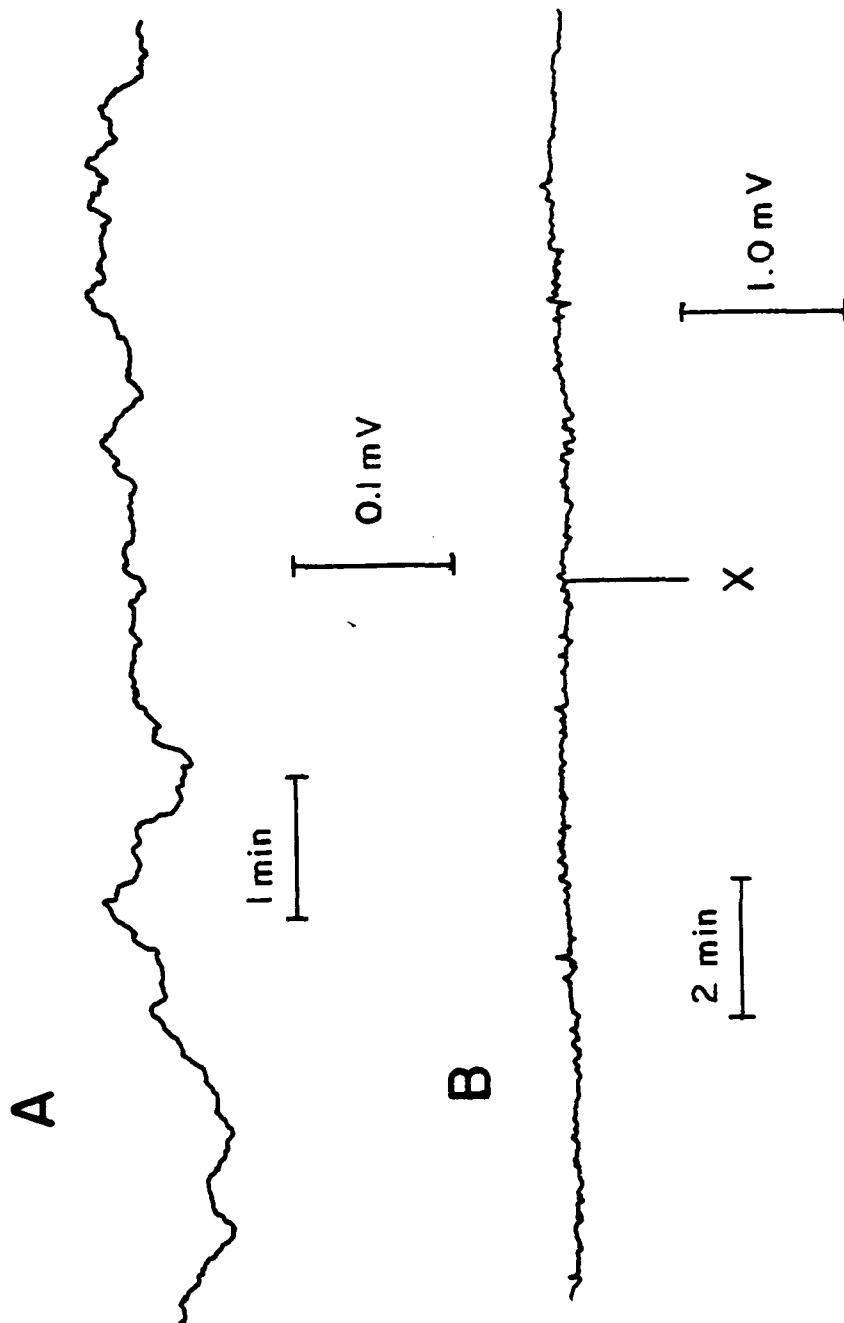


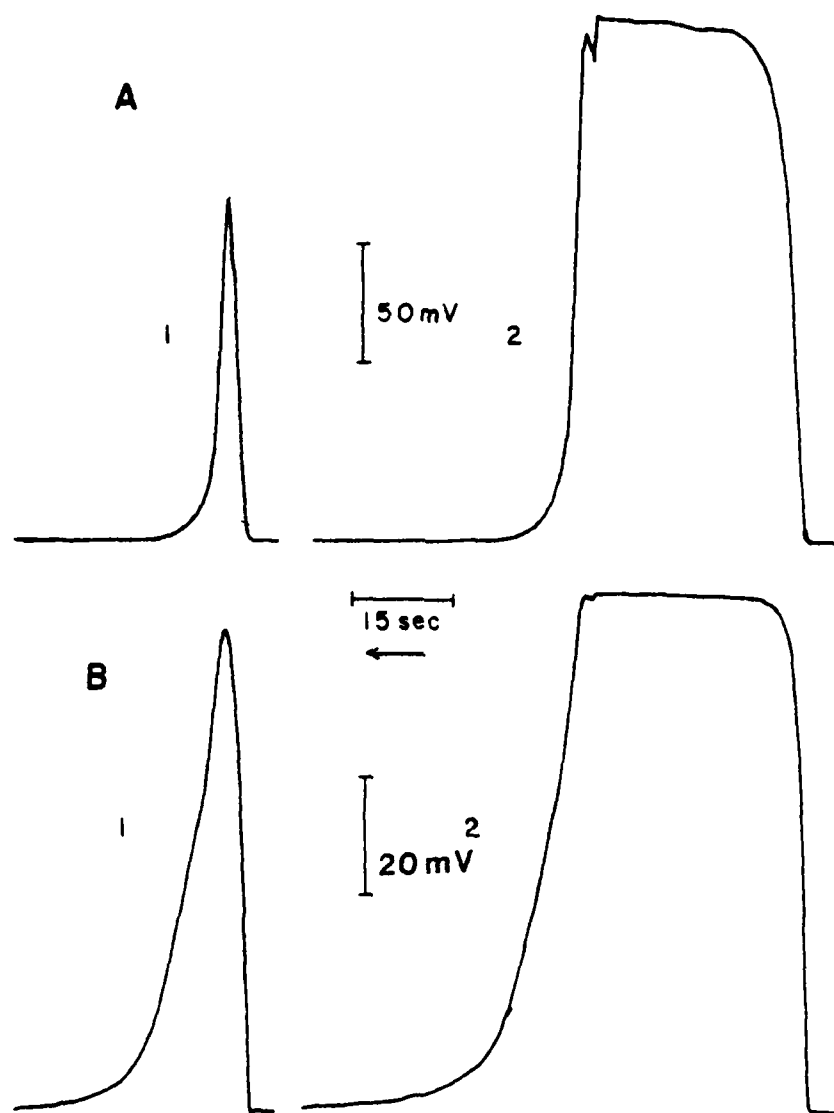
Figure 25. Dynamic Response of Flow-through Cupric Ion-selective Electrode.

Flow system configuration is as in Figure 13, although without delay coil. The column effluent flow was simulated by an identical pumping/pulse dampening system, with a 5 mL sample loop placed between the pulse dampener and junction. (E, Figure 15). The reactant channel solution was 0.01 M CuEDTA (prepared as in text) in 0.1 M KNO_3 , pH adjusted to 4.0 with KOH and HNO_3 , 25°C. Column effluent solution was simulated by 0.1 M KNO_3 , and sample solution was 10^{-4} M $\text{Cu}(\text{NO}_3)_2$ in 0.1 M, KNO_3 , 25°C. Flow-through electrode and potentiometric cell were the same as in Figure 23. Flow rate was 1.0 mL/min/channel.

- A. Concentration response (antilogarithm of potential, assuming 29.6 mV/decade[Cu(II)]) as a function of time.
- B. Cell potential as a function of time.

Samples of the following volumes were injected:

1. 50 μL .
2. Volume required to reach steady-state potential.



The measuring apparatus is configured similar to the detector calibration apparatus (two-channel pump, streams combined), but no delay coil was inserted between the stream juncture and flow-through electrode. The combined stream flow rate was 2.0 mL/min, and the two solutions contained 0.01 M CuEDTA and 0.1 M KNO_3 (background and sample). The solution in the sample loop was 10^{-4} M $\text{Cu}(\text{NO}_3)_2$ + 0.1 M KNO_3 .

Figure 25B is the potential response directly from the electrode, and Figure 25A is the response of the system linearized (after antilog transducer). Curves 1 are 50 μL injections from a timed loop (3 sec), which makes 100 μL samples when combined with the background stream. Curves 2 are long-loop injections where the signal was allowed to reach essentially steady-state level. The spike at the end of Curves 2A and 2B was caused by the switching of the sample loop valve, causing a momentary blockage of flow in that channel and thus a temporary flow of low Cu(II) concentration before the line leading from the valve to the stream junction is flushed out.

The figure shows the apparent spreading effect of direct potential measurements. The potential signal is expanded with respect to a true concentration signal at low concentrations and compressed as concentration increases. If the electrode response is approximated at 30 mV/decade (Nernst slope, Equation 1, for a divalent ion), then 9 mV below the peak signal represents half the concentration of the peak.

The rise and fall curves of the steady-state peaks can be crudely approximated by a simple exponential in this experiment. Data are tabulated in Table V for the experiment described above over a range of flow rates from 0.5 to 4.0 mL/min total. The various values of τ will

Table V. Dynamic Concentration Response of Flow through Electrode^a

Flow Rate (mL/min)	$\omega_{1/2}$ ^b		Rise			Fall		
	(sec)	(μ L)	τ_1 ^c (sec)	τ_2 ^c (sec)	τ_3 ^c (sec)	τ_1 ^d (sec)	τ_2 ^d (sec)	τ_3 ^d (sec)
0.5	11.8	98	2.9	3.0	3.9	3.8	4.0	5.5
1.0	5.2	86	2.3	1.8	1.7	1.5	1.4	1.6
2.0	2.5	84	2.7	2.5	2.7	1.5	1.6	1.9
4.0	1.7	112	1.2	1.2	1.2	1.9	1.7	1.8

a. Conditions: Valve connected to detector with less than 10 μ L of tubing. Sample loop total volume 5.0 mL. Background channel 0.01 M CuEDTA, pH 4.0, sample channel 0.1 M KNO₃, sample loop 10⁻⁴ M Cu(NO₃)₂ + 0.1 M KNO₃. All measurements at room temperature.

b. Width at half-height for 100 μ L (combined streams) injection.

c. Time constants (τ_1, τ_2, τ_3) were calculated from the time required to rise to 63%, 86%, and 95% of the steady-state signal, respectively.

d. Time constants (τ_1, τ_2, τ_3) were calculated from the time required to fall to 63%, 86%, and 95% of the steady-state signal, respectively.

all be equal only if the data fit a true exponential equation, and this is not quite true here. The measurement is complicated by the presence of low-pass filters after both the electrometer and antilog transducer with approximately one second time constants. Thus, the electronic filtering is not small enough to prevent interaction with the electrode's dynamic response.

For two reasons, we were satisfied that the electrode per se was not a major limiting dynamic factor as it was in the early stages of this work. First, the experimental half-width was essentially equal to the sample volume for small-volume injections (Table V). This indicates a minimum of mass dispersion in the electrode. Second, the time constant of the electrode (and electronics) is relatively very short compared to the other time constants (i.e., mass dispersion in the delay coil, see IV.C.1) in the assembled detector. The variance of an observed peak (σ_T) is related to the variance in the peak itself (σ_p) and the spreading due to the observation system (σ_s) according to the following equation:

$$\sigma_T = \sqrt{(\sigma_p)^2 + (\sigma_s)^2} \quad (80)$$

In this case, in order to obtain the spreading of the peak due only to the electrode, we must use the spreading due to an exponential response to a step function. Sternberg (122) has found that for the function

$$f(t) = 1 - \exp(-t/\tau) \quad (81)$$

where τ is the first-order time constant,

$$\sigma^2 = \tau^2 \quad (82)$$

or

$$\sigma = \tau$$

(83)

Since this is the case, and Equation 80 shows that variances spread geometrically, we can calculate that a τ for the electrode of 2 sec will affect the spreading of a peak by less than 5% if the peak itself is over ten seconds long. In Section IV.C.1, we have shown that peaks are intrinsically longer than that except at high flow rates (4.0 mL/min total flow rate), and thus the response time of the electrode is negligible.

The fact that we were able to approximate an exponential electrode response function is significant, even though the fit of our data to an exponential curve is not perfect. This points mechanistically to a mass-transfer response process for this particular electrode, which is one of the main theoretical models of electrode response. One significant advantage in using a flow-through electrode to demonstrate a mass-transfer electrode mechanism rather than a dip-type electrode suspended in a solution is that liquid flow across the surface of the electrode is controlled much better with a flow-through electrode than with a dip-type electrode. Laminar or turbulent flow past a flow-through electrode surface can be sustained or changed at will by varying the flow rate and/or flow stream dimensions. A mass-transfer response mechanism will show a marked difference between the rate of response under laminar and turbulent flow conditions, with much slower response under laminar flow. This was shown by Mertens (57), who compared response rates using Auto-analyzer (laminar flow) and homemade jet-impact (turbulent flow) equipment. The flow past an electrode

suspended in a stirred solution is complicated, and any mass-transfer mechanism may result in fast electrode response. None of the mechanistic conclusions reached above can then be found using a suspended dip-type electrode.

Our experiments showed that our electrode design has very fast response compared to the few reports found in the literature in dynamic response of flow-through electrodes under similar conditions. Thompson and Rechnitz (77) show from data presented in their paper that a well polished Cd(II) electrode requires approximately six seconds to reach within 3 mV of steady-state (79% concentration response) for a 10^{-5} to 10^{-4} M Cd(II) concentration jump. Van der Leest (118) constructed a chloride-selective flow-through electrode which required approximately 30 seconds to respond to within 6 mV (79% concentration change) of steady-state for a chloride concentration change from 2×10^{-4} M to 5×10^{-3} M. With a flow-through cupric ion electrode, Van der Linden and Oostervink (28) claim 90% response in six seconds (corresponding to a first-order time constant of 2.6 seconds) for a change in cupric ion concentration between two unspecified levels. The fact that the two cupric ion levels were not specified makes this figure impossible to compare our experimental results, since the rate of approaching steady-state for a concentration change depends strongly on the initial and final levels of measured ion concentration (61,62, Section II.C.6).

C. Assembled Detector System

1. Dynamic Response to Changes in Cu(II) Concentration.
 - a. Dynamic response to varying sample size.

We constructed the detector as described in Section III.C. The

delay coils (2.5 m of 0.05 cm I.D. tubing heated and 0.5 m of 0.05 cm I.D. tubing at room temperature) were chosen for a delay time of 37 sec at 1 mL/min flow rate, which we determined would allow most metal ion-CuEDTA reactions tested to reach equilibrium. The sample loop was 5 mL in volume (5 m of 0.8 mm I.D. tubing) and samples of varying size were injected by switching the sample loop into the flowing stream for specific timed intervals.

Injections of 10^{-4} M $\text{Cu}(\text{NO}_3)_2$ in 0.1 M KNO_3 were made of 50, 100, 200, 300, 500, and 1000 μL nominal volumes at flow rates of 0.25, 0.50, 1.0, and 2.0 mL/min/channel. Traces of the concentration (antilog) response at the electrode are shown in Figure 26 for the injections at 1.0 mL/min/channel. These show the changing size and shape of the output with the volume of sample injected.

In this work, we have used the peak width of half maximum ($\omega_{1/2}$) due to its ease of measurement as an experimental measure of dispersion. To compare results directly with theory, it is necessary to compute the peak variance. For the 50 μL peaks at each flow rate, we computed the variance according to its statistical definition

$$\sigma = \sqrt{\frac{\sum h_i (t_i - \bar{t})^2}{\sum h_i}} \quad (84)$$

where h_i is the height of the peak at time t_i and \bar{t} is the time of the peak mean, computed by the formula

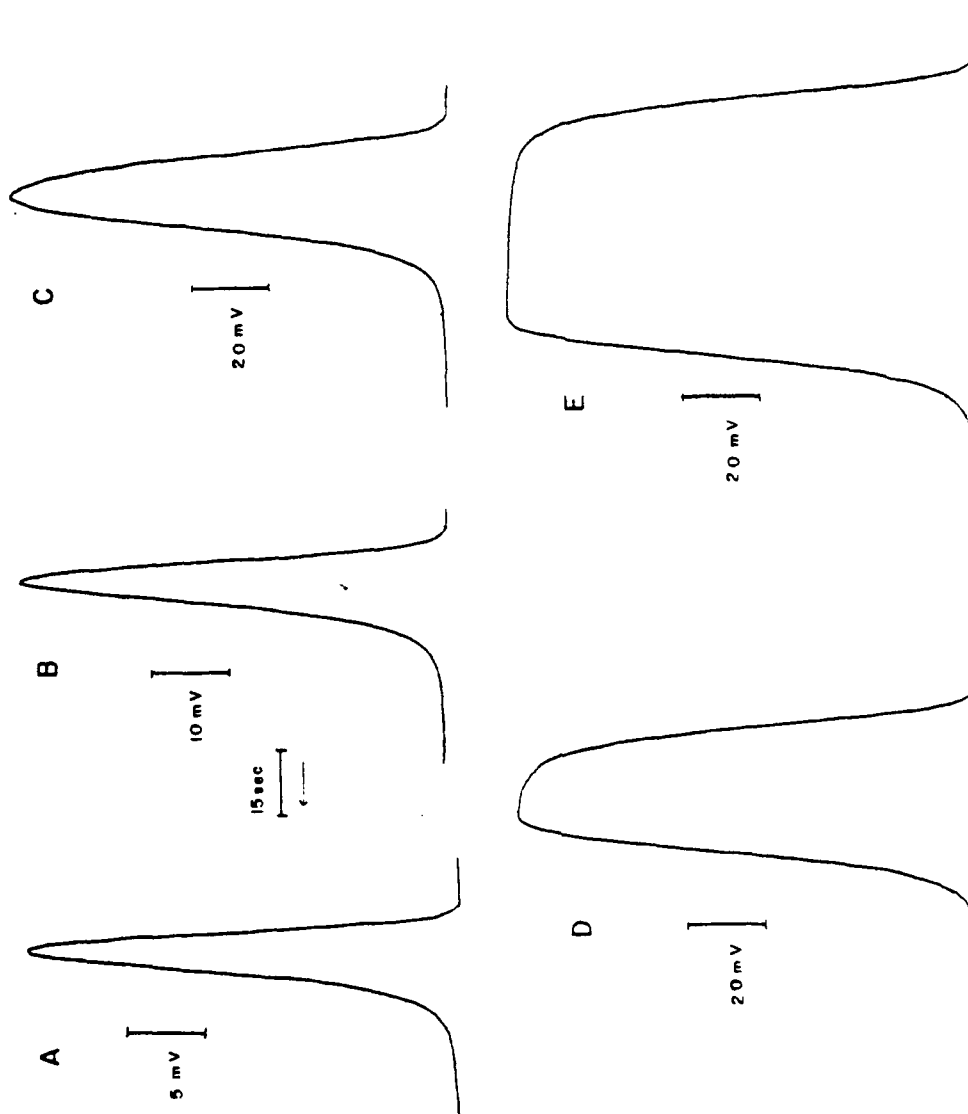
$$\bar{t} = \frac{\sum h_i t_i}{\sum h_i} \quad (85)$$

Figure 26. Dynamic Detector Response as a Function of Sample Volume.

Flow system was constructed as in Figure 25, but including the following delay coils in series: 2.0 m of 0.5 mm diameter Teflon tubing heated to 75°C, 0.5 m of 0.5 mm diameter Teflon tubing, room temperature. Solutions used were identical to those in Figure 25, and flow-through electrode and potentiometric cell were the same as in Figure 23. Flow rate was 1.0 mL/min/channel. Concentration response (as in Figure 25) was used.

Nominal volumes injected (see text):

- A. 50 μ L.
- B. 100 μ L.
- C. 300 μ L.
- D. 500 μ L.
- E. 1000 μ L.



Since data acquisition was manual, only 9 to 12 points were taken per curve. Variances for 50 μL input peaks are necessarily broader than those which would have been obtained for a true "delta" or "impulse" function. We estimated $\omega_{1/2}$ for an impulse function by graphically extrapolating $\omega_{1/2}$ for finite sample volumes to a sample volume of zero, as in Figure 27 for a flow rate of 0.5 mL/min/channel. This value, termed $\omega_{1/2}^0$, was then multiplied by the quantity $\sigma/\omega_{1/2}$ for the 50 μL peaks to obtain the variance for an impulse response (σ_{exp}) in Table VI.

Peak symmetry and $\omega_{1/2}/\sigma$ values for the 50 μL peaks decrease with increasing flow rate. This is caused by the two processes controlling the peak dispersion, laminar ("streamlining") flow of the liquid through the tube, and radial diffusion of solute molecules in the liquid. As discussed in the section on streaming potentials in ionic fluids (I.C.5), liquid at the center of a confined flowing stream will move at a faster rate than liquid at the walls of the tube, due to stagnation at the liquid-surface interface and the viscosity of the liquid. This produces an asymmetrical concentration profile ("tailing") across the length of the peak, with the leading edge of the peak comprised of the solute moving through the center of the tube, and the trailing edge comprised of solute moving in the flow lines closer to the walls of the tube. Radial diffusion tends to counteract this phenomenon by transporting solute molecules across the velocity gradients, reducing dispersion and making the peak more symmetrical.

Taylor has shown that a finite time is required for laminar convection and radial diffusion to interact so that the flow profile reaches

Figure 27. Peak Width at Half Height Squared as a Function of Sample Volume Squared for the Detector.

Conditions were identical to Figure 26, except the flow rate was 0.5 mL/min/channel. Concentration response (as in Figure 25) was used.

Upper line: theoretical line of $\omega_{1/2}^2 / V_s^2 = 2.0^2$, with intercept $(350 \mu\text{L})^2$.

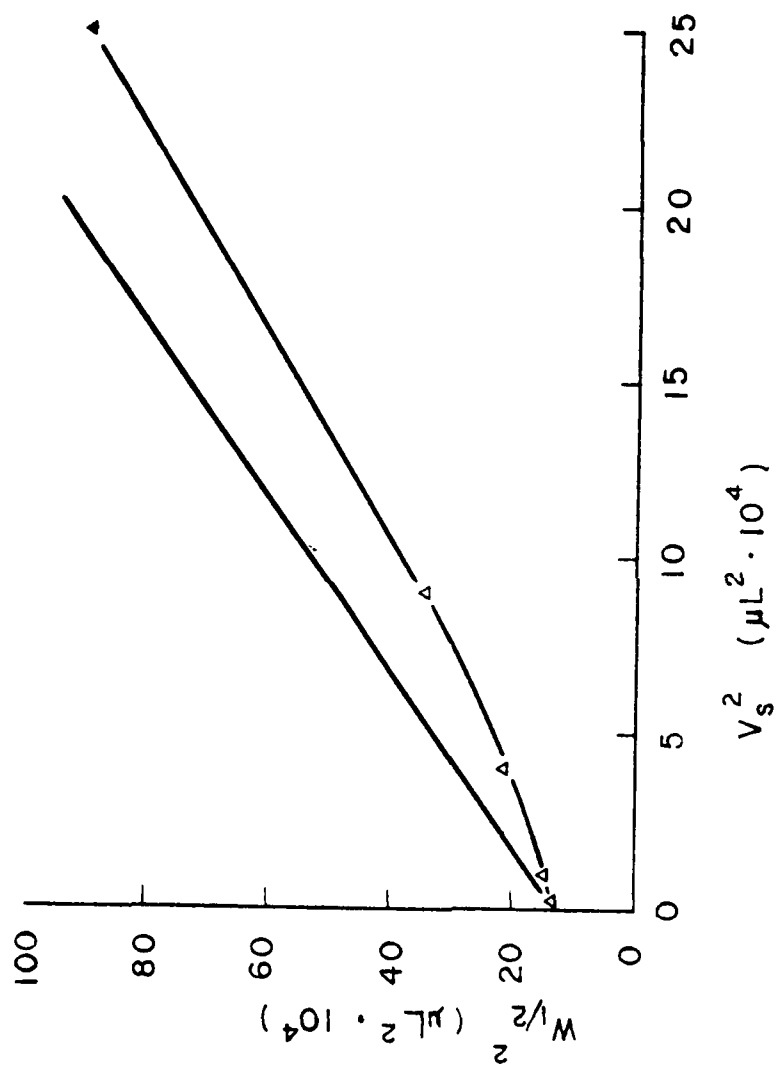


Table VI. Evaluation of Dispersion Due to the Detector.^a

Flow Rate (mL/min/ channel)	$\omega_{1/2}/\sigma$ ^b	$\omega_{1/2}^0$ ^c (μ L)	σ_{exp} ^d (μ L)	σ_{theory} ^e (μ L)	(slope of $\omega_{1/2}^2$ vs V_s^2) ^{1/2} , ^f
0.25	2.17	350	161	160	1.62
0.5	1.75	353	201	226	1.85
1.0	1.69	345	204	320	1.75
2.0	1.11	320	289	452	1.5 , 2.0 ^g

a. Detector configuration and conditions are given in Figure 26. Samples were 10^{-4} M $\text{Cu}(\text{NO}_3)_2$ in 0.1 M KNO_3 , volumes were estimated by timing the amount of sample injected.

b. Ratio of peak width at half-maximum height to variance for a 50 μ L sample. The variance of the peaks was determined graphically (see text).

c. Obtained as the y-intercept of the plot of $(\omega_{1/2})^2$ as a function of sample size squared (V_s^2). A representative plot is shown in Figure 27.

d. Product of $\omega_{1/2}^0$ and $(\omega_{1/2}/\sigma)^{-1}$.

e. Values were computed from Equation 96, using $r = 0.025$ cm, $L = 300$ cm, $D_m = 5 \times 10^{-6} \text{ cm}^2 \text{ sec}^{-1}$, and $F =$ indicated flow rate (mL/sec total).

f. Slopes were computed from data at 300 μ L and 500 μ L sample volumes.

g. Slope was computed from data at 500 μ L and 1000 μ L sample volumes.

steady-state, namely (119),

$$T_{ss} = r^2 / 14.4 D_m \quad (86)$$

where T_{ss} is in seconds, r is the radius of the tube (cm), and D_m is the molecular diffusion coefficient ($\text{cm}^2 \text{sec}^{-1}$). For CuCl_2 in 0.1 M NaCl (similar to our system), $D_m = 5 \times 10^{-6} \text{cm}^2 \text{sec}^{-1}$ (121), and $r = 0.025$ cm, thus $T_{ss} = 8.7$ sec. In our system, the transit time through a tube of 0.5 mL volume ranges from 60 sec (0.25 mL/min/channel flow rate) to 7.5 sec (2.0 mL/min/channel flow rate). Thus, in our system, Taylor's criterion is not always satisfied. Residence times less than that described by Equation 85 result in asymmetrical peaks, as reported by Hofmann and Halasz (120).

In Table VI, σ_{exp} values are compared to σ_{theory} obtained from Taylor's equation for dispersion of solutes in liquids flowing in a tube (119):

$$\bar{C} = \frac{M}{\pi r^2} \left(\frac{\exp[-(L-x)^2 / L^2 4\delta]}{2(\pi\delta L^2)^{1/2}} \right) \quad (87)$$

In this equation, \bar{C} is the concentration (molar) of a solute measured at distance x (cm) from the point of injection of the solute into a flowing stream, M is the absolute quantity (moles) of solute injected into the tube, r is the radius of the tube (cm), L is the distance (cm) from the point of injection to the point of maximum solute concentration, and δ is a dimensionless dispersion number,

$$\delta = D_a t / L^2 \quad (88)$$

Here, t is the time (sec) for the liquid to traverse the distance L , and D_a is termed the axial diffusion coefficient, given by the formula (120)

$$D_a = D_m + r^2 u^2 / 48 D_m \quad (89)$$

D_m is the molecular diffusion coefficient ($\text{cm}^2 \text{sec}^{-1}$), and u is the average linear velocity of the fluid (cm sec^{-1}).

We are interested in the spreading of a peak in terms of peak volume, not length along a tube, so we can convert Equation 86 into volume terms using the following relations:

$$t = V/F \quad (90)$$

$$L = V/\pi r^2 \quad (91)$$

$$x = V_x/\pi r^2 \quad (92)$$

$$u = F/\pi r^2 \quad (93)$$

$$D_a = F^2/48 D_m \pi^2 r^2 \quad (94)$$

where V is the total volume of the tube (cm^3), F is the volumetric flow rate of the solution ($\text{cm}^3 \text{sec}^{-1}$), and V_x is the volume of the tube from the point of injection to point x . Equation 86 then becomes

$$\bar{C} = \frac{48 D_m M}{2 \pi r^2 F L^2} \exp[-(V-V_0)^2 \cdot 12 D_m / \pi r^4 L F] \quad (95)$$

The variance of the peak described in Equation 94 is equal to its second moment (122), and this is given by

$$\sigma_{\text{exp}} = \sqrt{\sigma_{\text{exp}}^2} = \left(\frac{\pi r^4 L F}{24 D_m} \right)^{1/2} \quad (96)$$

This produces the well-known result that sample spreading in an open tube is proportional to the square of the radius and square root of the length of the tube (120).

The extremely close agreement between σ_{theory} and σ_{exp} at very low flow rates must be viewed as being somewhat fortuitous in view of our arbitrary choice of $D_{\text{Cu}^{2+}} = 5 \times 10^{-6} \text{ cm}^2 \text{ sec}^{-1}$ in 0.1 M KNO_3 at room temperature as well as the approximate value used for the tube radius. The data clearly indicate that the experimental variance does not increase in proportion to the square root of flow rate or linear velocity. This square root dependence is tacitly assumed by Ruzka and Hansen *et. al.* (119) in their work on "Flow Injection Analysis."

Our values of σ_{exp} at higher flow rates are significantly lower than those predicted by Equation 96. There are several reasons for this discrepancy. At the higher flow rates, the residence times of a peak in our system approaches and even drops below T_{ss} (Equation 85) required for Taylor's equation to be valid. Here, the laminar flow profile is not fully developed and turbulence lowers peak spreading. This is one great problem in reconciling peaks in "Flow Injection Analysis" with fluid flow theory (119), where the statement is made "within the range of tube lengths and diameters used in Flow Injection systems, D_f [dispersion] is independent of tube diameter for the same residence time T ." This statement is in direct conflict with Equation 95, derived from Taylor's original work.

Another reason for the discrepancy between our values of σ_{exp} and σ_{theory} is the fact that our system is heated. This will increase D_M , and thus lower total dispersion, according to Equations 94 and 96.

A third characteristic of our system which lowers the dispersion of a peak is the coiling of the delay line between sample loop and detector. Recent experimental work by Hofmann and Holasz (120) as well as the theoretical studies of Nunge et. al. (120a) demonstrate a very complex dependence of variance on flow rate in open helically coiled tubes. In general, at intermediate and high flow rates σ will be smaller than that predicted by Equation 96 due to the induction of secondary radial flow by the centrifugal force on the fluid as it moves in a curved tube. This secondary flow of liquid in the tubing stabilizes the flow profile and reduces laminar dispersion. Hofmann and Holasz (120) have shown that this can have a large effect on dispersion in situations where the diameter of the coil is over 100 times the diameter of the tube. This effect becomes more significant with higher flow rate, and this is evident in our examples where spreading diverges from theory as flow rate is increased.

Finally, the observed dispersion in our system is influenced by the method of introduction of a sample into the flowing stream. The evidence for this conclusion follows: Ideally, the total variance (σ_T) of a peak traveling through a system which causes spreading is related to the variance due to the sample volume (σ_s) and dispersion caused by the flow system (σ_d) through the following relation (122):

$$\sigma_T = \sqrt{(\sigma_s)^2 + (\sigma_d)^2} \quad (97)$$

A plot of σ_T^2 (or, in our case $\omega_{1/2}^2$) against σ_s^2 for varying sample sizes would then result in a straight line with an intercept at $\sigma_s^2 = 0$ equal to σ_d^2 and a slope of $(1.0)^2$ for spreading in a single stream,

or $(2.0)^2$ for dilution of the sample with a second stream of equal flow rate, as in our detector. Figure 27 is a plot of $\omega_{1/2}^2$ against V_s^2 for our detector, and it is clear that the observed slope is not 4.0. The slope of the line between $V_s = 300 \mu\text{L}$ and $V_s = 500 \mu\text{L}$ are shown in Table VI for all flow rates tested.

In order to explain the discrepancy between spreading in our system with respect to dispersion theory, we have developed a model of fluid flow through a reactor such as ours.

In the analysis of flow dispersion above, we have assumed constant flow at all times, and this is not the case. We have incorporated a pulse-dampener between the pump and sampling valve consisting of a fluid capacitor and resistor, as described in Chapter III. This acts as a low-pass filter to decrease the effects of a pulsating input stream, with pulses occurring slower than five times per second. The filter, then, was constructed with a time constant of over five seconds in order to accommodate this frequency. In this way, a very steady flow was maintained.

Our sampling technique consisted of switching in and out a Teflon sample loop, 0.8 mm I.D. x 5 m long. The resistance to fluid flow of this loop was not negligible compared to the other fluid resistors (pulse dampener, delay coil) in the flow system. Upon switching in this loop, the resistance of the arm of the flow system increased, and the flow rate dropped, as the fluid capacitor filled with liquid to compensate for the increased back-pressure beyond it. Since the capacitor-resistor system produced a low-pass filter, and the pump delivered liquid at a constant rate, the flow rate at the output of the

system exponentially approached the original flow rate. This phenomenon can be modeled by the following sequence, illustrated in Figure 28A:

$$0 < t < T_1 : f(t) = F_o \quad (98)$$

$$t = T_1 : f(t) = F_o - \Delta F_o \quad (99)$$

$$T_1 < t < \infty : f(t) = (F_o - \Delta F_o) + \Delta F_o (1 - e^{-(t-T_1)/k}) \quad (100)$$

In the above, t is time, $f(t)$ is the instantaneous flow rate at time t , T_1 is the point of switching in the sample loop (increased resistance), F_o is the original flow rate, ΔF_o is the change in flow rate due to the instantaneous increase in resistance of the system, and k is the time constant (first-order) of the fluid capacitor-resistor system. As can be seen from Equation 85, at long times, the flow rate reaches F_o , the original system flow rate.

The integrated output of the system before the sample loop is switched in is then

$$\int_0^{T_1} F_o dt = F_o T_1 \quad (101)$$

Since we are interested in a loss of liquid output caused by the sampling process, the change in system output after the sample loop is switched in relative to the unperturbed system is

$$\int_{T_1}^{\infty} F_o - \left\{ (F_o - \Delta F_o) + \Delta F_o (1 - e^{-(t-T_1)/k}) \right\} dt = \Delta F_o k \quad (102)$$

Figure 28. Model of Liquid Flow Rate and Accumulated Output Volume for Sample Input (Sampling Loop) for the Detector System.

F_0 is the original liquid flow rate.

ΔF_0 is the change in flow rate at the point of switching in (or out) the sample loop.

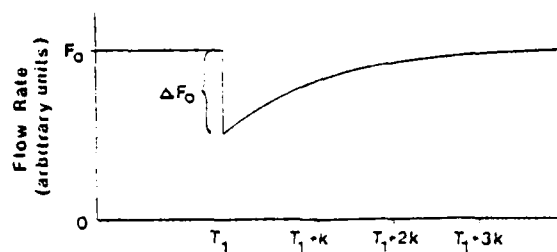
T_1 is the time at which the sample loop is switched in.

T_2 is the time at which the sample loop is switched out.

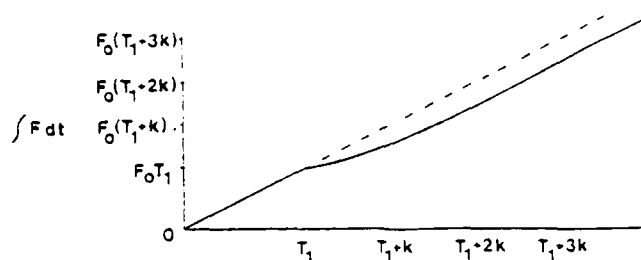
k is the first-order time constant for the fluid filter (see text).

All figures are plotted against time.

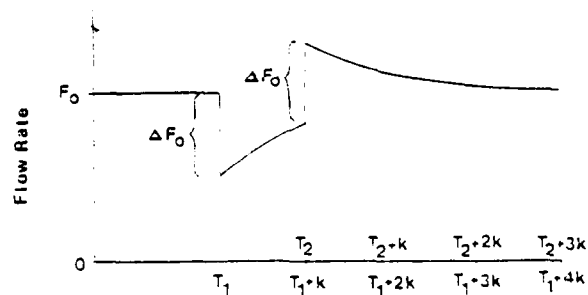
- A. Flow rate when sample loop is switched in at T_1 .
- B. Accumulated output volume for Plot A. Broken line is continuation of original slope.
- C. Flow rate when sample loop is switched in at T_1 and switched out at $T_2 (= T_1 + k)$.
- D. Accumulated output volume for Plot C. Broken line is continuation of original slope.



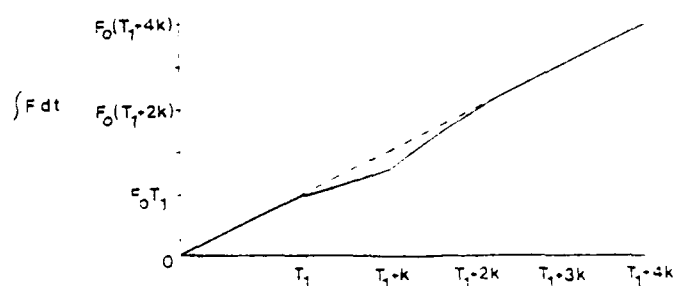
A



B



C



D

Time
(arbitrary units)

The integrated output of the flow system is plotted against time in Figure 28B. This shows that a finite amount of output is lost, i.e., trapped in the fluid capacitor. From examination of this figure, it is also obvious that the amount of sample taken over a period of time T_1 to $(T_1 + a)$ is less than would be found if the flow rate remained constant with time.

In our system, however, we are concerned with finite-sized sample loops. If the loop is switched out of the flow system, the resistance to flow is less, and the flow rate increases. For this model, we assume that the flow rate increased the same amount that it decreased upon switching in the sample loop, ΔF_o . It then again settles to the original flow rate F_o . This more complete model is given below, and illustrated in Figure 28C.

$$0 < t < T_1: \quad f(t) = F_o \quad (103)$$

$$t = T_1: \quad f(t) = F_o - \Delta F_o \quad (104)$$

$$T_1 < t < T_1 + a: \quad f(t) = (F_o - \Delta F_o) + \Delta F_o (1 - e^{-(t-T_1)/k}) \quad (105)$$

$$t = T_2: \quad f(t) = f(T_1 + a) + \Delta F_o \quad (106)$$

$$T_2 < t < \infty: \quad f(t) = (f(T_1 + a) + \Delta F_o) - \left[(f(T_1 + a) + \Delta F_o) - \Delta F_o (1 - e^{-(t-T_2)/k}) \right] \quad (107)$$

Here, a is a finite time after T_1 where the sample loop is switched out, and T_2 is the time immediately after $(T_1 + a)$, where the flow rate has increased by ΔF_o . The integrals of each of these segments can again be computed

$$\int_0^{T_1} F_o dt = F_o T_1 \quad (108)$$

$$\int_{T_o}^{T_1+a} F_o - \left\{ (F_o - \Delta F_o) + \Delta F_o (1 - e^{-(T-t_1)/k}) \right\} dt = \Delta F_o k (e^{-a/k} - 1) \quad (109)$$

$$\int_{T_2}^{\infty} F_o - \left[\left\{ (F_o - \Delta F_o) + \Delta F_o (1 - e^{-a/k}) + \Delta F_o \right\} - \left\{ (F_o - \Delta F_o) + \Delta F_o (1 - e^{-a/k}) + \Delta F_o - F_o \right\} \right. \\ \left. \times (1 - e^{-(t/T_2)/k}) \right] dt = \Delta F_o (1 - e^{-a/k}) \quad (110)$$

where Equations 108 and 109 are again the difference in output between the model and the unperturbed system. This integral is plotted against time in Figure 28D.

One important point is that the integral given by Equation 108 and that given by Equation 109 sum to zero. This result is what is expected, that the output of the system is equal to that of the unperturbed system at long times. That has to be true because the input to the system is constant and the initial and final fluid resistances are equal. Thus, the fluid capacitor cannot hold more fluid (fluid "lost" in terms of output) at long-time steady-state than it held before the initial perturbation.

This model again shows that a timed sampled loop from t to $(T_1 + a)$ will not inject as much sample as would be derived assuming a constant flow rate. In addition, after the sample loop is switched out, a specific volume will pass by a point in less time than if the flow rate were constant.

Thus, since our samples were from a timed loop, they were smaller than the volumes calculated assuming a constant flow rate, and since

the peaks observed at the output of the detector were measured on a recorder with a constant time axis, they were apparently compressed again because of the second effect, although the actual volumes were not affected here. This explains the fact that in Figure 27, all points correspond to a lower sample size for specific $\omega_{1/2}^2$ values.

Finally, with very large samples the slope of the $\omega_{1/2}^2$ vs V_s^2 line should approach the theoretical value, since the digressions of flow rates from a constant value are transient in nature, as shown in Figure 28C. This does occur with our system, as shown in the data in Table V for a flow rate of 2.0 mL/min/channel. The slope of $\omega_{1/2}^2$ vs V_s^2 from 500 to 1000 μ L is exactly 4.0, confirming the model at large sample volumes.

Sternberg (122) has derived the equations describing the output response of a system with finite input sample width. As the sample width increases, the peak height rises to a maximum and the peak width increases, as shown in Figure 29. Schifreen, *et al.* (123) analyzed Sternberg's equations for the maximum peak height in terms of the variance due to the spreading in the device (σ_d) and sample size (θ). If their equation is normalized to the maximum obtainable peak height, then using H as the peak height for an individual sample and H_{ss} as the maximum obtainable peak height (steady-state), one obtains

$$H/H_{ss} = \text{erf} (\theta/2\sqrt{2}\sigma_d) \quad (111)$$

This equation was originally derived for Gaussian peaks in gas chromatography, and we have used it as our model here even though our peaks are not Gaussian. Using the data obtained from the sample volume

Figure 29. Detector Peak Height as a Function of Sample Volume.

Conditions were identical to Figure 26, except the flow rate was varied from 0.25 to 2.0 mL/min/channel. Concentration response (as in Figure 25) was used.

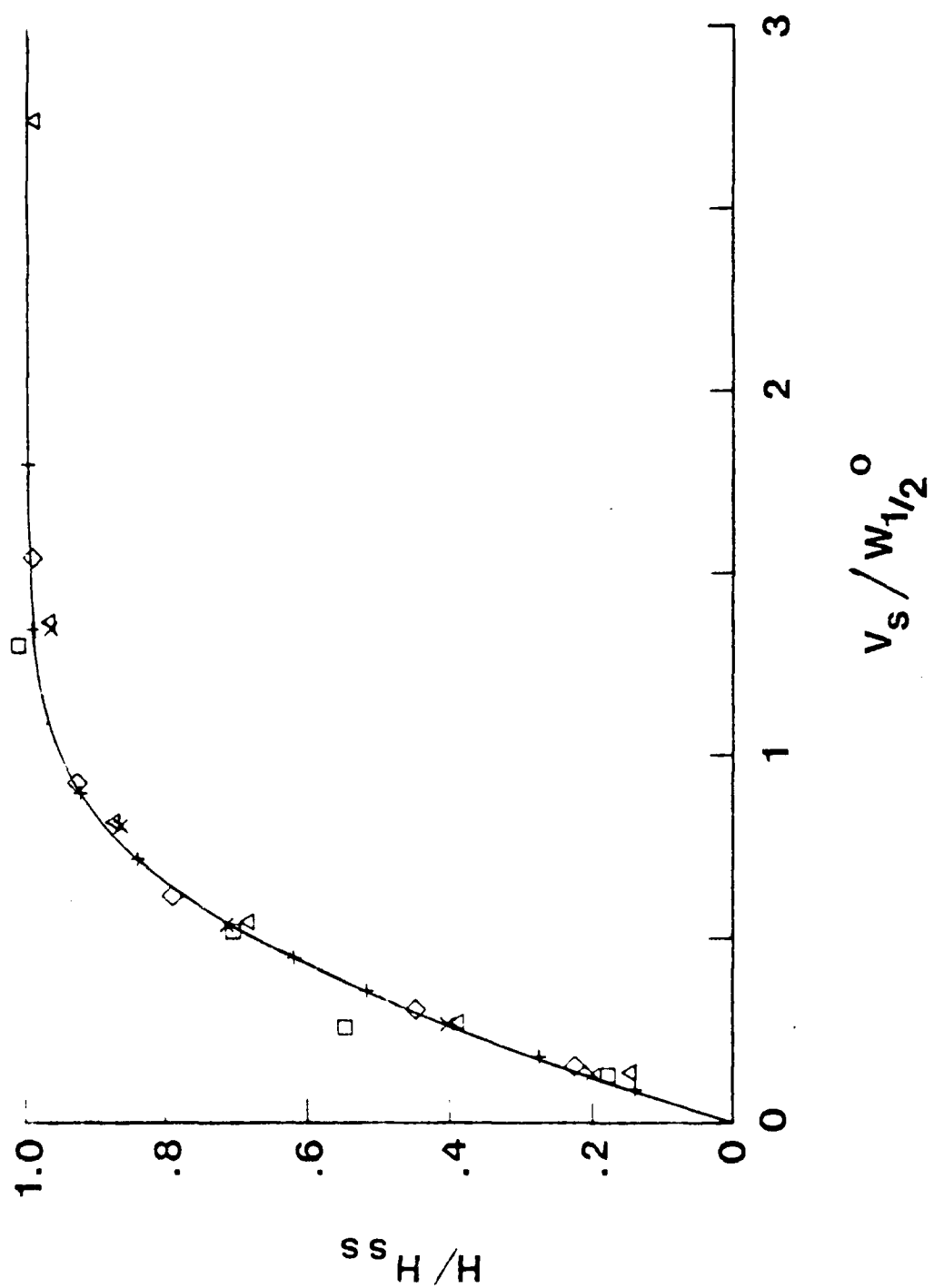
H / H_{ss} = Peak height normalized to steady-state peak height.

$V_s / \omega_{1/2}^0$ = Ratio of nominal sample volume to peak half-width at zero sample volume (see Table VI).

Theoretical curve calculated from Equation 111, using $\sigma = 0.8 \omega_{1/2}^0$ (+ , solid line).

Flow rates used (mL/min/channel):

- A. 0.25 (×).
- B. 0.50 (□).
- C. 1.0 (◇).
- D. 2.0 (Δ).



studies, and normalizing the individual peak widths to the minimum peak widths, $\omega_{\frac{1}{2}}^0$, we obtain Figure 29. The solid line is the response according to Equation 110, using $\sigma_d = 0.8 \omega_{\frac{1}{2}}^0$. The peaks thus lie very close to the theoretical curve using this value for σ_d . This value does not agree with those given in Table VI, but this is also because of the sample-compression characteristics of the system described earlier in this section and the different peak shape.

b. Peak return to baseline after injections of differing Cu(II) concentration.

A second characteristic important to the utility of a chromatographic detector is its recovery time after peaks of different magnitudes pass. This shows how soon the detector is able to see a small peak which follows a large one. We have defined the detector's recovery time for our purposes as the length of time required for the trailing edge of a steady-state peak to fall to a point 9 mV above the background cell potential. This point (9 mV above background) represents a Cu(II) concentration approximately twice the residual concentration from CuEDTA dissociation, or approximately 1 μM excess Cu(II) (see Equation 1).

This definition of recovery time is fundamentally different from the time for a peak to fall to half its maximum value. Our definition utilizes absolute concentrations of the peak and background, and thus for a specific relaxation function (as $C = C_0 e^{-t^2/\tau_r}$, a simplification of Taylor's equation) is concentration dependent. Time for a peak to fall to half maximum is a relative measure, and thus is not concentration dependent.

One point which must be mentioned is that the time for a peak to fall to half maximum as used in our detector refers to the concentration (antilog) output. If the potential response is used, then there is a concentration dependence, since the potential scale is logarithmic. This is illustrated in Table VII, where various representations of the recovery time are shown for different size peaks, according to the simple approximation of Taylor's equation (Equation 86) and thus our detector response function

$$C = C_0 e^{-t^2/\tau_r} \quad (112)$$

The recovery time as defined by our criteria are given in Table VIII for the detector using $\text{Cu}(\text{NO}_3)_2$ samples. The far right column consists of values calculated from Equation 112 using $\tau_r = 280 \text{ sec}^{-2}$.

Equation 112 describes a Gaussian peak centered at $t = 0$, with σ equal to $(\tau_r/2)^{1/2}$. Using τ_r calculated above, and a flow rate of 1.0 mL/min, we arrive at $\sigma = 197 \mu\text{L}$. This is in excellent agreement with σ_{exp} in Table VI which for 0.5 mL/min/channel is 201 μL . The agreement between the calculated points and those obtained experimentally and the calculated and experimental values of σ show a strong applicability of the model Equation 112 to our system. This also shows the validity of the definition of recovery time to the modeling of a system response to a real peak.

2. Effect of delay coil length (reaction time) on extent of displacement reaction for $\text{Ni}(\text{II})$.

Table VII. Various Measures of Recovery Time for a Detector
to the Concentration Function $C = C_o e^{-t^2/\tau_r}$.^a

C_o (dimensionless)	$\omega_{1/2}, c^b$ (sec)	$\omega_{1/2}, l^c$ (sec)	T_r^d (sec)
10^{-5}	0.83	1.07	1.52
10^{-4}	0.83	1.52	2.14
10^{-3}	0.83	1.86	2.63
10^{-2}	0.83	2.15	3.03

a. Definitions of symbols:

C = concentration at time t (arbitrary units)

C_o = maximum concentration (arbitrary units)

τ = second-order time constant (sec^2), set equal to 1.0

b. Defined as the time required to fall to $C = \frac{1}{2}C_o$.

c. Defined as the time required for $\log_{10} (C/10^{-6})$ to fall to half the value of $\log_{10} (C_o/10^{-6})$. Simulates the time in our detector for the potential to fall to half of its peak value.

d. Defined as the time required to fall to $C = 10^{-6}$.

Table VIII. Recovery Time for the Detector^a

Concentration Cu(II) (M)	Recovery Time ^b (sec)	Standard deviation of recovery time ^c (sec)	Calculated Recovery time ^d (sec)
10^{-6}	6	2	--
3×10^{-6}	16	2	16
10^{-5}	22	2	23
3×10^{-5}	29	1	31
10^{-4}	35	2	36
3×10^{-4}	42	1	40
10^{-3}	43	2	44
3×10^{-3}	45	3	47
10^{-2}	54	3	51

a. Detector configuration and conditions are given in Figure 26.

Cu(II) samples are solutions of the stated concentrations on 0.1 M KNO_3 .

b. Defined as the time required for the trailing edge of a steady-state peak to fall to a potential 9 mV above original potential. At this point, $[\text{Cu(II)}] = 2[\text{Cu(II)}]_{\text{background}}$.

c. Standard Deviations were obtained from three replicates.

d. Calculated with the equation $C = C_0 e^{-t^2/\tau_R}$, where $C = 10^{-6}$ M Cu(II) and $\tau_R = 280 \text{ sec}^{-2}$.

From the experiments with the dip-type electrodes, we had determined that the kinetics of exchange between Ni(II) and CuEDTA were the slowest of any metals we had tested. To determine the effect of exchange kinetics on the sensitivity and detection limit of the detector, we used two different heated delay coils, one 0.5 mm diameter x 5 m long (1.0 mL total volume), and the other 0.5 mm diameter x 2.5 m long (0.5 mL total volume). We also adjusted the flow rate to vary the residence time in the delay coils. From our earlier studies, we had concluded that the parameters for the system which presented an optimum trade-off of sensitivity and exchange kinetics for our purpose were a background solution of 0.01 M CuEDTA, adjusted to pH 4.00 and 0.1 M KNO_3 . The temperature of the heated portion of the delay coil was set at 75°C as a compromise to allow the reaction to proceed at the highest possible rate without constantly degassing the solution and forming bubbles in the coil. The solution flowing through the sample channel was 0.1 M KNO_3 and all samples were made in 0.1 M KNO_3 background. These parameters were used in all experiments with the assembled detector.

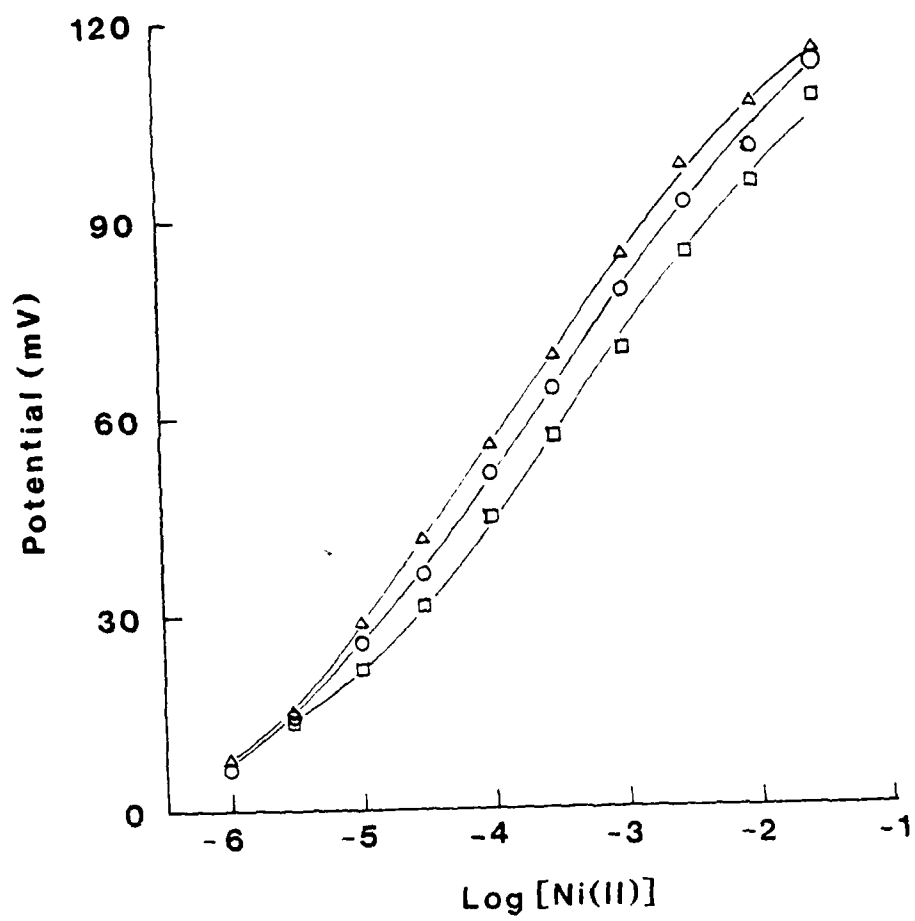
The results of these experiments are shown in Figure 30. There is a dependence of the magnitude of the steady-state signal on residence time, which is expected in the case of a kinetically slow reaction. The electrode measures free Cu(II) concentration at a specific point on the time axis of the reaction profile and thus reaches a steady-state potential governed by the extent of reaction at that particular time.

As can be seen from the figure, the sensitivity of the detector over most of the range is not affected by shortening the delay coil so

Figure 30. Steady-state Logarithmic Response of Detector to $\text{Ni}(\text{NO}_3)_2$ Samples.

Conditions were identical to Figure 26, except delay coil length and flow rate were varied. Sample solutions used were $\text{Ni}(\text{NO}_3)_2$ at concentrations shown in 0.1 M KNO_3 . Potentials plotted are the differences in cell potential from potential under original conditions, 0.01 M CuEDTA in 0.1 M KNO_3 , pH adjusted to 4.0 with KOH and HNO_3 .

- A. Delay coils 2.0 m long by 0.5 mm I.D. at 75°C (64 sec delay) and 0.5 m long by 0.5 mm I.D. at 25°C (17 sec delay). Flow rate 0.5 mL/min/channel, total delay coil volume 1.25 mL (Δ).
- B. Delay coils 1.0 m long by 0.5 mm I.D. at 75°C (33 sec delay) and 0.5 m long by 0.5 mm I.D. at 25°C (17 sec delay). Flow rate 0.5 mL/min/channel, total delay coil volume 0.75 mL (\circ).
- C. Delay coils 1.0 m long by 0.5 mm I.D. at 75°C (17 sec delay) and 0.5 m long by 0.5 mm I.D. at 25 °C (7 sec delay). Flow rate 1.0 mL/min/channel, total delay coil volume 0.75 mL (\square).



that the exchange reaction is not complete. However, the sensitivity at extreme lower levels of Ni(II) is lowered and the detection limit is raised. This is due to the fact that the absolute amount of Cu(II) produced is lower with a shorter reaction time.

From this data, we determined that a residence time of 60 sec (heated) and 15 sec (unheated) was sufficient to allow Ni(II) to reach equilibrium in its reaction with CuEDTA, and 30 sec (heated) and 15 sec (unheated) was sufficient for all other metals tested.

3. Detector response to various metals.

We tested the detector for response to various transitions and rare earth metal ions. Ions not soluble in aqueous solution at pH 4.0 were not considered feasible candidates under the conditions we used. Compounds soluble only in strong acid would change the pH of the CuEDTA stream upon mixing, and this would produce a signal from dissociation of the CuEDTA complex (see Equations 40-48) in addition to that from the ligand exchange. Buffering the CuEDTA solution would not help in this case, since the metals would precipitate as hydroxides.

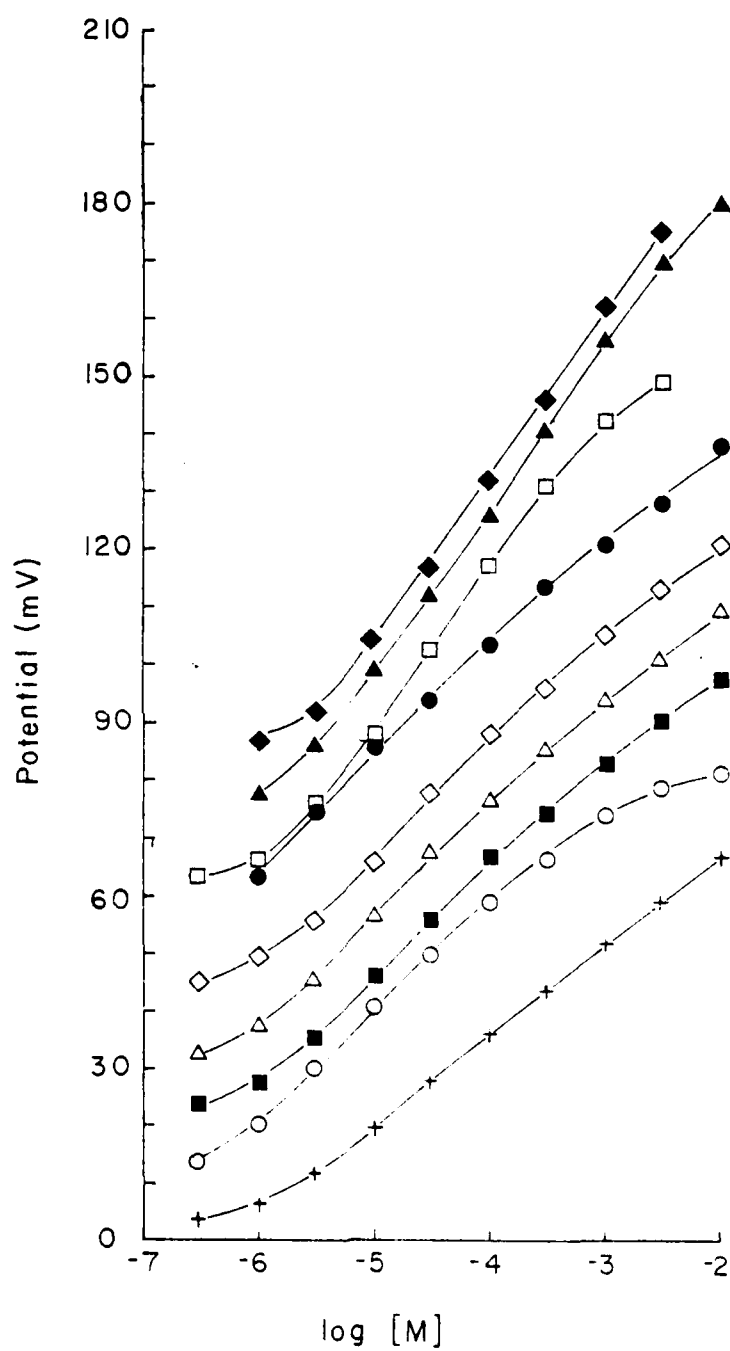
Ions soluble in pH 4 solution which could be detected with the system included Ni(II), Cu(II), Pb(II), Zn(II), Cd(II), Ce(III), La(III), and Co(II). Figure 31 is a plot of steady-state potential achieved for injections from 3×10^{-7} to 10^{-2} M metal ion. The curves are each successively offset 10 mV in order to make the figure more easily readable. The curves all exhibit a sigmoidal shape, like the theoretical curves in Chapter II.

We fit these curves to Equation 67, after subtracting the blank (0.1 M KNO_3) response and converting the potential readings to Cu(II)

Figure 31. Steady-state Logarithmic Response of Detector to Various Metal Ions.

Conditions were identical to Figure 26, except delay coil residence times for Ni(II) were 64 sec at 75°C and 17 sec at 25°C. Sample solutions used were metal salts at concentrations shown in 0.1 M KNO_3 . Potentials plotted are the difference between initial and steady-state cell potentials. Original solution was 0.01 M CuEDTA in 0.1 M KNO_3 , pH adjusted to 4.0 with KOH and HNO_3 . Plots for different metal salts are successively offset by about 10 mV for clarity of display.

- A. $\text{Cu}(\text{NO}_3)_2$ (◆).
- B. $\text{Ni}(\text{NO}_3)_2$ (▲).
- C. $\text{Pb}(\text{NO}_3)_2$ (□).
- D. $\text{Zn}(\text{NO}_3)_2$ (●).
- E. $\text{Co}(\text{NO}_3)_2$ (◇).
- F. $\text{Cd}(\text{NO}_3)_2$ (△).
- G. CdCl_2 (■).
- H. $\text{Ce}_2(\text{SO}_4)_3$ (○).
- I. $\text{La}(\text{NO}_3)_3$ (+).



concentration. For this purpose, we used a general multiparametric curve-fitting computer program developed by Meites (124). The program fits data to a user-entered equation, which can have up to nine adjustable parameters, by minimizing the sum of squares of deviations between the calculated and experimental curves. Results of the fit are given in Table IX. This table shows that the theory in Chapter II describes the steady-state response of the detector quite well. The values of β (Equation 61) calculated from the detector response to metals are all close to those calculated from literature values of the formal equilibrium constants of the individual metals and Cu(II) with EDTA (115). In addition, β^* and f values are all close to each other, indicating that the CuEDTA solutions produced by the method described earlier are very reproducible with respect to their stoichiometry. The computed value of β^* is low compared to that calculated from Equations 48-50 and 62; this is explained by the fact that the CuEDTA contains a slight excess of Cu(II) (Chapter IV.A.2) and discrimination between a low β^* value without excess Cu(II) and a high β^* value with a small amount of excess Cu(II) is possible only with a large number of data points at low values.

One significant point about the curves is that the data for the salts CdCl_2 and $\text{Cd}(\text{NO}_3)_2$ are almost identical. This is true even though the concentration of chloride at the upper end of the CdCl_2 curve (10^{-2} M) is approximately 100 times the free Cu(II) concentration. The experimental curves involving CdCl_2 , however, showed a small but definite overshoot at the trailing end of the peak at concentrations above 10^{-4} M. We postulate that this is caused by the transient effect chloride ion has on electrode response (66, vide infra).

Table IX. Experimental Estimates of the Dimensionless Parameters Governing the CuEDTA-Mⁿ⁺ Exchange Reaction.^a

Metal ion ^b	f ^c	β^*^d	β_{exp}^e	$\beta_{\text{lit}}^{e,f}$
Ni(II)	1.00000	6.0×10^7	0.12	0.66
Pb(II)	0.99992	4.2×10^7	0.39	0.33
Zn(II)	0.9998	3.0×10^7	1.1×10^{-3}	3.0×10^{-3}
Cd(II)	0.99999	5.9×10^7	2.5×10^{-3}	4.6×10^{-3}
Cd(II) ^g	1.00000	1.3×10^8	1.7×10^{-3}	4.6×10^{-3}
Co(II)	1.00000	3.4×10^7	4.3×10^{-3}	3.2×10^{-3}
Cc(III) ^h	1.00000	5.7×10^7	1.9×10^{-3}	1.6×10^{-3}
La(III)	0.99999	5.4×10^7	3.2×10^{-4}	5.0×10^{-4}

a. Detector configurations and conditions are given in Figure 26, and data are plotted in Figure 30. Parameters were obtained from a multiparametric least-squares fit of the experimental data to Equation 67.

b. Nitrate salts of metal ions were used, unless otherwise specified.

c. Defined in Equation 60.

d. Defined in Equation 62.

e. Defined in Equation 61.

f. Values were calculated from Reference 14 for ions at 20°C in 0.1 M KNO₃.

g. Chloride salt was used.

h. Sulfate salt was used.

The sigmoidal shape of the metal-response curves, while pleasing theoretically, limit the system's utility as a metal ion detector, since linear response plots are the easiest to interpret. For this reason, the linear portions of the curves were extracted and least-squares analysis was performed on the data. The results are given in Table X. The "signal-to-noise (S/N) ratio" has been defined for our purposes as the ratio of the potential difference between the lowest concentration studied and a blank (0.1 M KNO_3) injection to the standard deviation of the potential measurement for the lowest concentration studied. It is evident that micromolar concentrations can easily be detected and $3 \times 10^{-7} \text{ M}$ in all metals which we studied at that concentration.

The linear range of all of the metals we studied is at least three orders of magnitude, with slopes from 15 to 28 mV/decade and correlation coefficients at or above 0.997. This shows the ability of the system to accommodate wide variations in metal ion concentrations before sensitivity is lost.

Because of the analytical importance of the linear regions of the metal response curves, it is important to compare experimental curves to these predicted by our model using thermodynamic metal-ligand complex formation constants. In Table XI we compare the experimental slopes for metal ions over the linear ranges defined in Table X to simulated data over the same ranges. Complex formation constants from the literature (115) and from curve-fitting of the experimental data to the model (Table IX) were both used for comparison. The slope obtained experimentally is always within 1.5 mV/decade of the value obtained by

Table X. Linear Range of Steady-state Response of Detector for Metal Ions.^a

Metal ion ^b	S/N ^c	Linear Ranged (M)	Slope ^e (mV/decade[M])	Standard Deviation of Slope ^e (mV/decade[M])	Correlation Coefficient	Student's "t" ^e
La(III)	7.1	$3 \times 10^{-6} - 10^{-2}$	15.7	0.1	0.9999	190
Ce(III) ^f	11.6	$10^{-6} - 10^{-3}$	18.0	0.6	0.997	31
Cd(II)	20	$10^{-6} - 3 \times 10^{-3}$	18.7	0.4	0.999	45
Cd(II) ^g	21	$10^{-6} - 3 \times 10^{-3}$	18.4	0.4	0.999	47
Co(II)	25	$10^{-6} - 10^{-2}$	18.5	0.4	0.999	47
Zn(II)	70 ^j	$10^{-6} - 10^{-2}$	18.2	0.4	0.998	43
Pb(II)	7.5	$10^{-6} - 10^{-3}$	26.2	0.6	0.998	43
Ni(II)	41 ^j	$3 \times 10^{-6} - 3 \times 10^{-3}$	28.2	0.3	0.999	83
Ni(II) ^h	60 ^j	$3 \times 10^{-6} - 3 \times 10^{-3}$	26.0	0.6	0.999	42
Ni(II) ⁱ	55 ^j	$10^{-5} - 10^{-2}$	25.1	0.4	0.999	69
Cu(II)	40 ^j	$3 \times 10^{-6} - 3 \times 10^{-3}$	28.0	0.5	0.999	55

- a. Detector configuration and conditions are given in Figure 26, and data are plotted in Figure 30, unless otherwise specified.
- b. Nitrate salts of metal ions were used, unless otherwise specified.
- c. Computed as the ratio $(E_s - E_b)/S_s$, where $E_s - E_b$ is the difference in steady-state potential between a 3×10^{-7} M metal salt injection and blank injection (no metal salt added), and S_s is the standard deviation of steady state potential for a 3×10^{-7} M metal salt injection, using three replicates.
- d. Range of concentrations used in least-squares analysis of data.
- e. From linear least-squares analysis of data.
- f. Sulfate salt was used.
- g. Chloride salt was used.
- h. Conditions and data are given in Figure 29, middle curve (moderate delay coil length).
- i. Conditions and data are given in Figure 29, lower curve (shortest delay coil length).
- j. $E_s - E_b$ is computed using 10^{-6} M metal salt instead of 3×10^{-7} M.

Table XI. Comparison of Experimental and Theoretical Slopes of Metal Ion Response over the "Linear" Range of the Detector^a

Metal ion ^b	Slope ^c (mV/decade[M])	Reference Slope ^d (mV/decade[Cu])	Theoretical Slope (exp) ^e (mV/decade[M])	Theoretical Slope (lit) ^f (mV/decade[M])
La(IV)	15.7	29.9	15.8	16.3
Ce(III) ^g	18.0	30.2	18.4	18.2
Co(II)	18.5	29.9	19.4	18.9
Cd(II)	18.7	30.4	19.0	20.0
Cd(II) ^h	18.4	29.5	18.4	20.6
Zn(II)	18.2	29.2	15.4	16.9
Pb(II)	26.2	30.0	26.5	26.3
Ni(II)	28.2	31.9	27.3	29.7

a. Conditions as in Figure 26, and experimental data plotted in Figure 30.

b. Nitrate salt of metal ion used, unless otherwise specified.

c. From Table X, over the same concentration range.

d. $E_{(10^{-3} \text{ M Cu(II)})} - E_{(10^{-4} \text{ M Cu(II)})}$ taken previous to response curve.

e. Least-squares analysis of linear range using β_{lit} from Table X.

f. Least-squares analysis of linear range using β_{exp} from Table X.

g. Sulfate salt was used.

h. Chloride salt was used.

our model. The "reference slope" is the slope of the electrode response to cupric ion on the day that the specific calibration curve was run. Again, this value can vary by a few percent because of the state of the electrode and ambient conditions. We think that this is again excellent agreement between our experimental values and the model, and further demonstrates the validity of the technique.

4. Detector response to common anions (excluding halides).

The detector was tested for response to some common anions as their sodium or potassium salts. Injections of deionized water and 0.1 M KNO_3 were used as blanks, and all other anions were injected at a concentration of 0.01 M. In all cases, the electrode response was allowed to proceed to steady-state.

The anions H_2PO_4^- (adjusted to pH 4.0), SO_4^{2-} (pH 4.0) and biphthalate ($\text{HC}_8\text{H}_4\text{O}_4^-$, pH 4.0) gave very small responses. When the pH was not adjusted to 4.0, as in the case of CO_3^{2-} (pH 6.9) and SO_4^{2-} (pH 6.0), the potential shifted several millivolts negative. This was determined to be caused by a shift in the $\text{Cu} + \text{EDTA} \rightleftharpoons \text{CuEDTA}$ equilibrium towards formation of the complex because of the increase in pH. We reached this conclusion because of the different results of the SO_4^{2-} experiments at pH 4 and pH 6, where SO_4^{2-} is in the same form in both cases. Results for this set of experiments are given in Table XII.

5. Detector response to halide ions.

The halide ions were tested for response in the same way as the previous anions. In these cases, however, the peak shapes were very different. For F^- , Cl^- , and Br^- , as the peak front passed the electrode,

Table XII. Steady-state Reponse of the Detector to Common Anion Salts.^a

Anion	Steady-state potential ^b (mV)	Standard deviation of potential ^c (mV)
d	0.86	0.12
NO_3^- e	2.45	0.09
H_2PO_4^-	2.5	0.4
$\text{HC}_6\text{H}_4\text{O}_4^-$	2.5	0.5
SO_4^{2-}	-0.96	0.05
SO_4^{2-} f	-7.1	0.1
HCO_3^- g	-8.8	0.1

a. Detector configuration and conditions are given in Figure 26.

Samples consisted of 0.01 M solutions of the sodium or potassium salts of the anions in 0.1 M KNO_3 , with the pH of the sample solution adjusted to 4.0 with HNO_3 , unless otherwise specified.

b. Difference between peak potential and original cell potential.

c. Standard deviations were obtained from three replicates.

d. KNO_3 was omitted from sample.

e. Concentration of NO_3^- was 0.1 M.

f. pH was measured to be 6.0.

g. pH was measured to be 6.9.

the potential shifted negative, indicating an apparent decrease in Cu(II) concentration. The potential then settled back to a value close to the background. As the sample tail passed, the converse occurred, the potential shifting sharply in the direction of higher Cu(II) concentration, and again settling to the background value. These peaks are shown in Figure 32. These results can be explained qualitatively using the model of transient electrode response proposed by Morf (65) (see Section I.C.6). He proposed a model for transient electrode response based on a heterogenous membrane electrode, which explained potential overshoots in the case of interfering ions of the same charge as the measured ion. If ions of opposite charge of the measured ion are considered, an overshoot in the opposite direction (lower apparent measured ion concentration) is possible with this model.

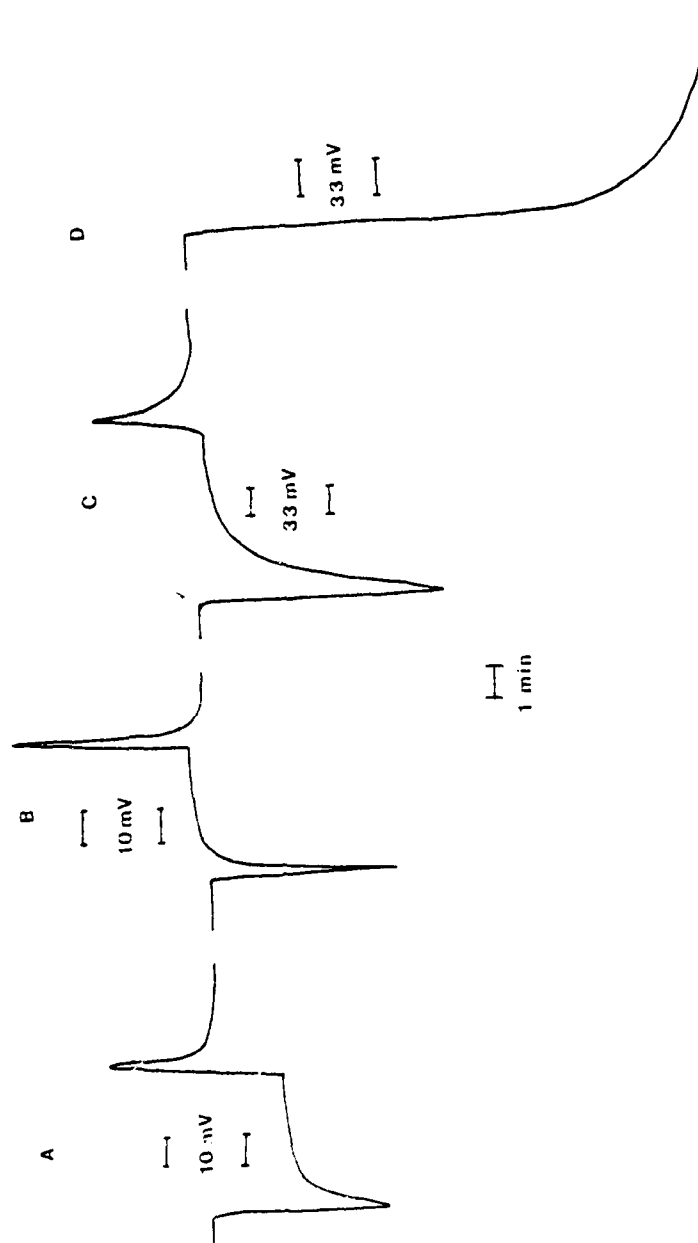
The detector response to I^- was completely different. The electrode potential shifted strongly toward lower Cu(II) activity, but the peak leveled off to a steady-state value during the sample injection. After the sample tail passed, the electrode potential returned to the original value. The electrode, however, was no longer responsive to a 10^{-4} M Cu(II) sample, and proper (Nernstian) response to Cu(II) samples could not be restored by polishing the electrode.

The differences in response of the electrode to halides can be explained by the fact that silver halides are less soluble in the order $AgF < AgCl < AgBr < AgI$. Therefore, the interference by the four anions should be more pronounced in that order, if solubility of the silver salts is a factor, i.e., a coating of the silver halide forming on the surface. Also, the ternary salt Ag_3SI has been synthesized and

Figure 32. Dynamic Response of Detector to Potassium Halide Samples.

Conditions were identical to Figure 26. All samples were 0.01 M potassium halide in 0.1 M KNO_3 . Traces are cell potential as a function of time.

- A. KF.
- B. KCl.
- C. KBr.
- D. KI.



characterized (76), and this compound could form on the surface of the membrane when iodide is passed over.

Thus, in using the detector, one must avoid drastic pH changes, since they will alter the background Cu(II) concentration. Bromide and iodide should also be avoided, the first because it produces large and slow transients as it passes the electrode, and the second because it poisons the electrode.

V. CONCLUSION

In this report, we have described the development and operation of a liquid chromatography detector applicable to transition and rare earth metal ions. Crucial to the detector, we designed and characterized a flow-through cupric ion-selective electrode with Nernstian response down to at least 10^{-7} M Cu(II) and dynamic response better than those described in the literature under similar conditions.

The apparatus is simple and inexpensive to construct, and exhibits a detection limit of 1.5×10^{-10} mole metal ion absolute. Other reagents can be used to tailor the sensitivity and selectivity to specific applications, according to a theoretical model based on thermodynamic data of metal-ligand complex formation. The detector response agrees well with the theoretical model over a concentration range of 3×10^{-4} . Common anions which do not complex with Cu(II) or the metal ion measured do not interfere with response, although halide ions cause a transient shift in the electrode potential (except I^- , which poisons the electrode) in the order $F^- < Cl^- < Br^- < I^-$. This is due to the characteristics of the cupric ion-selective electrode itself. These ions, however, should be fairly easily eliminated from solutions by ion-exchange, should they be a problem.

APPENDIX. AN AUTOMATIC SIGNAL-OFFSET MODULE

A. Introduction

There are three common ways to transmit signals which vary over wide ranges to a single-range recording device: (1) conversion of the input signal to its logarithm, (2) attenuation of the input signal by an amplifier with switchable fixed gains, and (3) addition to the input signal of opposing fixed potentials with a summing amplifier.

The first option can provide a dynamic range of typically four orders of magnitude (125), but the precision of output referenced to the signal is poor, particularly when large signals are being measured. Also, data is not easily interpreted without reconversion to its original form. The second option, attenuation, is widely used (126 and references therein), but again loses precision at high input signals, since the precision of output is controlled by the attenuator setting. The third option, addition of opposing potentials (offsets) has usually been used to add a single offset to a signal, only doubling the effective range of the recording device. This severely restricts the utility of such a system.

Here we describe a system for adding multiple offsets to an input signal, greatly extending the range of a recording device, while keeping the same absolute precision over the entire range. The system is designed to extend the range of a recording device by a factor of 16.

B. Functional Description

A block diagram of the automatic offsetting module is shown in Figure 33. The input signal is amplified by -1, -10, or -100. This is necessary for two reasons. First, the subsequent electronics are designed for a full-scale output of approximately 1 volt. This first stage enables the user to work with signals much smaller than this. Second, the use of an inverting amplifier in this stage counteracts a second inversion by the summing amplifier to restore the output signal to its correct polarity.

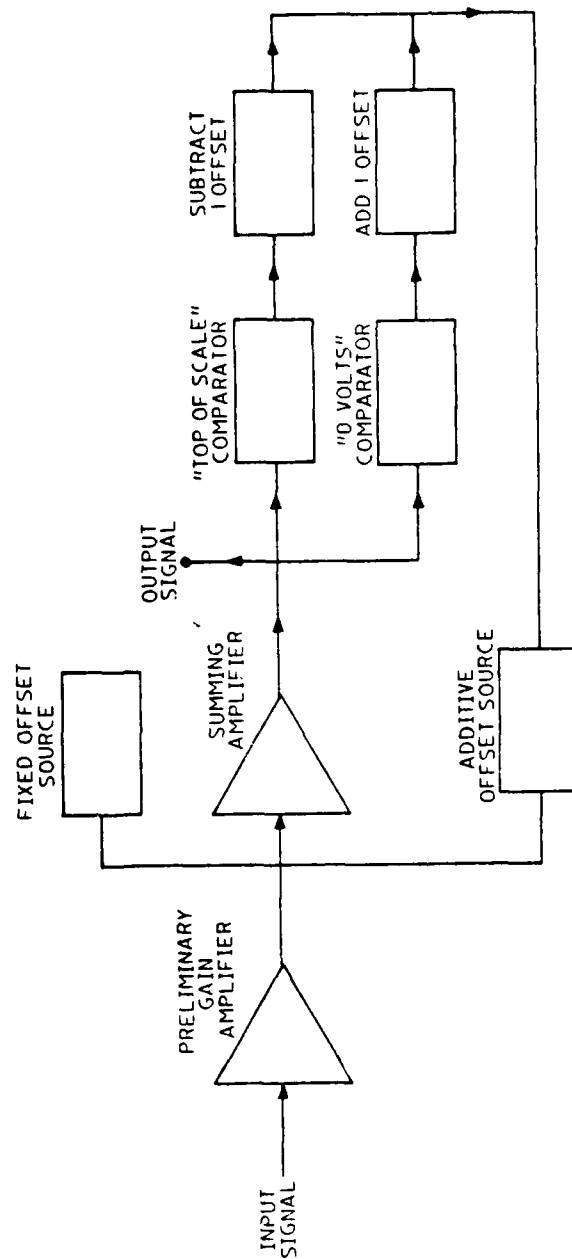
The next stage is the summing amplifier, where the incoming signal, any fixed offsets, and offsets due to the signal exceeding a set "top of scale" potential or falling below 0 volts are added to produce the output signal.

The output of the summing amplifier is also fed into two comparators. The first will change polarity when its input exceeds a "top of scale" potential set by the user. This sends a signal to the additive offset source (AOS) to subtract one "full scale" offset from the output of the summing amplifier, bringing it back within the boundary conditions.

If the output of the summing amplifier falls below 0 volts, the second comparator changes polarity, sending a signal to the AOS to add one "full scale" offset to the summing amplifier's output.

The AOS has the capability for adding or subtracting 15 offsets to the summing amplifier's output. If more offsets than this are needed, they must be applied externally before this offsetting circuit.

Figure 33. Block Diagram of the Automatic Offset Module.



The final element adds a user selectable fixed amount of offset to the input signal in order to be able to subtract an offset when the input signal to the preliminary amplifier falls below 0 volts, since the AOS is unipolar.

C. Operational Principles

The schematic diagram of the offset module is shown in Figure 34, with the components listed in Table XIII. The preliminary gain amplifier (OA1) is an Analog Devices 153K, which has very low voltage and current noise specifications (1 μ V and 10 pA p-p). Hence, a gain of 100 on a small signal is not overridden by background noise.

The summing amplifier (OA2) is a National Semiconductor LM741CN amplifier in the inverting configuration with a gain of -1 for the signal from OA1, and adjustable gains for both of the offset circuits.

The comparators (OA3A, OA3B) are each one-half of a dual 741-type amplifier (National Semiconductor 4458N dual op amp). As long as the output of OA2 is between 0 volts and "top of scale," the outputs of both comparators are at negative saturation. Consequentially, the bases of Q1 and Q2 (3140SK PNP transistors, RCA) are negative with respect to their emitters, and the transistors are switched "on." Their collectors are thus poised at 0 volts. This potential is fed into an input of IC1A and IC1B (both NAND gates) respectively. This sets the outputs of IC1A and IC1B constantly high, and no signals are sent to the AOS.

When the signal from the summing amplifier exceeds the set "top of scale," OA3A switches to positive saturation. This raises the potential of the base of Q1 above the emitter, and the transistor does not

Figure 34. Schematic Diagram of the Automatic Offset Module.

For types and values of components, see Table XIII.

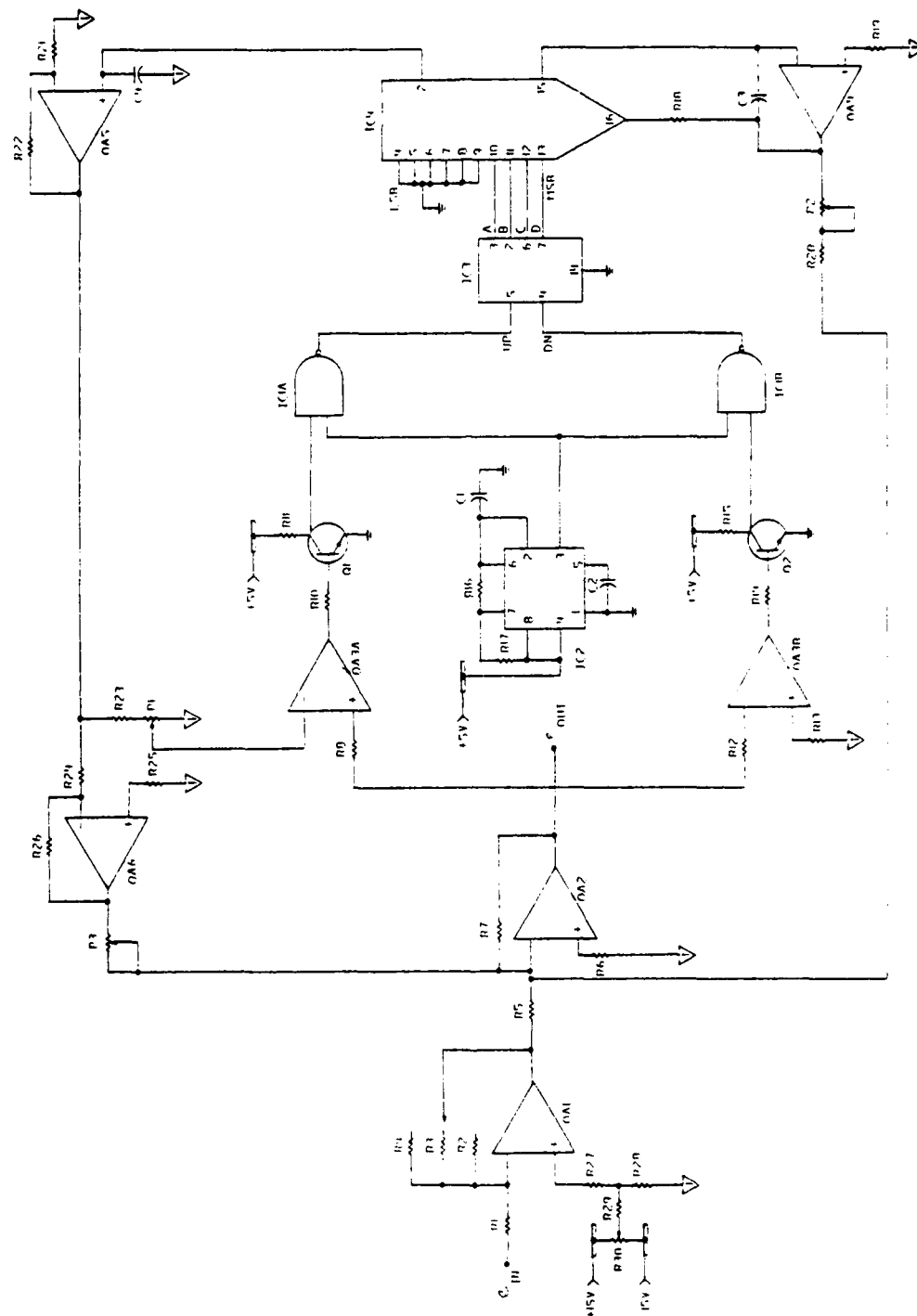


Table XIII. Components Used in the Circuit in Figure 34.

Resistors:

All fixed resistors, unless otherwise noted, are metal film, 1/4 W, 1% tolerance.

R1, R2, R5, R7, R21, R22, R24, R26, R27 - 10 K Ω .

R3 - 100 K Ω .

R4 - 1.0 M Ω .

R6, R19, R25 - 5 K Ω .

R8, R9, R12, R13 - 27 K Ω , 2%.

R10, R11, R14, R15, R17 - 1 K Ω , carbon, 1/4 W, 5%.

R16 - 10 K Ω , carbon, 1/4 W, 5%.

R18, R28 - 25 Ω .

R20 - 5.8 K Ω .

R23 - 59 K Ω .

R29 - 200 K Ω .

R30 - 50 K Ω , 22 turn trimpot.

P1, P3 - 20 K Ω , ten-turn potentiometer, 0.5% linearity.

P2 - 1 K Ω , ten-turn potentiometer, 0.5% linearity.

Capacitors:

All capacitors are mica, 10% tolerance.

C1 - 0.01 μ F.

C2 - 0.02 μ F.

C3 - 10 pF.

C4 - 5 pF.

Integrated Circuits:

OA1 - 153 K low noise operational amplifier (Analog Devices).

OA2, OA4, OA5, OA6 - LM741CN General purpose operational amplifier (National Semiconductor).

OA3 - 4558N dual general purpose operational amplifier (National Semiconductor)

IC1 - 7400 Quad 2-input NAND gate (Texas Instruments).

IC2 - NE555P Timer (Texas Instruments).

IC3 - 74193 Binary 4-bit up/down counter (Texas Instruments).

IC4 - AD561 10-bit digital-to-analog converter (Analog Devices).

Q1, Q2 - 3140 SK PNP transistor (RCA).

conduct. The input to IC1A from Q1 is then +5V, or "high." IC2 is a 555 timer configured to strobe between 0 and +5 volts at approximately 40 KHz. When IC2 goes "high," the output of IC1A goes "low," pulsing the "up count" input of IC3, a four-bit binary up/down counter. This pulse then adds one bit to the output word, which in turn feeds into the four most significant bits of IC4, a 10-bit digital-to-analog converter (Analog Devices AD561). The potential from IC4 through OA4 is proportional to the digital input, so each count "up" from IC3 raises the potential by 1/16 of the maximum output. This potential is then fed back into OA2 through resistor R18 and potentiometer P2, which can be adjusted to subtract a potential of one "full-scale" in the output of OA2. The procedure for adding a "full-scale" potential in the event of the output of OA2 falling below 0 volts is identical, involving OA3B, Q2, IC1B, and the "down count" input of IC3.

IC4, the digital-to-analog converter, has one other function. The output of Pin2, when fed into OA5, is a very stable reference voltage, its magnitude dependent on R21 and R20. This voltage is first fed through R21 and P1 to ground, and P1 is tapped to provide the "top of scale" potential for OA3A. The "top of scale" potential must be equal to or higher than the "full scale" offset set by P2. If this condition is not met, then the feedback loop can be unstable and cycle through the 15 available offsets. For a second reason, it is sometimes advantageous to have the "full scale" potential slightly less than the "top of scale." If a noisy signal is poised close to an offset point, and the "full scale" and "top of scale" potentials are essentially equal, then the module may rapidly add and subtract offsets according to the

noise on top of the signal. Lowering the "full scale" offset creates a small dead band which could prevent this from happening.

The output of OA5 is also inverted by OA6, and this output is fed through P3 into the inverting input of OA2. This provides a constant offset to be canceled by the AOS, enabling the user to set a negative non-zero offset for 0 volts input. In case the input signal then falls below 0 volts, a full-scale offset could be added by the AOS. If this were not the case, the word "0" from IC3 would be decremented to "15," subtracting 15 full scale offsets at the clock frequency, and will then recycle through the 15 offsets until the input signal again exceeds 0 volts.

Not shown in the circuit diagram is a BCD-to-7-segment-display decoder chip (7447) and corresponding 7-segment display. These are connected to the output of IC3, in order to show the user how many offsets out of the 15 have been used.

D. Application

The circuit is shown in use in Figure 35, where a synthesized signal (from a Wavetek Model 112 function generator) is shown on the lower trace and the output of the offset module (with a first stage gain of 1) on the upper trace. For clarity of illustration, the pen retracing the full-scale effects is not shown, although vertical lines would normally appear where offsets occur.

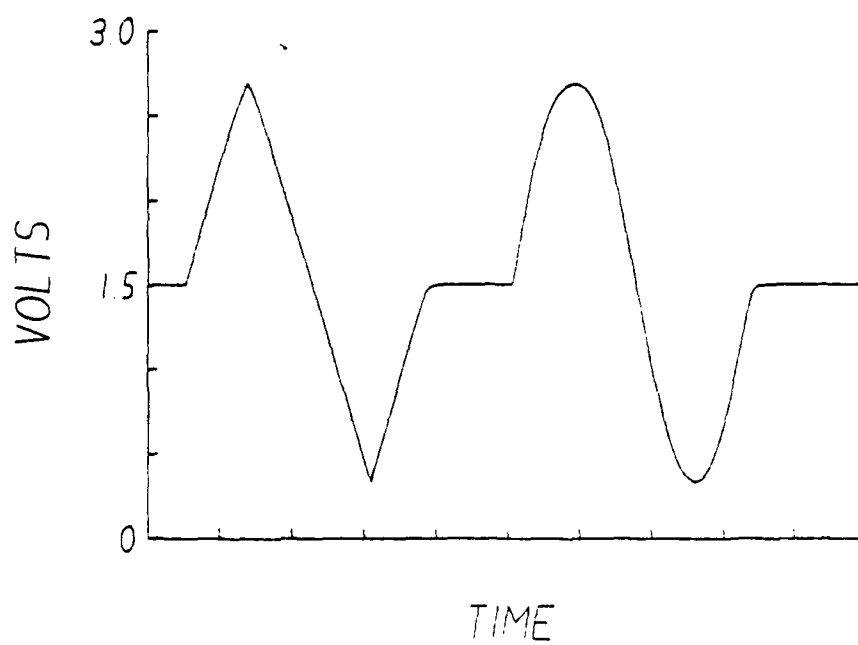
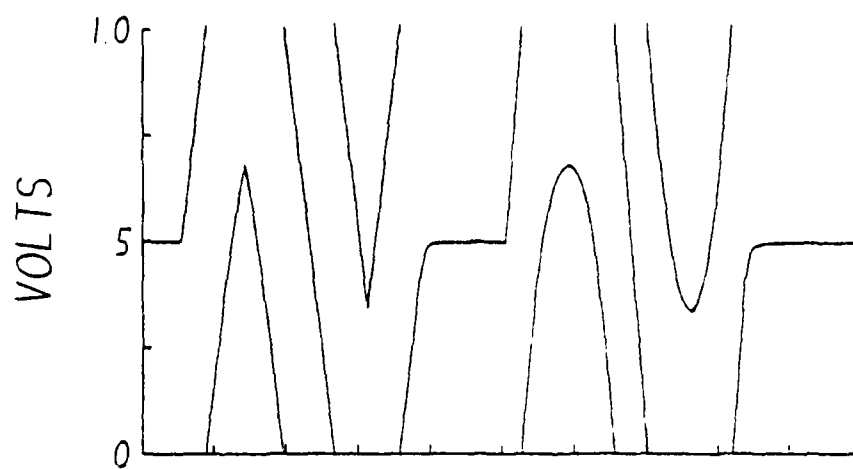
The precision of an offset point was determined using an Analog Devices AD2700 voltage reference source, a Leeds and Northrup K-3 potentiometer, and a Fluke Model 8800A 5-1/2 digit multimeter. A 20 mV signal was applied with a gain of 100 on the preliminary amplifier, and

Figure 35. Operation of the Automatic Offset Module.

Input to module, triangular and sine waves, approximately 0.05 Hz, 2.5 V. amplitude, centered at 1.5 V. above common.

Top trace: Output of offset module. Where pen has retraced full scale erased for clarity of display.

Bottom trace: Input to offset module.



the input slowly varied until the offset was triggered. The standard deviation of the offset point (measured at the input) was 0.02% ($N=11$), both for an addition and subtraction of an offset. This is better than the specified precision of the Fluke multimeter at a 20 mV input.

BIBLIOGRAPHY

1. Tanaka, Y.; Fujita, K. J. Chromatogr. 1975, 108, 255.
2. Seymour, M.; Fritz, J. S. Anal. Chem. 1973, 45, 1394.
3. Sisson, D. H.; Mode, V. A.; Campbell, D. O. J. Chromatogr. 1972, 66, 129.
4. Gilbert, T. W.; Dobbs, R. A. Anal. Chem. 1973, 45, 1390.
5. Dorsey, J. G.; Denton, M. S.; Gilbert, T. W. Anal. Chem. 1978, 50, 1330.
6. Warren, H. D.; McKay, D. P. J. Chrom. Sci. 1975, 13, 117.
7. Freed, D. J. Anal. Chem. 1975, 47, 186.
8. Araki, S.; Suzuki, S.; Yamada, M. Talanta. 1972, 19, 577.
9. Blaedel, W. J.; Todd, J. W. Anal. Chem. 1958, 30, 1821.
10. Buchanon, E. B., Jr.; Bacon, J. R. Anal. Chem. 1967, 39, 615.
11. Johnson, D. C.; Larochelle, J. Talanta. 1973, 20, 959.
12. Fritz, J. S.; Story, J. N. Anal. Chem. 1974, 46, 825.
13. Arguello, M. D.; Fritz, J. S. Anal. Chem. 1977, 49, 1595.
14. Neary, M. P.; Seitz, R.; Hercules, D. M. Anal. Lett. 1974, 7, 583.
15. Hartkopf, A.; Delumyea, R. Anal. Lett. 1974, 7, 79.
16. Delumyea, R.; Hartkopf, A. V. Anal. Chem. 1976, 48, 1402.
17. Tanaka, Y.; Muto, G. Anal. Chem. 1973, 45, 1864.
18. Small, H.; Stevens, T. S.; Bauman, W. C. Anal. Chem. 1975, 47, 1801.
19. Shultz, F. A.; Mathis, D. E. Anal. Chem. 1974, 46, 2253.
20. Loscombe, C. R.; Cox, G. B.; Dalziel, J. A. W. J. Chromatogr. 1978, 166, 403.
21. Kissinger, P. T. Anal. Chem. 1977, 49, 447A.

22. Fenn, R. J.; Siggia, S.; Curran, D. J. Anal. Chem. 1978, 50, 1067.
23. Swartzfager, D. G. Anal. Chem. 1976, 48, 2189.
24. Rabenstein, D. L.; Saetre, R. Anal. Chem. 1977, 49, 1036.
25. EG&G Princeton Applied Research Corp. Polarographic Instrumentation. 1978, 5.
26. Reeve, D. R.; Crozier, A. J. Chromatogr. 1977, 137, 271.
27. Wescan Instruments, Inc. Preliminary Information Model 213 Conductivity Detector. 1979.
28. Tesarik, K.; Kalab, P. J. Chromatogr. 1973, 78, 357.
29. Van der Linden, W. E.; Oostervink, R. Anal. Chim. Acta. 1978, 101, 419.
30. Carr, P. W. Anal. Chem. 1978, 50, 1602.
31. Frei, R. W.; Scholten, A. H. M. T. J. Chromatogr. Sci. 1979, 17, 152.
32. Orion Research Analytical Methods Guide, Ninth Edition, 1978.
33. Durst, R. A., ed. "Ion Selective Electrodes"; National Bureau of Standards Special Publication 314, 1969; Chapter 2.
34. Ibid., Chapter 6.
35. Ibid., Chapter 11.
36. Blaedel, W. J.; Dinwiddie, D. E. Anal. Chem. 1974, 46, 873.
37. Koryta, J. Anal. Chim. Acta. 1977, 91, 1.
38. Covington, A. K. CRC Crit. Rev. Anal. Chem. 1974, 3, 355.
39. Blum, R.; Fog, H. M. Electroanal. Chem. 1972, 34, 485.
40. Hansen, E. H.; Lamm, C. G.; Ruzicka, J. Anal. Chim. Acta. 1972, 59, 403.
41. Perrin, D. D.; Dempsey, B. "Buffers for pH and Metal Ion Control"; John Wiley and Sons: New York, 1974; Chapter 7.
42. Baumann, E. W. Anal. Chim. Acta. 1971, 54, 189.
43. Durst, Chapter 10.

44. Jensen, J. B. Anal. Chim. Acta. 1975, 76, 279.
45. Smith, M. J.; Manahan, S. E. Anal. Chem. 1973, 45, 836.
46. Heijne, G. J. M.; van der Linden, W. E.; den Boef, G. Anal. Chim. Acta. 1978, 98, 221.
47. Heijne, G. J. M.; van der Linden, W. E.; den Boef, G. Anal. Chim. Acta. 1978, 100, 193.
48. Butler, J. N. "Ionic Equilibrium - A Mathematical Approach"; Addison-Wesley: Reading, Mass., 1964; p. 437.
49. Ives, D. J. G.; Janz, G. J. "Reference Electrodes"; Academic Press: New York, 1961; Chapter 1.
50. Bates, R. G. "Determination of pH: Theory and Practice", 2nd ed.; John Wiley and Sons: New York, 1973; Chapter 3.
51. Robinson, R. A.; Stokes, R. H. "Electrolyte Solutions"; Academic Press: New York, 1959; p. 465.
52. Durst, Chapter 4.
53. Butler, J. A. V., ed. "Electrical Phenomena at Interfaces"; MacMillan Co.: New York, 1951; Chapter 3.
54. Glasstone, S. "An Introduction to Electrochemistry"; Van Nostrand: New York, 1942; Chapter 16.
55. Van den Winkel, P.; Mertens, J.; Massart, D. L. Anal. Chem. 1974, 46, 1765.
56. Rechnitz, G. A.; Lin, A. Anal. Chem. 1967, 39, 1406.
57. Mertens, J.; Van den Winkel, P.; Massart, D. L. Anal. Chem. 1976, 48, 272.
58. Toth, K.; Pungor, E. Anal. Chim. Acta. 1972, 64, 417.
59. Shatkay, A. Anal. Chem. 1976, 48, 1039.
60. Rangarajan, R.; Rechnitz, G. A. Anal. Chem. 1975, 47, 325.
61. Morf, W. E.; Lindner, E.; Simon, W. Anal. Chem. 1975, 47, 1596.
62. Blaedel, W. J.; Dinwiddie, D. E. Anal. Chem. 1975, 47, 1070.
63. Rechnitz, G. A.; Hameka, H. F. Z. Anal. Chem. 1965, 214, 252.
64. Lindner, E.; Toth, K.; Pungor, E. Anal. Chem. 1976, 48, 1071.

65. Morf, W. E. Anal. Lett. 1977, 10, 87.
66. Midgely, D. Anal. Chim. Acta. 1976, 87, 19.
67. Parthasarathy, N.; Buffle, J.; Haerdi, W. Anal. Chim. Acta. 1977, 93, 121.
68. Toth, K.; Pungor, E. Anal. Chim. Acta. 1971, 57, 131.
69. Ross, J. W. U.S. Patent 3,497,424; 24 February 1970.
70. Pick, J.; Toth, K.; Pungor, E. Anal. Chim. Acta. 1972, 61, 169.
71. Hepel, T.; Hepel, M.; Leszko, M. Analyst. 1977, 102, 132.
72. Hirata, H.; Higashiyama, K.; Date, K. Anal. Chim. Acta. 1971, 53, 202.
73. Heijne, G. J. M.; van der Linden, W. E.; den Boef, G. Anal. Chim. Acta. 1977, 89, 287.
74. Hansen, E. H.; Lamm, C. G.; Ruzicka, J. Anal. Chim. Acta. 1972, 59, 403.
75. Anfalt, T.; Jagner, D. Anal. Chim. Acta. 1971, 56, 477.
76. Van de Leest, R. E. Analyst. 1977, 102, 509.
77. Thompson, H.; Rechnitz, G. A. Chem. Instrum. 1972, 4, 239.
78. Heijne, G. J. M.; Van der Linden, W. E. Anal. Chim. Acta. 1977, 93, 99.
79. Heijne, G. J. M.; Van der Linden, W. E. Anal. Chim. Acta. 1978, 96, 13.
80. Blum, R.; Fog, H. M. J. Electroanal. Chem. 1972, 34, 485.
81. Hansen, E. H.; Ruzicka, J. Talanta. 1973, 20, 1105.
82. Nakagawa, G.; Wada, H.; Hayakawa, T. Bull. Chem. Soc. Japan 1975, 48, 424.
83. Hulanicki, A.; Lewenstein, A. Talanta. 1976, 23, 47.
84. Jyo, A.; Hashizume, T.; Ishibashi, N. Anal. Chem. 1977, 49, 1868.
85. Olson, V. K.; Carr, J. D.; Hargens, R. D.; Force, R. K. Anal. Chem. 1976, 48, 1228.
86. Sekerka, I.; Lechner, J. F. Anal. Lett. 1978, A11, 415.

87. Fung, Y. S.; Fung, K. W. Anal. Chem. 1977, 49, 497.
88. Crombie, D. J.; Moody, G. J.; Thomas, J. D. R. Talanta. 1974, 21, 1094.
89. Jasinski, R.; Trachtenberg, I.; Andrychuk, D. Anal. Chem. 1974, 46, 365.
90. Oglesby, G. B.; Duer, W. C.; Millero, F. J. Anal. Chem. 1977, 49, 877.
91. Ross, J. W., Jr.; Front, M. S. Anal. Chem. 1969, 41, 1900.
92. Mascini, M. Anal. Chim. Acta. 1971, 56, 316.
93. Van Oort, W. J.; Van den Bergen, V. W. J.; Griepink, B. Z. Anal. Chem. 1974, 269, 184.
94. Napoli, A.; Mascini, M. Anal. Chim. Acta. 1977, 89, 209.
95. Baumann, E. W.; Wallace, R. M. Anal. Chem. 1969, 41, 2072.
96. Sucha, L.; Valentova, M.; Suchanek, M.; Urner, Z. Scientific Papers of the Institute of Chemical Technology, Prague. 1973, 1973, 99.
97. Van der Meer, J. M.; den Boef, G.; van der Linden, W. E. Anal. Chim. Acta. 1975, 76, 261.
98. Van der Meer, J. M.; den Boef, G.; van der Linden, W. E. Anal. Chim. Acta. 1975, 79, 27.
99. Van der Linden, W. E.; Oostervink, R. Anal. Chim. Acta. 1978, 101, 419.
100. Tanaka, N.; Kato, K. Bull. Chem. Soc. Japan 1959, 32, 1376.
- 100a. Tanaka, N.; Kato, K.; Tamamushi, R. Bull. Chem. Soc. Japan 1958, 31, 283.
101. Kato, K. Bull. Chem. Soc. Japan 1960, 33, 600.
102. Tanaka, N.; Kamada, M. Bull. Chem. Soc. Japan 1962, 35, 1596.
103. Tanaka, N.; Osawa, H.; Kamada, M. Bull. Chem. Soc. Japan 1963, 36, 530.
104. Bydalek, T. J.; Margerum, D. W. J. Amer. Chem. Soc. 1961, 83, 4326.
- 104a. Smith, G. F.; Margerum, D. W. Inorg. Chem. 1969, 8, 135.

105. D'Olieslager, W.; Choppin, G. R. J. Inorg. Nucl. Chem. 1971, 33, 127.
106. Leitinen, H. A. "Chemical Analysis"; McGraw-Hill: New York, 1960; Chapter 13.
107. Johansson, G.; Edstrom, K. Talanta. 1972, 19, 1623.
108. Malmstadt, H. V.; Enke, C. G.; Crouch, S. R. "Electronic Measurements for Scientists"; W. A. Benjamin: Menlo Park, California, 1974; p. 348.
109. Adams, R. E.; Betso, S. R.; Carr, P. W. Anal. Chem. 1976, 48, 1989.
110. Diefenderfer, A. J. "Principles of Electronic Instrumentation"; W. B. Saunders: Philadelphia, 1972; p. 313.
111. Bakalyer, S. R.; Bradley, M. P. T.; Hongamen, R. J. Chromatogr. 1978, 158, 277.
112. Zipper, J. J.; Fleet, B.; Persone, S. P. Anal. Chem. 1974, 46, 2111.
113. Papastathopoulos, D. S.; Nikolelis, D. P.; Hadjiioannou, T. P. Analyst. 1977, 102, 852.
114. Kirschner, S. J. Amer. Chem. Soc. 1956, 78, 2372.
115. Sillen, L. G.; Martell, A. E. "Stability Constants of Metal-ion Complexes"; The Chemical Society, London Special Publication 17, 1964, and Supplement 1, 1971.
116. Negus, L. E.; Light, T. S. Instr. Tech. Dec. 1972, 23.
117. Laidler, K. J. "Chemical Kinetics"; McGraw-Hill: New York, 1965; Chapter 1.
118. Van de Leest, R. E. Analyst. 1976, 101, 433.
119. Ruzicka, J.; Hansen, E. H. Anal. Chim. Acta. 1978, 99, 37.
120. Hofmann, K.; Halasz, I. Anal. Chim. Acta. 1979, 173, 211.
- 120a. Nunge, R. J.; Lin, T. S. AIChE J. 1973, 19, 1280.
121. National Research Council "International Critical Tables", Vol. 5; McGraw-Hill: New York, 1929; p. 65.
122. Sternberg, J. C. in Giddings, J. C., ed. "Advances in Chromatography", Vol. 2; Dekker: N. Y., 1966; Chapter 6.

123. Schifreen, R. S.; Hanna, D. A.; Bowers, L. D.; Carr, P. W. Anal. Chem. 1977, 49, 1929.
124. Meites, L. "The General Multiparametric Curve-fitting Program CFT-3"; Clarkson College of Technology, Potsdam, N.Y., 1973.
125. Analog Devices Data Acquisition Catalog, Model 759 Logarithmic Transconverter, 1978, p. 221.
126. Ramaley, L.; Surette, D. P. Chem. Instrum. 1978, 8, 181.